Design and Implementation of a High Precision Profilometer

by

Tarzen Kwok

B.S., Mechanical Engineering (1992)

University of Hawaii
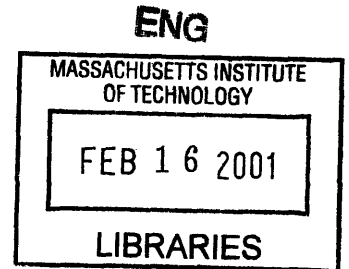
Submitted to the Department of Mechanical Engineering
in Partial Fulfillment of the Requirements for the degree of
Master of Science in Mechanical Engineering

at the

Massachusetts Institute of Technology

February, 1995

Signature of Author_____

Department of Mechanical Engineering
January 20, 1995

Certified by_____

Dr. Kamal Youcef-Toumi
Associate Professor
Thesis Supervisor

Accepted by_____

Dr. Ain A. Sonin
Chairman, Department Committee on Graduate Students

Barker Eng

Design and Implementation of a High Precision Profilometer

by

Tarzen Kwok

Submitted to the Department of Mechanical Engineering
on December 16,1994 in partial fulfillment of the
requirements for the degree of Master of Science in
Mechanical Engineering

ABSTRACT

A high precision profilometry system was developed primarily for the inspection of two-sided sample specimens. Based upon system specifications and requirements, it was found that the most suitable profilometry technique was atomic force microscopy (AFM). The major components of the profilometer were: 1) a commercial atomic force microscope, 2) customized sample positioning hardware, 3) image processing and control software, and 4) system calibration procedures.

The primary focus of this thesis is on the design and implementation of the customized blade positioning hardware, consisting of two linear stages stacked to form an X-Y table and a novel 'flip' stage which allows both sides of the sample to be measured by the AFM. The flip stage uses a kinematic coupling design to achieve the necessary positioning precision and stability. A homogeneous transformation matrix (HTM) method was developed for calculating the profiling errors due to stage positioning errors.

The actual performance and calibration of the profilometer system was investigated through various tests, including: 1) measurement / positioning repeatibility tests of individual components, 2) measurement accuracy tests (documented in a seperate report), and 3) other tests, such as determination of measurement sensitivity, drift rates, and system natural frequency.

Thesis Supervisor: Dr. Kamal Youcef-Toumi
Title: Associate Professor of Mechanical Engineering

Acknowledgements

This thesis (and more importantly, the work that it documents) is dedicated to my parents, whose support and advice I will always cherish.

I would like to acknowledge the support of the following persons in making this project a success and my graduate studies here at M.I.T. a truly educational and productive experience:

Professor Youcef-Toumi: even though you are a very busy person, you always kept an open ear to my problems and gave me suggestions; you taught me to work independently.

Dr. Eric Liu: your persistance (e.g. I must admit at one time no one believed in the 'flip' stage concept except you), countless ideas, and time / resource management skills are traits that I hope to learn and apply (the sooner the better!). You were instrumental in guiding the course of this project.

Cheng-Jung Chiu: your work on the software / control side of this project allowed me to concentrate my efforts on the hardware design; without your help I would of (literally) drop dead from exhaustion; thanks a million!

Fred Cote: as the LMP research shop technician, the tireless enthusiasm and dedication with which you helped countless numbers of graduate students is truly inspirational. I have learned machining and so much more from you-- I guess the only way to 'repay' you is to design things which are truly useful and easy to manufacture.

Tetsuo Ohara: thank you for your guidance, advice and practical experience; best of luck on the development of your 'Nanowave' sensor.

Engineers **Brian Bosy** and **Joseph Depuyut** provided me with constructive criticisms and practical engineering advice on the sample positioning hardware.

T.J. Yeh: without the company of 'Tomato Juice' (or was that 'Tom and Jerry' ?), working in the lab would of been a truly lonesome experience; I always enjoyed our open, frank discussions (on everything except technical things, that is). Your friendliness, and genuine concern for others (despite your claim of being anti-social) will always be remembered and serve as a role model for me and many other people. Although we must each go our own seperate ways, hopefully our friendship will not come to an end.

Fellow lab members and graduate students (past and present) **Mitchell, Henning, Pablo, Irene, Yuri, Francis, Jake, Shih-Ying, Harry, Herman,Henry, Toshi** (my officemate), among others; in each of you I see personal traits that explain why M.I.T. is a great institution.

Last but not least, I would like to thank the many part / machine shop vendors whose products / services were used in the profilometer. Special thanks goes out to **Leslie Regan** for granting me a super long extension on my thesis.

Table of Contents

List of Tables and Figures

List of Tables

List of Figures

1 Introduction

1.1 Problem Statement

This report documents the design and implementation of the custom hardware components developed for a high resolution, high precision two-sided sample profilometer system.

The geometric profile of the two-sided sample can be described by two parameters: D, which is the horizontal distance from the *identified* tip, and T, which is the vertical distance from the surface of the sample to the hypothetical line that intersects the identified tip and runs parallel to the sample support body. D and T can be further decomposed as follows:

$$D = D_0 + E_{D1} + E_{D2} \qquad\qquad (1.1)$$

$$T = T_0 + E_{T1} + T_{T2} \qquad\qquad (1.2)$$

D_0 and T_0 refer to the true dimensions of the sample E_{D1} and E_{T1} refer to the errors associated with the location of the tip, and E_{D2} and T_{T2} refer to the general systematic / random errors (i.e. 'uncertainty') associated with the measurement technique used. These parameters are graphically shown in Figure 1.1 and Figure 1.2. The target specifications for the profilometry system are listed in Table 1.1 below:

Range:		
	D0,max	20 µm from tip
	T0,max	0 to ≈ 4.0 µm
Resolution:		
	D0	≤ 0.02 µm (20 nm
	T0	≤ 0.001 µm (1 nm)
Errors:		
	ED1	≤ ± 0.02 µm (20 nm)
	ED2	≤ ± 0.005 µm (5 nm)
	ET1	≤ ± 0.02 µm (20 nm)
	ET2	≤ ± 0.005 µm (5 nm)
D & T linearity		≤ 1% (with respect to the full measurement range)
Measurement technique		
restrictions:		**must be non-destructive**

Table 1.1 Profilometry system target specifications

In addition to the above specifications, the following constraints were also present:

1) time to complete project: ≈ 1 year;
2) reliability and ease-of-use.

1.2 Scope of Work

As mentioned earlier, this report deals primarily with the custom hardware developed for the profilometer. The major hardware components of the profilometer are:
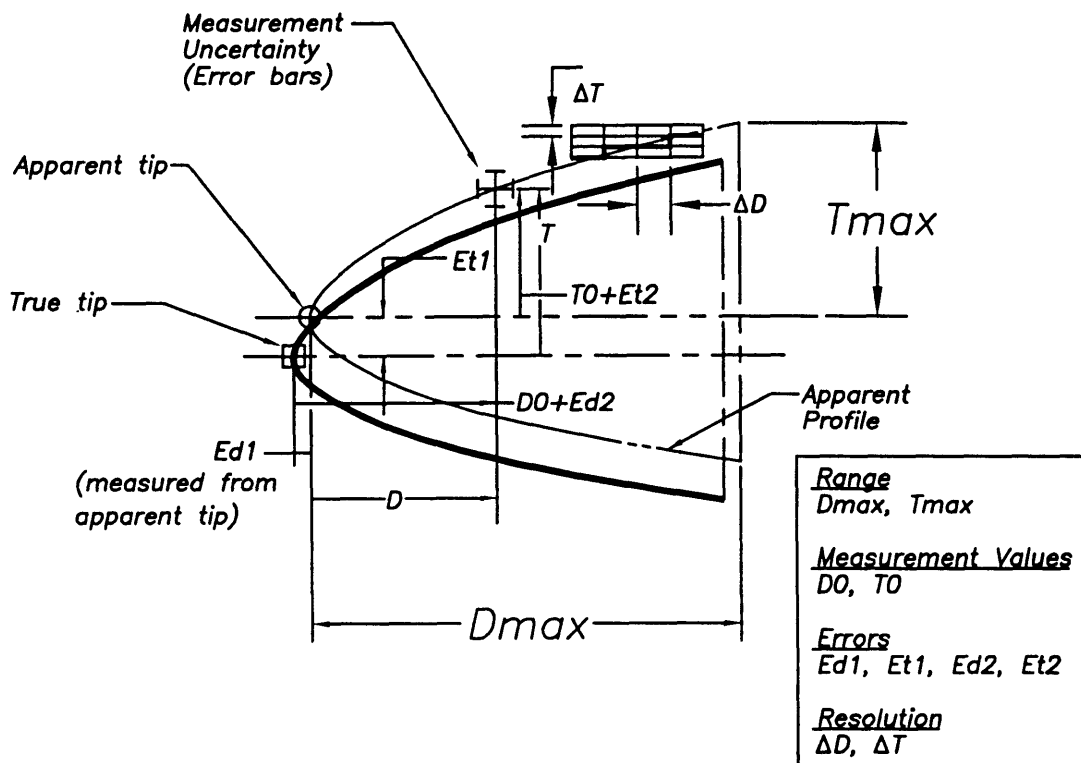
Figure 1.1 Sample profile measurement definitions
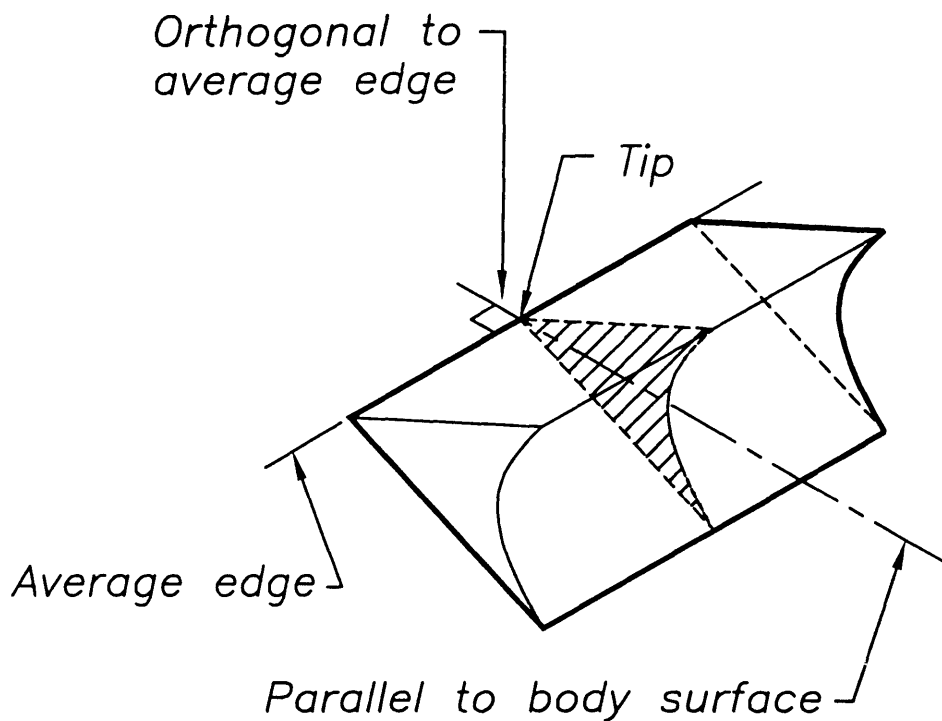
Figure 1.2 Datum surfaces for profile measurements

9

1) measurement probe subsystem;
2) sample positioning subsystem;
3) electronic / optics subsystem.

Each of these components is further discussed in the following chapters; chapter two deals primarily with the measurement probe subsystem, a brief mention is made of the electronic / optics subsystem; chapters three and four discuss the sample positioning subsystem, and chapter five presents the actual implementation of the entire hardware unit and an evaluation of its performance. Finally, conclusions and recommendations are given in chapter six.

It should be mentioned that a very important part of the entire profilometer system is the actual profiling process / procedure, as implemented through software. Issues here includes selection of profiling parameters, identification of the tip and subsequent generation of the sample profile, and an examination of the sources and effects of measurement errors. These topics are covered in a seperate report [A1].

2 Profilometer Design

2.1 Introduction

In this chapter, the profilometry method and physical configuration for the profilometer are chosen. This is followed by a brief description of the actual measurement probe and associated electronics / optics subsystems.

2.2 Profilometry Methods

Profilometry techniques that were considered included the well-established methods (i.e. scanning electron microscope, mechanical stylus, optical stylus, and the atomic force microscope), as well as methods under research and development (e.g. scanning near-field optical microscope). In the following subsections, a brief description of the operating principle, and strengths and weaknesses of each profiling technique is given.

2.2.1 Scanning Electron Microscopy (SEM)

In scanning electron microscopy (SEM), an electron beam bombards the sample surface, resulting in secondary surface electron emissions; these emissions are then collected to form the data image. SEM's are powerful metrology instruments, capable of resolutions as high as 5 nm [A2] and a linewidth measurement linearity of 1% [A3]. For three-dimensional profilometry, SEM is *not* a viable option because the SEM data is inherently two-dimensional in nature; to obtain an accurate profile the sample must be imaged through a cross-section (i.e. the sample must be physically modified, which is unacceptable). Despite this shortcoming, SEM data still provides a highly informative, 'photorealistic' image of the sample surface, thus SEM complements (rather than competes) with the profilometry technique that will be developed.

2.2.2 Conventional Mechanical Stylus

In the conventional stylus method, a stylus with a sharp tip is mechanically dragged along the surface. This is shown in Figure 2.1. The deflection of the hinged stylus arm is measured and recorded as the surface profile. The use of a hinged stylus arm allows measurement of very rough surfaces (peak-to-peak heights > 1 mm) . On the other hand, since the hinged stylus arm is partially supported by the stylus itself, physical rigidity limits the minimum stylus tip radius and hence the lateral resolution to about 0.1 μm [A4]. Probe-to-surface contact forces range from 10^{-3} to 10^{-6} N [A5].

2.2.3 Optical Methods

In optical profilometry, many different optical phenomena (such as interference and internal reflection) can be utilized. The most popular technique is based on phase-measuring interferometry, where a light beam reflecting off the sample surface is interfered with a phase-varied reference beam as shown in Figure 2..2 , and the surface profile is deduced from the fringe patterns produced. With a collimated light beam (i.e. the light is made to travel in parallel lines) and a large photodetector array, the entire surface can be profiled simultaneously. This and other conventional optical methods are limited in lateral resolution by the diffraction limit of the visible light used (

Figure 2.1: STYLUS WORK SENSOR MOTOR/GEARBOX –HORIZONTAL DRIVE STRAIGHT DATUM BEARINGS VERTICAL COLUMN
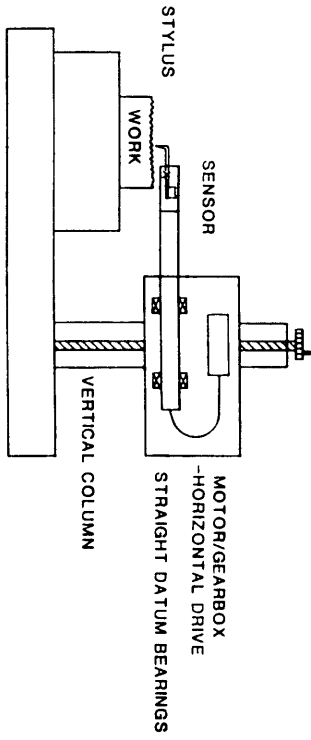
Figure 2.1: Conventional mechanical stylus, from [A4]

AMPLITUDE

mm
10
1
100
10
1
100
10
1
μm
0·1
nm
0·01

0·1   1   10 100 | 1   10 100 | 1   10 100 | 1   10 100 1000
      nm   μm   mm

SURFACE WAVELENGTH

PROBE

STYLUS
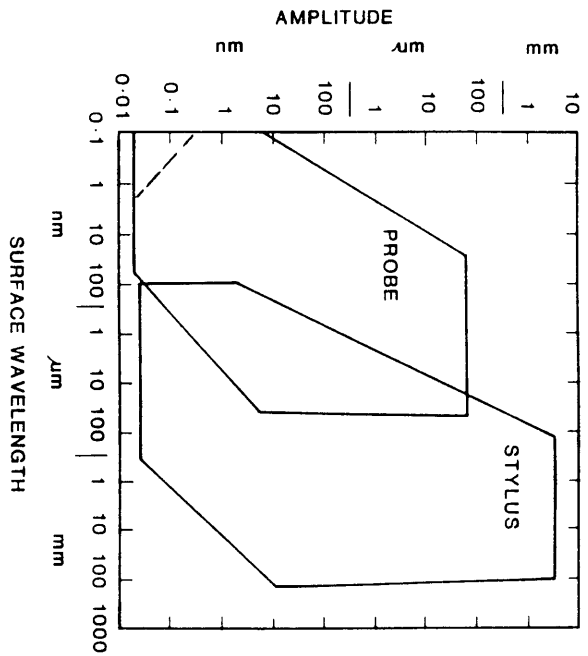
Figure 2.3: Measurement range of various profilometry techniques, [A4]

source
half mirror
reference mirror
detector
servo
surface
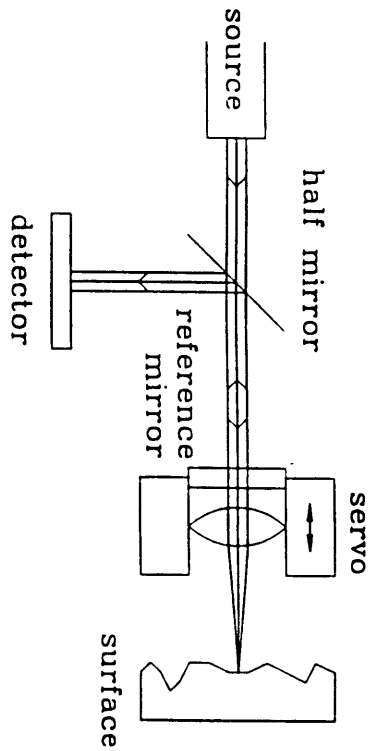
Figure 2.2: Phase-measuring interferometry, [A4]

TO THREE ORTHOGONAL ACTUATORS

SPECIMEN

TUNNELING PROBE TO MONITOR BEAM DEFLECTION
FLEXIBLE CANTILEVER AND PROBE
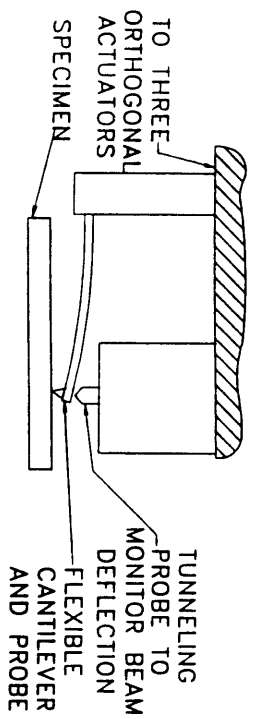
Figure 2.4: Contact mode atomic force microscope, here a tunneling sensor is used for beam deflection detection, other methods can be used as well, [A4]

≈ 0.5 μm) [A4]. In addition, measurement values are dependent on the surface reflectivity of the material being profiled.

2.2.4 Scanning Probe Microscopy (SPM)

Based upon the lateral resolution requirement only (≤ 0.02 μm), it should be obvious that the conventional methods described above are not suitable profiling solutions. Currently, only the recently developed scanning probe microscopes can meet the 20 nm lateral resolution requirement, see Figure 2.3. In these microscopes, an atomically sharp (or nearly so) tip is moved over the sample surface with a piezoelectric fine positioner, seperated from the surface by a small gap (which is on the order of nanometers or less). Scanning probe microscopes investigated were the contact atomic force microscope, the scanning tunneling microscope (STM), scanning near-field optical microscope (SNOM), scanning capacitance microscope, scanning thermal microscope, and other variations of atomic force microscope, such as non-contact (long range) atomic force, magnetic and electrostatic force microscopes.

In the contact mode atomic force microscope, a cantilver beam mounted microstylus is moved relative to the sample surface using piezoactuators, see Figure 2.4; with the deflection of the cantilever is taken to be a measure of the surface topography. Atomic force microscopy offers ultrahigh lateral and vertical resolution (<1 nm possible), however, the maximum surface roughness that can be profiled is much less than that of the conventional stylus due to the limited deflection of the stylus cantilever, see Figure 2.3. Probe-to-surface contact forces range from 10^{-8} N to 10^{-11} N.

In the scanning tunneling microscope (STM), the quantum tunneling current between the probe tip and sample is measured. The STM is attractive because it is a non-contact device (i.e. no surface damage, potential for high speed profiling) with the highest resolution of all the 'scan probe' microscopes, however, it can only be used on electrically conducting surfaces.

In the scanning near-field optical microscope (SNOM), the focusing limit of conventional far-field optics is bypassed by bringing a 20 nm diameter light aperature approximately 5 nm from the surface; the resulting transmitted or reflected light is then collected to form an image. SNOM technology is still very much in the research stage-- the minimum achievable lateral resolution so far, 12 nm, has been limited by the ability to form the light apertures reproducibly [A6], although it should be noted that commercial SNOM's have begun to appear in the marketplace [A7].

In the non-contact atomic force microscope, long range Van de Waals forces are measured by vibrating the cantilever stylus in a vertical direction, near its resonance frequency, and detecting the change in vibrational amptitude of the beam due to a change in the force gradient (i.e. because of changes in the surface profile) [A8]. The non-contact atomic force microscope offers non-invasiveness profiling; compared to contact atomic force microscopy however, the technique has several disadvantages. First, Van de Waals forces are hard-to-measure 'weak' forces, hence the microcope is more susceptible to noise. Secondly, the probe tip must be servoed to a fixed height above the sample (typically a few nanometers)-- this must be done slowly to avoid 'crashing' the tip. Thirdly, since the tip is always floating above the surface, the effective tip radius is increased and hence the achievable lateral resolution is decreased as well [A9].

Finally, in the scanning thermal microscope, the measured temperature of an AC current heated tip is a function of gap spacing [A10]. The magnetic and electrostatic force microscope measure the force due to a magnetic and electrostatic potential field, respectively [A11,A12]. The electrostatic force microscope is different from the scanning capacitance microscope [A13], which measures the capacitance between the probe tip and sample. These methods were not designed to measure topography directly-- the sensed quantity is actually a function of both the surface topography and other surface properties (e.g. local dielectric constant).

2.3 Selection of Profilometry Method

The profilometry technique(s) which will be used was selected based upon the following criteria (in order of importance):

1) *profiling requirements:* measurement range, resolution, repeatibility, and non-destructive profiling;
2) *sample surface characteristics:* sample with/without non-conductive thin-film, range of surface roughness which has to be measured;
3) *profilometer requirements:* offline measurement, one machine for both conductive and non-conductive samples;
4) *time to completion/cost.*

A comparison of the different possible profiling methods showed contact atomic force microscopy to be the most promising profilometry technique. The reasons for this, in terms of the selection criteria above, are as follows:

1) *profiling requirements:* a 20 μm x 20 μm x 4 μm (height) profiling volume, with 20 nm lateral resolution can be achieved with existing scanning piezoactuator designs [A14]; a 20 nm resolution for the force sensing stylus is also achievable-- micromachined tips with radius <10.0 nm have been consistently produced[A15]. In addition, closed-loop control of the piezoactuator will minimize the effects of piezoactuator nonlinearities and drift (alternately, image processing techniques can be used), thus insuring high measurement repeatibility. Lastly, even though contact measurement is used, this is still expected to result in non-destructive profiling-- more fragile biological samples have been imagedwithout damage using contact forces as high as 10^{-8} [A16].
2) *surface sample characteristics:* the AFM can be used to profile both conductive and nonconductive surfaces; thin film characterization is one field where AFM's are actively being used [A17]; the surface roughness that can be measured is dependent on the overall size of the stylus (this is a problem common to all scanning probe microscopes)-- note however that high height-to-width aspect ratio micromachined tips [A18] which will minimize this problem.
3) *profilometer requirements:* since measurements are performed offline, profiling speed may not be a major issue; current AFM systems have scan rates from 1 Hz to 10 kHz [A19]. As mentioned in (2), because the AFM is capable of profiling both conducting and nonconducting surfaces, only one machine is required.
4) *time to completion/cost:* all the technologies mentioned in (1) to (3) above are either well established or under rapid development, thus the creation of a working system within one year's time is definitely possible.

Note that scanning tunneling microscopy has similar attractive features; so the STM could be used to profile the uncoated (i.e. electrically conductive) samples; (hardware changes to the profilometer would be minimial). For consistent measurements however, AFM would be the first method of choice, because even the uncoated sample might have a nonconductive oxide/contamination layer/spot that would render the STM inoperative [A19].

2.4 Profilometer Configuration

Having selected a profilometry method, the next step was to decide on a physical configuration for the profilometer. An exhaustive listing of all possible probe(s) / sample arrangements is given in Figure 2.5; each configuration was then subsequently examined for feasibility and technical merit.

As its name suggest, the two scanner / two probe / stationary sample configuration would have each side of the sample profiled by a seperate probe. A simultaneous scanning two probe AFM is definitely doable [A20], however, the hardware cost of two measurement probe systems could be prohibitively high. Other critical issues include alignment and calibration of the two probes.

In the one scanner / three-contact point probe / stationary sample configuration, a special three-contact point probe profiles the sample by moving from one side of the sample to the other. Macroscopic versions of such probes are used in industrial coordinate measuring machines (CMM) to measure hard-to-reach spots, and an SPM system with a three-contact point probe has been developed by [A21], see Figure 2.6. The advantage of this configuration-- the use of only one scanner and probe along with a stationary sample, is offset by the need to develop a reliable sensing / control scheme for the three-contact point probe-- this is not a trivial task!

In the one scanner / one probe / 'flip' sample configuration, a special positioning device 'flips' the sample from one side to the other, allowing a single conventional AFM unit to be used. The technical issues which must be resolved include accurate reconstruction of the sample profile and the precision positioning / alignment of the sample.

A variation of the above concept would be to have the sample rotating continuously while the AFM is operating. Because the sample has an essentially 'thin' profile (i.e. a high D to T ratio), maintaining contact between the AFM probe and the sample would require complex (non-circular) positioning of the sample with nanometer level accuracies; this configuration would only be advantageous for profiling near the tip region, where the profile is circular in nature.

Lastly, in the one scanner / two probe / 'stationary' sample configuration, two probes are mounted face-to-face on a single scanner, with the sample profiled one side at a time. In this configuration only one scanner is utilized, and the sample is required to move through a small range of motion; technical problems that must be overcome include development of a two probe head, operation of the AFM with the probe 'upside down', and alignment and calibration of the two probes.

In conclusion, the three-contact point probe and continuous sample rotation configurations were not pursued further because they presented significant technical difficulties without offering any substantial advantages. For the two probe configurations (either with one scanner or two), their primary advantage is that the
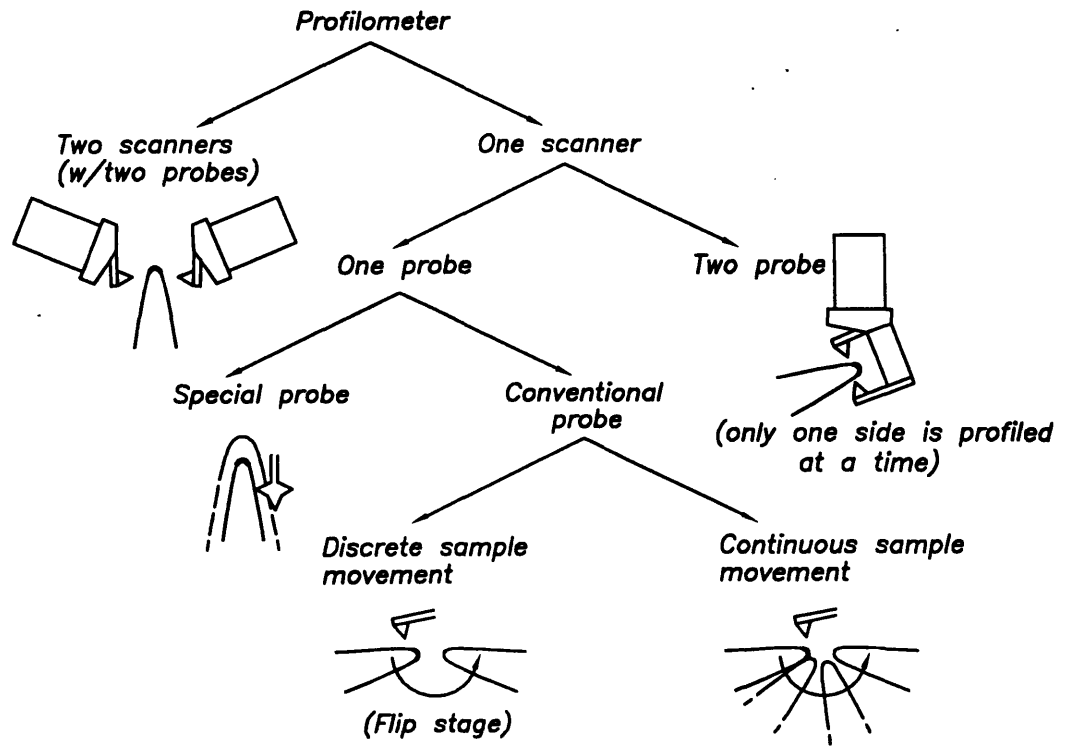
Figure 2.5: *Possible measurement probe(s) / sample position configurations*
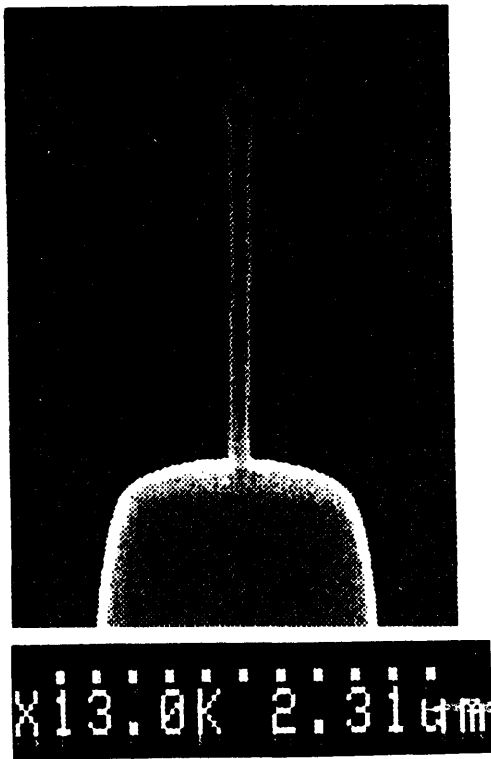
Figure 2.6: *Three contact point AFM probe, from [A21]*
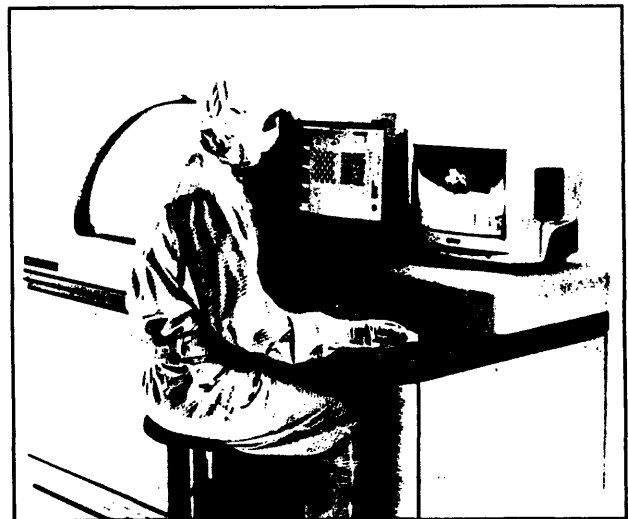
Figure 2.7: *Park Scientific Instruments AutoProbe XL, from [A23]*

sample only needs to be moved (if at all) through a small range of motion. This means that it can be positioned with great accuracies (for example, high sensitivity, short range screw type angular adjustments can be used). Also, the sample can be fixtured more rigidly than with a movable mount. A closer examination of the two probe configuration however revealed the following disadvantages:

1) *probe alignment:* the critical issue of probe alignment was investigated experimentally; using an optical microscope, probe alignment on the order of $\pm 5 \mu m$ was achieved, (this is unacceptable), greater alignment accuracies would require a novel alignment scheme or the alignment under the visiual inspection of an SEM; (see Appendix A for more information);

2) *probe calibration:* the micromachined cantilever force sensors used in AFM's show large variations in their sensitivity (on the order of 20 - 50% [A2]); a two probe configuration would obviously suffer from this additional source of error; note that experimental methods for determining the cantilever force constant are currently being researched;

3) *development time:* in the opinion of Marco Tortenese (coinventor of the 'Piezolever', a type of AFM force sensor [A22]) and manager of AFM probes at Park Scientific Instruments [A23]), development of a two probe system would involve considerable resources; in addition, if commercial AFM components were used, this would surely involve close cooperation with the AFM manufacturer;

4) *hardware requirements:* as mentioned earlier, hardware costs could be prohibitively high because of the need for two scanner units, cameras, and / or electronics. More importantly, it was realized that the AFM would be used for purposes other than two-sided sample profilometry, therefore use of the two probe configuration may require a seperate probe unit for general measurements.

Thus it was concluded that the most reasonable configuration to implement was the 'flip' sample concept. The use of a single conventional AFM unit significantly shortens the time and resources required to develop the profilometer, in addition, only one scanner / probe needs to be calibrated. On the other hand, a high precision sample positioner device needs to be developed.

2.5 Measurement Probe Hardware Description

In order to minimize development time and maximize reliability / ease-of-use, it was decided that a commercially available AFM should be used if at all possible. A detailed survey of AFM's from leading vendors Digital Instruments [A24], Park Scientific Instruments, and Topometrix [A7] revealed that the profilometer requirements were best met by the Park Scientific Instruments 'XL', see Figure 2.7. In addition to satisfying all the AFM profiling specifications, the XL has the following noteworthy features:

1) *closed-loop / independent sensor monitoring* of piezoelectric scanner motion minimizes positioning errors under all scan conditions;

2) *'user-friendly' operations* including pre-aligned probe / scanner head, automated operation thru a Windows interfaced computer program (that includes post-processing), high magnification optics for sample feature / probe alignment, and turnkey operation with built-in customized / preconfigurated electronics;

17

3) *design for industrial environments* with integral vibration / acoustic shielding and large sample positioning stage;

Note that at the time this is being written, an improved version of the XL, called the 'M5', will be introduced to the market shortly; this instrument features multi-mode imaging capabilites (i.e. contact / tapping mode AFM, non-contact mode AFM, LFM and MFM) and improved enviromental noise shielding. Detailed descriptions of the commercial AFM survey and the XL itself are given in a seperate report [A1].

2.6 Summary

Contact mode atomic force microscopy (AFM) was found to be the most ideal technique for profilometry. Then it was determined that the optimal (in terms of technical performance, time / resources available, and reliability / ease of use) profilometer hardware configuration should consist of a commercial AFM (the Park Scientific Instruments XL) and a custom sample positioning system-- a sample 'flip' stage plus X-Y positioning stages.

3 Sample Positioner Design Concept

3.1 Introduction

The design concept for the sample positioning subsystem is developed in this chapter. First, the necessary engineering specifications are drawn up, this is then followed by an overview of precision positioning methods. From this overview, potential design concepts of the sample positioner are synthesized and subsequently evaluated to arrive at a suitable solution.

3.2 Sample Positioning Requirements

The engineering specifications for the sample positioner consist of the range of motion (both angular and linear), and the required positioning resolution and precision. These specifications were developed with respect to the sample positioning and AFM scanner coordinate systems shown in Figure 3.1. The coordinate system origin lies on the centerline of rotation, with the 'X' axis parallel to the reference mounting surface (i.e. the granite table) and pointing into the sample, the 'Y' axis on the centerline of rotation (i.e. along the sample edge), and the 'Z' axis normal to the granite surface. Note that when the sample is flipped, the coordinate system does not change orientation.

The angular positioning range for the sample is determined by the minimum sample tilt angle α (defined positive with the sample is tilted downwards). Mechanical clearance between the scanner and the sample body dictates a minimum tilt angle of about 8°; thus the sample must be 'flipped' through a maximum angle of 164°. For a D profiling range of 20 μm, the maximum allowable tilt angle of the long range scanner (100 μm x 100 μm x 8 μm (vertical Z range)) is 24° (see Figure 3.2); for the short range scanner (10 μm x 10 μm x 2.5 μm) the maximum allowable tilt angle is 15 ° (for a max. D profiling range of 10 μm, of course).

Profiling the sample vertically (i.e. α = 90°) was also considered, but it was realized that doing so would result in significant measurement error due to AFM probe / sample tip shape convolution. This can be understood by modelling the probe and sample tip as circular arcs of radii R_1 and R_2; from Figure 3.3 it can be seen that the resultant profile image would have an effective radius of $R_1 + R_2$ [B1]. The convolution problem is examined in greater detail in a seperate thesis [A1].

For the X / Y positioning range, this is dictated by three requirements: the sample profiling range, the general sample profiling range, and ease-of-loading sample requirements. For the two-sided sample profiling, a conservative estimate for the required X profiling range is $\approx$ 280 μm, in the Y direction, the edge length which can be profiled is limited to about 0.75". For general sample profiling, a minimum X/Y positioning range of about 2" x 2" is desirable. Finally, for ease-of-loading, one of the axis should move out about 6" from under the scanner head towards the user (this is due to the particular dimensions of the XL).

The resolution and precision with which the sample must be positioned was determined by the original profiling specifications and the profiling procedure. Of the six positioning errors, three translational (δ_x, δ_y, δ_z) and three rotational (ε_x, ε_y, ε_z), the most important errors are ε_y, (the sample tilt angle error) and δ_y (the sample edge shift error due to the flipping operation), followed by ε_x(the sample yaw angle error) and ε_z (the sample roll angle error). The planar AFM probe-to-sample tip alignment error (δ_x)
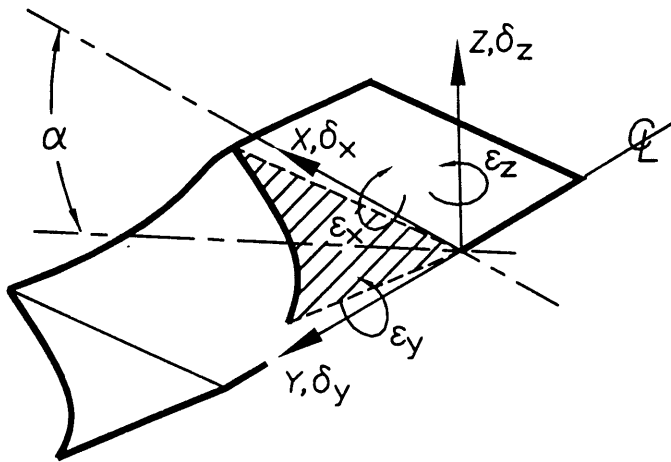
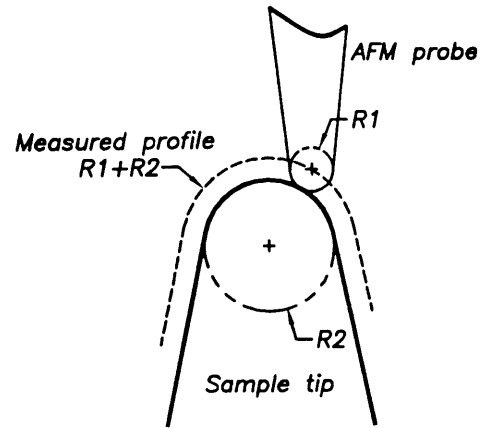*Figure 3.1: AFM / sample positioner / sample coordinate system*

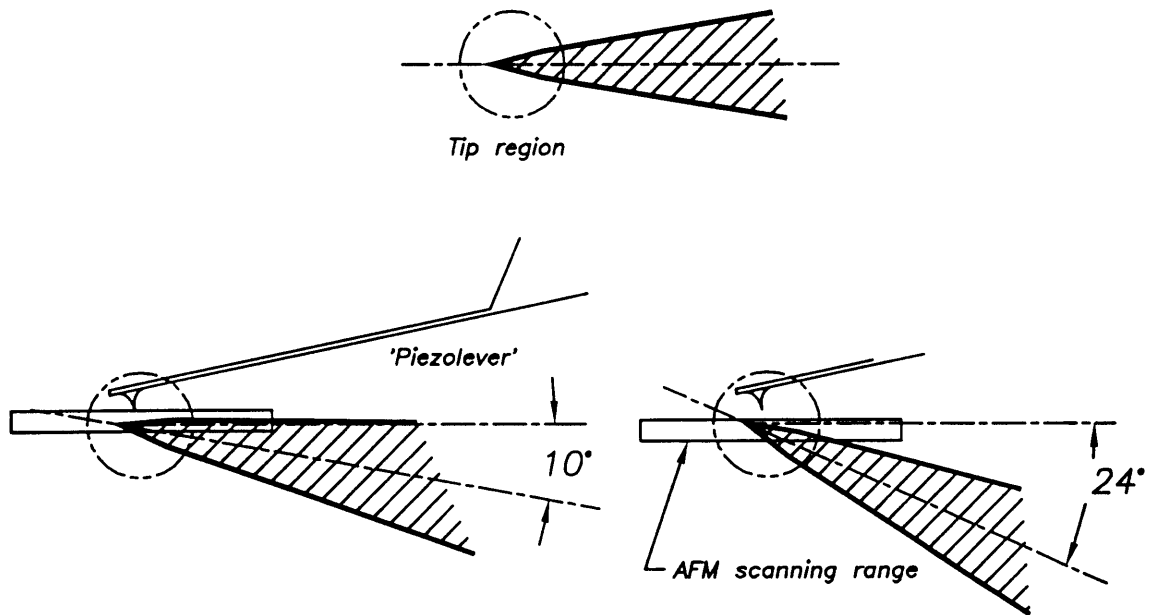*Figure 3.3 Profiling the sample vertically*

Figure 3.2: AFM scanning range and sample geometry

is not as critical because coarse alignment is always done visually before measurements are taken; (fine alignment is accomplished with the AFM). Finally, δ_z is not important because measurements are made with respect to a relative reference (the located sample tip). Target design values for the positioning errors are given in Table 3.1 below. *For the initial design development phase (described in this chapter), emphysis will be placed on meeting the target positioning error specifications of ε_y and δ_y (because these are the most critical errors).*

Error Name	Target Design Positioning Error	Explanation / Numerical Calculation of Target Design Positioning Error
Sample tilt angle error (ε_y)	$\approx \pm 20$ *arc-sec.*	Assuming that the sample is tilted flat with the sample tip on the centerline of rotation, an angular error of ± 20 *arc-sec.* would produce an ET2 error of ≈ 2 *nm* at D = 20 μm, this 2 *nm* value was allocated from the maximum specified ET2 of ± 5 *nm* (the rest of the error is allocated to the AFM).
Sample edge shift error (δ_y)	± 1 μm	This is the shift in position along the sample edge due to the flip operation. The target values were deemed reasonable given the performance of high precision bearings (i.e. axial runout); in addition, the effect of this error is mitigated by the use of averaging in the recorded measurement.
Sample yaw angle error (ε_z)	$\approx \pm 40$ *arc-sec.*	Using a similar procedure as with ε_y , an ED2 error of ± 4 *nm* from ε_z was considered reasonable; ε_z is not as important an error as ε_y because when tilted at the proper angle the sample is essentially flat (no large variations in the more critical dimension T). One assumption made here is that the sample edge alignment stops are sufficiently large so the average sample edge is aligned with the centerline of rotation.
Sample roll angle error(ε_x)	$\approx \pm 40$ *arc-sec.*	Calculation similar to above, resulting in an ET2 error of ± 4 *nm*; the effect of this error is mitigated by the use of averaging in the recorded measurement.
planar AFM probe-to-sample tip alignment error (δ_x)	± 2 μm (initial AFM probe-to sample tip alignment) ± 10 μm (flip offset)	There are actually two errors here, one for the initial alignment before profiling (a value of ± 2 μm was selected, this is described below), and another due to the flip operation (a value of about ± 10 μm is reasonable enough so that the operator does not have to move the sample excessively to align).
vertical AFM probe-to-sample tip alignment error (δ_z)	Not applicable	Measurements are made with respect to a relative reference (the located sample tip), so this is not an important error.

Table 3.1 Target design values for the positioning errors

The values listed in Table 3.1 are the resultant errors; to actually determine the source of errors-- the errors due to a specific positioning device, a homogeneous transformation matrix (HTM) based error calculation procedure was developed, see chapter 4. In general, the most important geometric source of error is the linear amplification of an angular error, also known as a sine error or the Abbé principle. For a small angular error ε, the formula for this is simply:

$$\delta = l\,\varepsilon \qquad\qquad (3.1)$$

where δ is the linear error and l is the amplification arm measured from the point of interest to the source of the error (typically at the bearings). The Abbé principle can be

put to good effect in angular positioning by maximizing l, thereby minimizing the angular error (or thought another way, maximizing the sensitivity) from a positioning / sensing element placed at l.

The required positioning resolution is dictated by the accuracy / precision desired, (ideally it should be about two to ten times smaller than the accuracy desired), so referring to Table 3.1 again, the desired 'flip' stage resolution is $\approx 2 - 10$ *arc.-sec.* (based on ε_y), for the y stage about 0.1 - 0.5 μm (based on δ_y), and finally for the X stage about 0.5 - 1 μm (based on δ_x). Note that a unique requirement for the X axis is the initial alignment of the AFM probe tip with the sample tip; experimental investigations had shown that the probe tip can be as much as 10 μm off the edge without seriously damaging the probe tip; to be on the safe side, an initial AFM probe-to-sample tip alignment goal of 1 - 3 μm in the X direction was sought.

In addition to meeting all of the specifications above, the dimensions of the sample positioner was bounded by the following space constraints:

1) the sample positioning system can have a maximum vertical heigh of 4", with the AFM head positionable from $\approx 2.63"$ to 4" above the reference granite surface;
2) when the AFM probe is in contact with the sample, vertical clearance between the AFM Z stage assembly and the probe contact point (i.e. 'flip' stage axis of rotation) is about 0.38" for about a 4" length on the axis of rotation (centered about the contact point); beyond that there is a 0.75" vertical clearance on one side of the Z stage.

Extensive modification of the XL was not allowed because this would have introduced lengthy delays into the project.

3.3 Precision Positioning Methodologies

Precision positioning for dimensional metrology can be achieved via one (or combination) of three general schemes: electromechanical positioning, mechanical positioning, and error-mapping. The advantages and disadvantages of each scheme should be kept in mind when specific positioning devices and design concepts are discussed in subsequent sections.

With electromechanical positioning, high precision / sensitive actuator(s) and sensor(s) are used to servo in onto the desired position (i.e. closed-loop control). Advantages include high positioning flexibility and reduced or no wear problems. The principal disadvantage of this technique are possible instablity and stiffness problems due to an untuned controller and/or system nonlinearities and noise.

In precision positioning by mechanical design, positioning accuracy is achieved via. mechanical means (e.g. jaw type couplings, kinematic couplings, pins, etc.). Advantages include simplicity in controls and operation, and potentially higher mechanical stability and stiffness than with other methods. Disadvantages include limited positioning flexibility and possible wear problems.

Lastly, in precision positioning by error-mapping, positioning accuracy is improved via. online or offline (i.e. post-processing) compensation of highly repeatible errors. A related offline compensation technique is to have a high precision sensor monitor the position of an open-loop actuator. Use of offline compensation for

dimensional metrology assumes that positioning accuracies are sufficient so as not to affect the measurement process. The principal advantage of this method is low cost implementation thru software. Error-mapping however can only be used to *enhance* positioning accuracy.

3.4 'Flip' Stage Design Concepts

Design concepts for the 'flip' stage are developed in this section. The use of existing off-the-shelf rotary positioning devices was looked into first, but it was found that these devices did not meet the profiling specifications or space constraints, hence the need for custom hardware.

Off-the-shelf rotary positioning devices can be divided into three goups, rotary tables, gimbal mounts, and short range positioners (i.e. tilt stands). Rotary tables are 360° range angular positioning devices which utilize a wide variety of positioning technologies (e.g. motorized gear drive, direct-drive, jaw-coupling). They were found to be unsuitable for use as a sample 'flip' stage in terms of the following:

1) *engineering specifications*: a 1" to 2" base diameter would be the ideal size, motorized rotary stages however usually have base diameters of 3" and larger; a small rotary stage [B2] (the 'world's smallest') of 1" base diameter was found, but this did not the meet specifications (e.g. angular positioning accuracies of ± 37 *arc-sec.* > target accuracy of ± 20 *arc-sec.*[1])

2) *cantilever effect*: size constraints imposed by the AFM and the sample specimen meant that the sample must be mounted on a significant cantilever (i.e. the structure that supports the sample, approx. 2" long, is greater than or equal to the rotary stage base diameter of 1 to 2"); this was highly undesirable because of the potential for large scale mechanical vibrations at the free end.

Short range angular positioners, including gonimeters (typical range ± 45°) and tilt stands (typical range ± 2.5°) could not be used because of the 164° angular range of motion required. A noteworthy feature of gonimeters (they look like cradles) is that they have a virtual axis of rotation; this means that if the sample could be referenced against its back edge, then the entire length of the sample can be profiled.

Gimbal type mounts are structually different from rotary tables in that the payload is supported at both ends by bearings. Off-the-shelf gimbal mounts are typically used for optical components and feature 360° pitch and yaw movements; these were too bulky in size to adopt for usage.

3.4.1 'Flip' Stage Design Concept #1: Precision Gimbal Mount

In this design concept, the sample is servo positioned with a precision gimbal mount configuration 'flip' stage (see Figure 3.4) The basic components of the gimbal type mount-- actuator / drivetrain combination, feedback position sensors, and end-support bearings, were each examined in detail. For the highest precision, a direct drive torque motor with the rotary encoder mounted directly on the output shaft should be used, along with seperate precision sensors for rotary position homing and axial runout.

---

[1] On this rotary stage the positioning encoder is NOT located on the output shaft but on the motor end instead; since specifications were measured using the positioning encoder, actual positioning accuracies are likely to be worse.

As for the end support bearings, space limitations dictates the use of deep groove radial contact bearings-- these bearings however need to be carefully preloaded in order to minimize friction (while still providing adequate stiffness), axial runout, and wobble.

For the actuator and drivetrain, a low acceleration requirement and small sample holder inertia (based upon previous designs) meant that a corresponding low maximum output torque and speed is required(2.64 *oz-in.* [18.6 *mN-m*] and 15 *rpm*, respectively). The calculations are straightforward and is given in Appendix B. In addition to these requirements, zero speed positioning stability (i.e. minimal jitter) was essential because of the high measurement resolution sought (i.e. ET2 < ± 5 *nm*). Actuator / drivetrain combinations investigated were: 1) conventional microstepping motor with zero backlash timing belt / metal band transmission, 2) DC servo motor with conventional gearing, 3) direct drive torque motor, and 4) direct drive ultrasonic motor. From this survey it was found that the direct drive torque motor offered the highest positioning precision.

A conventional microstepping motor features zero speed stability and easy control; however they generate considerable heat and their noncumulative positioning accuracy, even in microstepping mode, is typically ± 3 - 5% of the full step angle [B3] (thus for a high resolution 5-phase, 0.72° full step angle stepping motor, the best unloaded motor positioning accuracy is 78 *arc-sec.*)[2].

A DC servo motor with a gear speed reducer (a timing belt provides inadequate speed reduction) is likely to have low positioning accuracy / repeatibility due to friction, wobble, and backlash in the gearing.

With a direct drive torque motor[3] no gearing is used, so in theory the positioning resolution is limited only by the rotary encoder resolution; (note that this is true for brushless motors only, for brushed motors, there is a limit due to the brush contact area). Unlike a gear reducer where rotational stiffness is achieved via. mechanical means (i.e. gears), a direct drive torque motor system relies on the servo to provide the rotational stiffness.

Lastly, the use of a direct drive ultrasonic motor was considered. In these motors, rotary motion is generated through the elastic wave movement (i.e. electrically induced modal vibration) of a ring shaped piezoelectric element, see Figure 3.5; note that other piezo configurations are possible, but the ring shape is most common. Ultrasonic motors offer some unique advantages, such as high torque at low speeds (making direct drive possible), 'locked' position even with no power to the motor (due to the frictional preload force between the rotor and stator), and the potential for precision positioning (due to the fine control possible with the piezoelement) [B4]. Since these motors rely on friction for movement, this means that the minimal incremental motion is limited by the surface properties of the rotor / stator interface and also that motor life is somewhat limited due to wear. To the best of the author's knowledge, currently available rotary ultrasonic motors (e.g. the 30 *mm* O.D. Shinsei USR-30 with a 49 *mN-m* rated torque and 2000 *h* life) have not been used for precision positioning. Note however that high precision (5 *nm* resolution) linear motors are commercially available[B30].

---

[2]For repeatibility, [B3] states that this is typically ± 5 *arc-sec.* (motor unloaded, one revolution returning to start point from same direction); however, when the total system is considered (with drivetrain, bearing, load), the positioning repeatibility is likely to be worse.

[3]Small direct drive torque motors can be obtained from Inland motors (e.g. 6.6 *oz-in.* peak torque 1.125" O.D. miniature torque motors are available), there are other vendors as well.
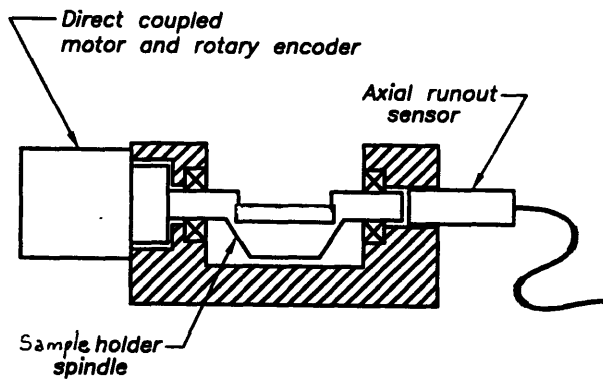
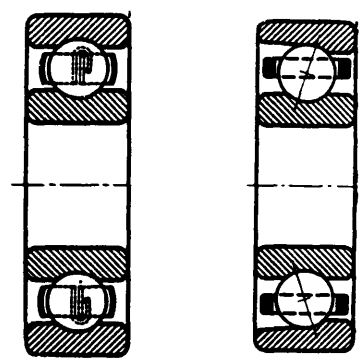Figure 3.4: Flip stage design concept #1: precision gimbal mount

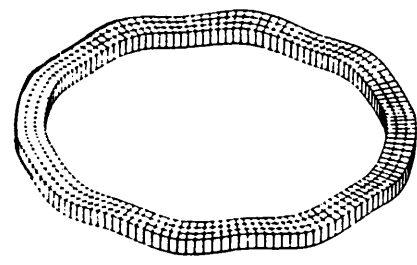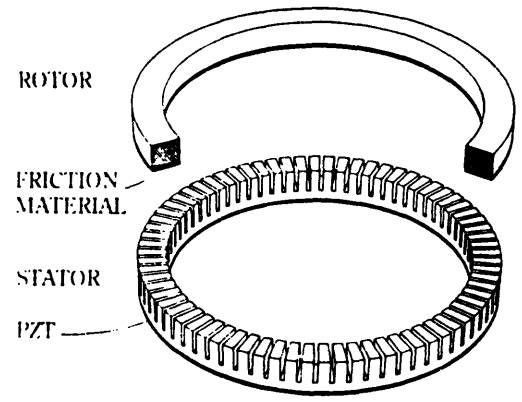Figure 3.6: Deep groove radial (left) and angular contact bearings (right); (from [B9])
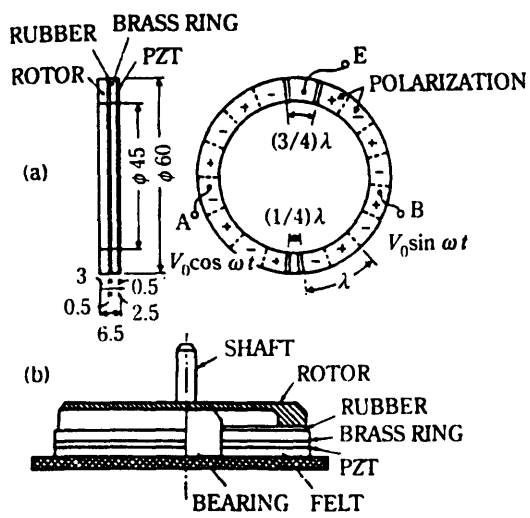
Figure 3.5: Ultrasonic rotary motor; components of motor (left), 9th bending mode of piezo ring (lower), isometric view of rotor / stator (right), from [B4]

25

Another major component of the precision gimbal mount stage are the rotary and linear position feedback sensors. For the rotary sensor, space constraints limits the available choices to incremental rotary encoders[4], with applicable models listed below. (Note that the performance of the optical encoders are barely adequate for this application).

	Resolution	Accuracy	Size	Cost
Gurley Precision Inst. 8311 incremental optical encoder [B25]	9 *arc-sec.* (80X electronic interpolation)	18 *arc-sec.* (incremental) 50 *arc-sec.* (absolute)	1.07" diameter 1.80" length	$1568 (sensor and electronics)
Gurley Precision Inst. 8314 incremental optical encoder [B25]	6.4 *arc-sec.* (80X electronic interpolation)	15 *arc-sec.* (incremental) 40 *arc-sec.* (absolute)	1.40" diameter 1.85" length	similar to above
Canon K-1 laser rotary encoder [B26]	1 *arc-sec.* (16X electronic interpolation)	5 *arc-sec.*	1.40" diameter 1.90" length	$4000 (sensor and electronics)

Table 3.2   Applicable precision incremental encoders

In using these incremental rotary encoders, two additional sources of errors need to be considered-- a limit switch referencing error and a coupling-to-output shaft misalignment error. Typical limit switches can have hysteresis (to minimize false triggering) of 10% - 20% of their maximum detection distance [B5], so for a short range 0.6 *mm* range proximity sensor placed 1" from the center of rotation, this means a repeatiblity of 486 *arc-sec.*! Greater repeatibility requires the use of a seperate precision sensor (e.g. dimensional gage LVDT). Another source of error comes from the coupling misalignment between the encoder and the output shaft (i.e. for the encoders above a seperate coupling is required, high precision "hollow" shaft encoders were found to be too bulky); equations for this type of error are given in [B6].

For linear displacement sensors (used mainly to measure the sample edge shift error δ_y), several choices are available:

	Range	Resolution	Accuracy	Size	Cost
Kaman SMu-9100 inductive sensor [B27]	25 *μm*	< 2.5 *nm*	250 *nm* nonlinearity	0.19" diameter	$1595 (sensor and electronics)
Mechanical Technologies ASP-1-ILA capacitive sensor [B28]	25 *μm*	0.4 *nm* (16 bit A/D conversion)	±0.1% full range nonlinearity (25 nm)	0.093" diameter	$3000 (sensor and electronics)
Lucas 004 XS-B miniature LVDT [B29]	250 *μm*	3.8 *nm* (16 bit A/D conversion)	±0.3% full range nonlinearity (750 nm)	0.03" diameter core	$627 (sensor and electronics)

Table 3.3   Applicable sample edge shift sensors

---

[4] The well known high precision rotary transducer "Inductosyn" was too bulky; (the smallest diameter sensor is 3" in diameter, with a measurement accuracies of ± 4.5 *arc-sec.*).

Note that these sensors measure δ_y indirectly by monitoring the spindle shaft axial runout. Error correction would consist of offseting the AFM scanner by the amount δ_y in the Y direction (this is assuming that the error is within the range of the scanner). Direct AFM measurement of δ_y is possible for small sized scans, this will be discussed later.

Finally for the end support bearings, several different types of bearings were investigated. Ultra high precision air bearings (e.g. axial and radial runout < 0.05 μm for a 4″ diameter bearing [B6]) could not be used because of their bulky size, and the open air discharge to the environment would be a major source of measurement noise. Other ultraprecision bearings have similar problems as well-- magnetic bearings (bulky, large heat generation [B6]) and hydrostatic bearings (bulky, messy oil lubrication). Rotary flexural bearings [B7] possess high mechanical stiffness (because of their one piece construction) and positioning repeatiblity (solid deformation), but range is limited to 60° (± 30°). Thus the only option is conventional mechanical bearings; space constraint dictates a maximum bearing outer diameter of about 16 mm (0.63 $in.$), and in this size range deep groove radial contact bearings("instrument bearings") are the most common, see Figure 3.6. Radial error motions on the order of about 5 - 10 μm can be expected [B8, B9], with axial runout being larger because the grooves do not provide significant axial support[B6]. It is possible to use 16 mm O.D. angular contact bearings [B9] (in pairs to provide bidirectional support see Figure 3.6). Ideally they provide both radially and axially constraint, so error motions (both radially and axially) can be on the order of 1/4 - 1 μm [B6]. Unfortunately, bearings of this size are not commonly used and must be custom made by the ball bearing manufacturer.

In terms of an overall system performance using the selected design elements (i.e. direct drive motor with rotary, linear, and limit switch sensor in conjuction with deep groove radial ball bearings) the following should be kept in mind:

1) *servo stability (jitter)*: for a low speed application such as this[5], sources of instability are either mechanical (friction, which can cause limit cycling[6][B6]), electrical (i.e. drift in electronics, electrical noise in encoder, motor,amplifiers) or control (untuned gains). Jitter is typically minimized by specifying a control deadband; for the torque motor this has to be carefully chosen because the motor provides no holding torque once inside the control deadband (i.e. position is maintained by friction only).

2) *stiffness vs. precision tradeoff for bearings*: because bearings are mechanically overconstrained (i.e. nonkinematic, see the next section for an explanation), they are extremely sensitive to mounting conditions and preloads; for example, press-fitting a bearing in too small a hole or applying a larger than necessary preload can dramatically increase the friction in the bearing, thereby reducing the angular positioning repeatibility (from arc-seconds to arc-minutes) and altering the dynamic characteristics (e.g. settling time). For overconstrainted designs there is always a tradeoff between stiffness (maximize friction) vs. precision (minimize friction).

---

[5]High speed applications must also contend with other effects, such as dynamical excitation of the motor, coupling, etc.

[6]Limit cycling can occur when the feedback encoder has a resolution greater than the smallest incremental motion, without a large enough control deadband, the system will continually oscillate about the desired position. Note that there are causes of limit cycling as well.

3.4.2 'Flip' Stage Design Concept #2: Kinematic Mechanical Fixture

In this concept, the sample is mounted on a movable fixture with three balls as locating elements. Referring to Figure 3.7, the fixture is mechanically clamped against and uniquely located by a tetrahedron, 'V' and flat on a reference structure; (actually there are two symmetrically located flats, thus allowing both sides of the sample to be profiled). This type of fixture is known as a Kelvin clamp or kinematic coupling. A kinematic coupling provides good mechanical stability and high positioning repeatibility; the reasons for this are explained below.

In mechanical positioning devices, the positioning elements (i.e. locators / bearings) are either of a kinematic or an elastic design (or a combination of the two). For a purely kinematic design, two relative motion parts are constrained at exactly 6 - n independent points, where n is the number of degrees of motion of the device. This is the complete opposite of an elastic design, where two relative motion parts are elastically deformed in order to conform to one another. It is easier to achieve high positioning repeatibility with kinematic designs because mating parts contact at finite (and often exactly the same) points, so easy-to-manufacture, high precision balls can typically be used as locating elements. In elastic designs, mating parts contact at infinite and often different points, so a high degree of workmanship is required to produce the required matching forms and good surface finishes. Properly built kinematic designs also possess high stability because the mating parts contact at the minimum number of points required for stability; (this is like comparing a (kinematic) three-legged stool to an (elastic) four-legged one). A disadvantage of kinematic designs however is that they have a lower stiffness than elastic designs because of their smaller contact areas; this is generally not a major issue in instrument design because of the small forces involved.

In terms of actual performance, kinematic couplings have long been known to provide highly repeatible fixturing [B10]. In [B11], a Kelvin clamp mounted sample with an 'X' mark surface feature was measured using a conventional stylus profilometer; relocation repeatiblity of the measured 'X' was found to be 1.8 ± 0.3 μm. In [B12], linear and angular positioning repeatibility of a 356 mm diameter kinematic coupling was found to be ≈ 0.3 μm and 0.4 arc-sec. respectively after an initial 50 cycle wear-in period.

Another type of coupling capable of high positioning repeatibility is the serrated jaw type (also known as Hirth or curvic) coupling used in some indexed rotary tables and machine tools, see Figure 3.8. Depending on the size of the coupling, the number of indexable angles ranges from 32 (11.25°) up to 1440 (0.25°). For large rotary tables, the indexing accuracy can be on the order of ± 0.25 arc-sec. and even as high as ± 0.1 arc-sec. [B13]. This high degree of accuracy comes from the elastic averaging of a large number of precisely machined and finely lapped teeths. A unique property of the serrated jaw coupling is that positioning repeatibility can actually *increase* with greater usage-- a large number of random indexings creates a self-lapping process whereby teeth form errors are corrected[B13].

The serrated jaw concept was investigated experimentally by measuring the positioning repeatibility of a reference surface attached to the movable half of a 0.75" dia., 303 stainless steel serrated jaw coupling[7]. The data for the positioning repeatibility is shown in Figure 3.9; after an initial wear-in period, the coupling displayed a steady position drift-- it was suspected that this was caused by uneven wear due to one side of

---

[7]The coupling was actually designed to couple motion transmission shafts; they were obtained from PIC Design, 86 Benson Road, P.O. Box 1004, Middlebury, CT 06762, Tel. (800) 243-6125, Fax. (203) 758-8271.
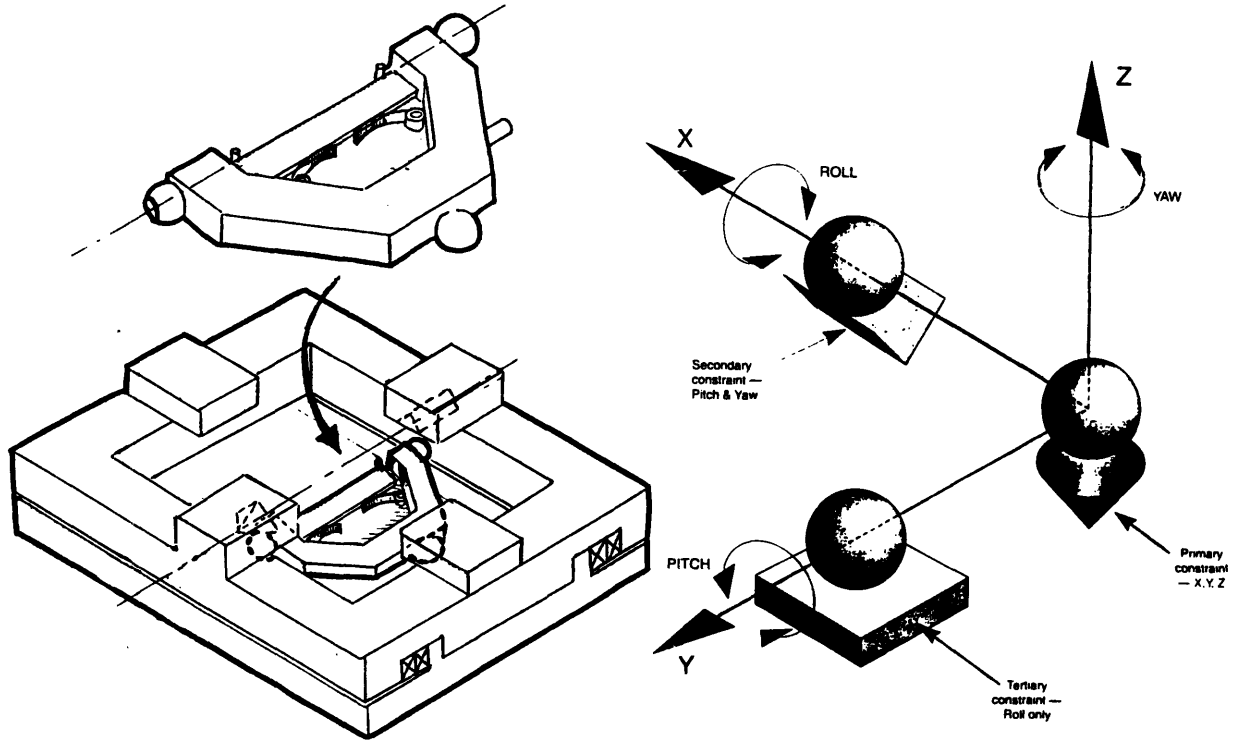
Figure 3.7: Flip stage design concept #2: kinematic mechanical fixture; initial design sketch (left), underlying kinematic concept (right, from [B19]).
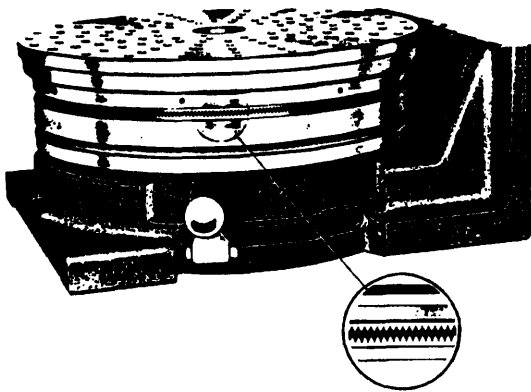

Figure 3.8: Serrated jaw coupling rotary table (from [B13])
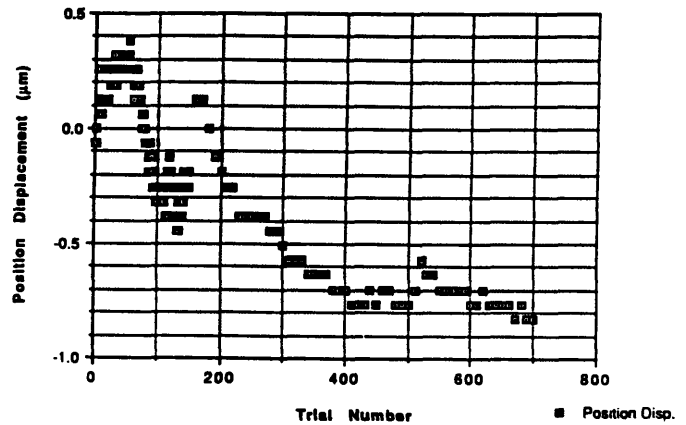
Figure 3.9: Serrated jaw coupling repeatibility experiment results.

the coupling being engaged before the other side. Despite the potential for good positioning repeatibility, the serrated jaw concept was eventually dropped for the following reasons:

1) *high manufacturing costs*: the required manufacture specifications (e.g. machining precision, processes required) and wear-in period / procedures for a suitable serrated jaw coupling must be determined through extensive (and costly) prototyping-- this would be a significant research undertaking in itself; in contrast, kinematic couplings are much simplier in structure, their properties are better known, and off-the-shelf components are readily available;

2) *uneven wear / dirt contamination*: these two items could significantly affect the positioning repeatibility-- uneven wear arising from indexing to a few selected angles only, in addition, dirt contamination would also have an effect due to the greater surface contact area of the serrated jaw couplings (some sort of built in air blower might be required);

3.4.3 'Flip' Stage Design Concept #3: Coarse / Fine Positioner

The final 'flip' stage design concept consist of a coarse / fine positioner arrangement. Coarse positioning would be accomplished with a gimbal type stage (perhaps a stepping motor / timing belt drivetrain for zero speed stability), and fine positioning would be done with a high resolution actuator (e.g. fine screw actuator [B14] or piezostack [B15]) mounted on a tilt platform, see Figure 3.10. Assuming the fine actuator has an Abbé offset of 2" from the center of rotation, use of a fine screw actuator (with 0.1 μm resolution, much higher for the piezostack) can result in a tilt angle positioning resolution of 0.4 *arc-sec.*. Measurement of the sample tilt angle would require a custom designed sensor (probably optical in nature), see Figure 3.10.

Another way of achieving coarse / fine positioning is to use two concentric rotary stages-- the inner stage providing the coarse positioning, and the outer stage (referenced against a fixed frame) providing the fine positioning (via a tangential drive) once it is locked onto the inner stage. This configuration was not an option due to space constraints.

Finally, it should be noted that an ultrasonic motor technology coarse / fine positioner under development has been able to achieve a positioning resolution of 1 *arc-sec.* over a 360° range [B16]. Coarse positioning is done with a conventional wave action ultrasonic rotary motor (refer back to section 3.4.1), while fine positioning is accomplished with torsion action elements. Again, development of this design into a robust solution would require considerable time and resources.

3.5 X-Y Stage Design Concepts

For the linear X-Y stages, two possibilities were considered, commercially available stages-- conventional linear mechanical stages and two-dimensional linear motors (i.e. Sawyer motor), and customized AFM stages as used on some commercial AFM's.

3.5.1 X-Y Stage Design Concept #1: Commercial X-Y Stage
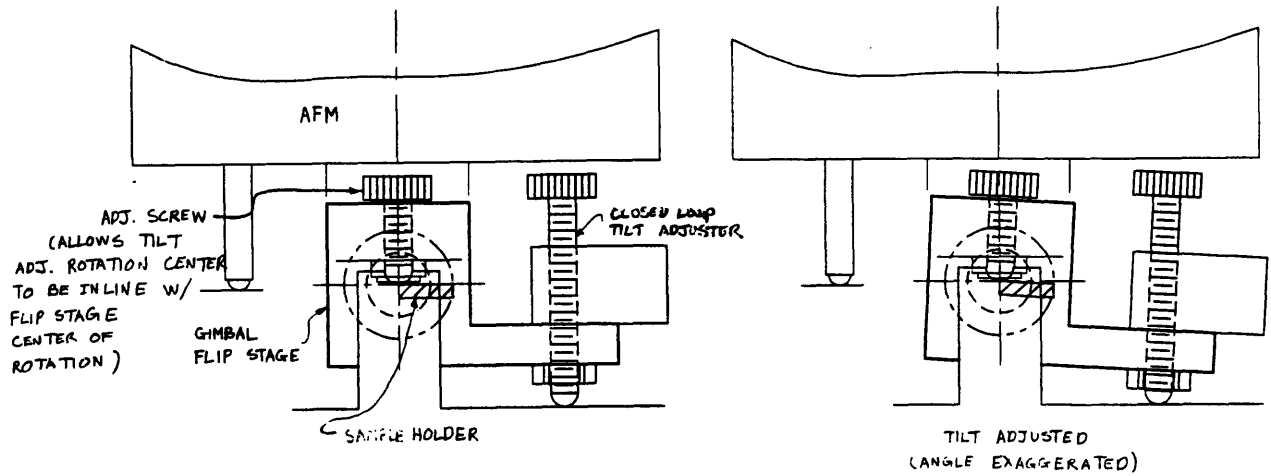
Figure 3.10: Flip stage design concept #3: coarse / fine positioner (initial sketch)

Angular error due to stage flatness error
(based upon flatness calibration curve for Aerotech ATS100-200 linear stage)
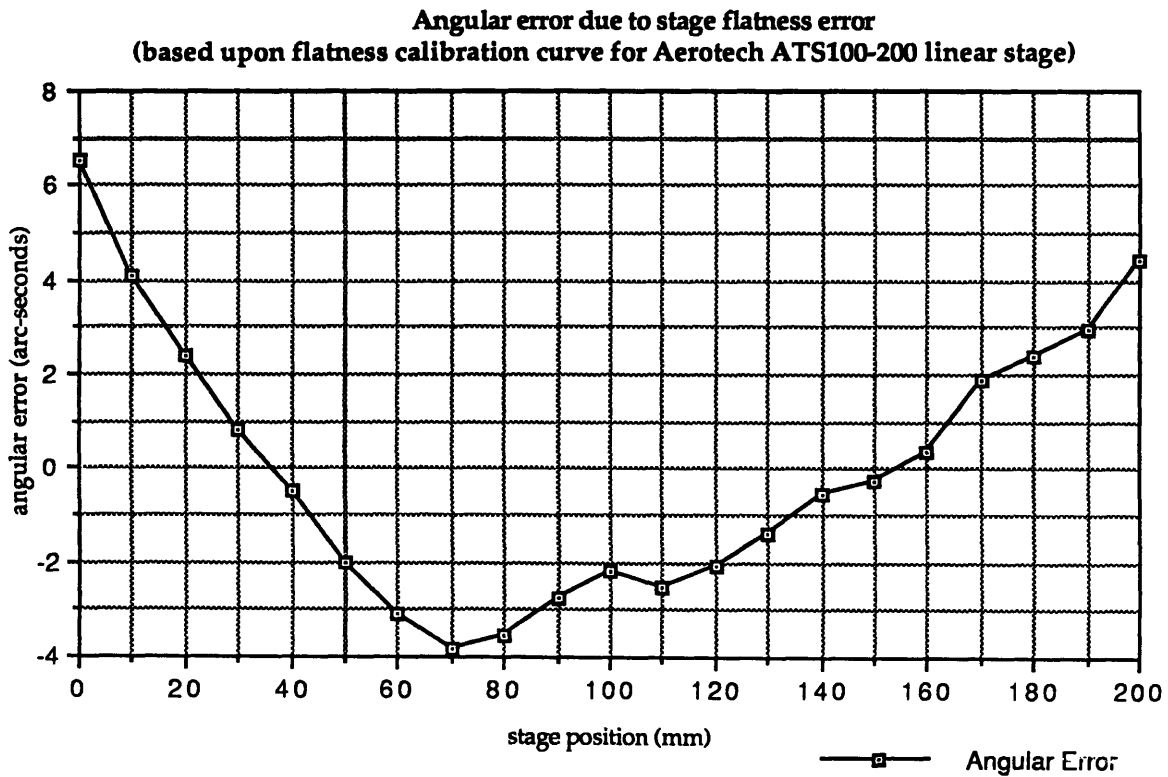
stage position (mm)

Angular Error

Figure 3.11: Typical flatness calibration curve for precision linear mechanical stage
(from [B21])

31

This design concept consist of using high precision conventional linear mechanical stages in a stacked arrangement. These stages were found to provide the necessary stability and positioning accuracy[8]. A two dimensional linear motor based stage was also investigated (it offered some unique advantages) but was not pursued due to technical issues.

In conventional linear mechanical stages, many different types of linear bearings (linear ball bushings, ball bearing slides, crossed roller bearings, recirculating ball linear guides) and drivetrains (leadscrews, ballscrews, timing belt) are available. For precision positioning with the highest possible stiffness, crossed roller bearings and recirculating ball linear guides are used in conjunction with a ballscrew. Advantages of conventional linear mechanical stages include usage of commonly available actuators (i.e. steppers, DC servos) and easy incorporation of various position sensors for closed-loop positioning (rotary / linear encoder, laser interferometer).

During the initial design phase, there was concern as to whether these stages could provide the required mechanical stability (remember, nanometer level noise performance was sought). This concern were dispelled when a literature survey revealed that atomic resolution (i.e. nanometer-to-subnanometer floor noise) was possible with properly designed STM systems which used conventional mechanical staging [B17, B18]. For example, [B18] used a 150 x 150 mm stroke conventional X-Y table[9] and obtained atomic images.

Another source of concern was the angular positioning accuracy of these stages. Specifications for the angular error range from < 5 arc-sec. (high precision) to $\approx$ 25 arc-sec. (typical cross-roller tables) [B19] to as high as 45 arc-sec. [B20]. However, because of the short range of motion required during profiling ($\approx$ 280 μm), the actual angular error is much smaller. For example, a typical flatness error calibration curve for a 200 mm travel precision linear stage is shown in Figure 3.11 [B21]; the maximum angular error is $\approx$ 5.5 arc-sec., and over a 300 μm length can be as small as 0.25 arc-sec.

A two dimensional linear motor based stage [B22] was also investigated. In this design, two one-dimensional linear motors are integrated into one structural frame (the "platten") and made to travel over an orthogonal grid metal base plate. The envisioned advantages of this concept was the ability to utilize several plattens on one base plate and a high positioning stiffness ($\approx$ 300 lbs clamping force!) achieved by turning off the platten's air bearing and letting the built in magnet clamp itself to the base plate. Unfortunately, the available motors were too bulky; in addition, they sometimes rotate unexpectedly during a commanded move, therefore requiring additional closed-loop angular positioning (with a custom angle sensor) for alignment [B23]. Thus this idea was not pursued further.

3.5.2 X-Y Stage Design Concept #2: Customized AFM Stage

With this concept, X-Y positioning would be accomplished by two stacked stages-- a lower stage supported by five air bearings moving on a 'V' and flat, and an upper stage with cross-roller way bearings, see Figure 3.12. During profiling, the air bearings would be turned off so that the lower stage sits solidly on the granite. This idea

---

[8]Higher precision active air bearings (by active I mean the air is left on all the time) were not considered an option because the bearings would be bulky, and significant floor noise could come from fluxuations in the air supply and the acoustic noise of discharging air.

[9]The 'floor' noise is dependent on all mechanical and electrical subsystems of the AFM, not just the X-Y staging, so careful consideration of all possible sources of noise is required.
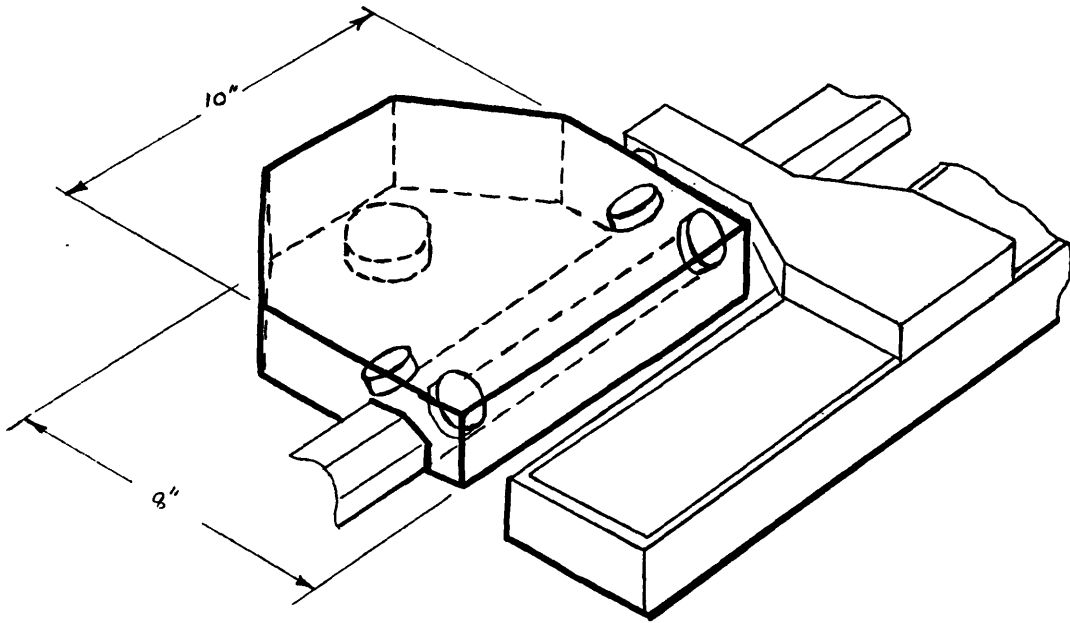
Figure 3.12: X-Y stage design concept #2: customized AFM stage (initial sketch)
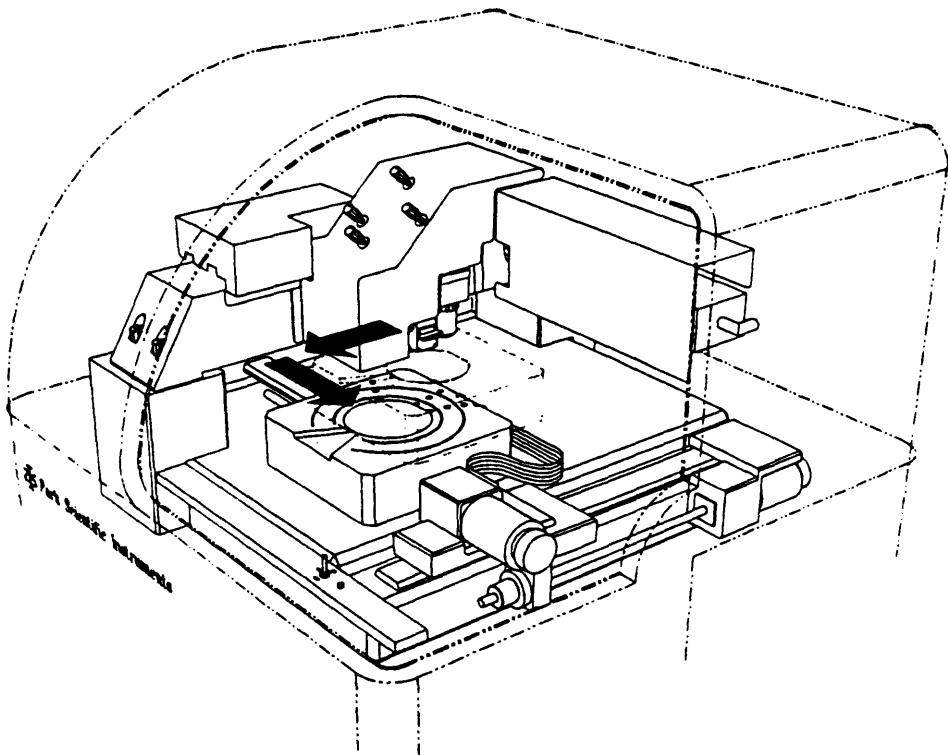

Figure 3.13: Park Scientific Instruments XL X-Y stage (from [A23])

was a spinoff of the original XL X-Y stage, an innovative design consisting of a large metal block (the 'chuck') that floats (via. air bearings) directly over a reference granite surface, see Figure 3.13. When the AFM is in use the air bearings are turned off. The main advantages of this design were: 1) a more rigid structure than conventional staging due to its one piece construction, 2) small angular errors because the chuck is referenced against a very flat granite table, and 3) a large sample area (8" x 8"). The use of this stage was not an option at the time because of the extensive hardware modifications required to accomodate the custom 'flip' stage, the low positioning resolution (5 μm step size), and high costs.

Another possibility considered was to use a novel mechanism that lifts the sample from the X-Y positioning stages and clamps it to the AFM assembly above, thereby resulting in a shorter, more rigid structual loop (possibly with subanstrom floor noise). Such mechanisms are used in the Topometrix Voyager[A6] and the Dektak SXM AFM (developed by IBM) [B24] for semiconductor wafer samples. Again, because of the extensive modifications that would be required, this concept was not pursued further.

3.6 Evaluation and Selection of Design Concept

The design concepts for the 'flip' stage and X-Y stages are examined in this section. Based upon a comparative evaluation, design concepts for the 'flip' stage and X-Y stages were selected; for the critical 'flip' stage, the selected concept was also verified experimentally.

3.6.1 Concept Evaluation and Selection

A comparison of the 'flip' stage concepts is given in Table 3.4 below:

Concept	Positioning Methodology	Advantage(s)	Disadvantage(s)
Precision servo gimbal mount	Electromechanical positioning	+ no or very little wear problems; + any tilt angle possible; + straightforward design;	- need to fine tune and 'tweak' system in order to minimize jitter / stability problems (may require skilled technician); - electromechanical components may be costly;
Kinematic mechanical fixture	Mechanical positioning plus error mapping	+ mechanically simple design; + if properly designed, high inherent mechanical stability (i.e. low measurement noise); + kinematic design means good positioning repeatibility, can use error mapping to increase measurement accuracy; + uses low cost components;	- if possible, design device to wear in noncritical direction or minimize thru proper material selection; - limited tilt angles;
Coarse / fine positioner	Electromechanical positioning	+ offers the most precise positioning possible; + no or very little wear problems; + any tilt angle possible;	- for this particular application, probably need to develop own tilt angle sensor; - coarse / fine positioner can be clumsy to control; - electromechanical components may be costly;

Table 3.4 Comparison of 'flip' stage concepts

Based upon the comparison, it was concluded that the 'best' concept to pursue was the kinematic mechanical fixture, for the following reasons:

1) *performance*: kinematic couplings have a proven record of providing high positioning repeatibility [B10, B11, B12] (sufficient for this application); this, in conjunction with error-mapping can produce highly accurate measurements;

2) *positioning requirements*: as mentioned earlier, accurate profilometry requires that the sample be tilted at not too great an angle ($\approx$ -8° to -24°, profiling the sample vertically results in significant convolution problems), so in this respect the kinematic coupling is ideal because it provides precision end-of-motion range positioning; in addition, it was observed that only one or two tilt angles was needed, this can be easily provided for in the kinematic coupling fixture thru the use of modular angle setting blocks;

3) *operating requirements*: because of its inherent precision (i.e. kinematic design) and simplicity, the kinematic coupling fixture requires less 'tweaking' and adjustments to make it work than other designs (e.g. in the gimbal mount design, careful preloading of the bearings and fine-tuning of the servo drive is required in order to achieve the desired precision). The need for adjustments should be minimized as this may required the services of a (costly) skilled technician.

In all fairness, the advantages and disadvantages of the kinematic mechanical fixture design in comparison to the other concepts was aknowledged and deemed acceptable (i.e. *no design is perfect in all respects*). Note that the precision gimbal mount concept was chosen as a backup solution.

As for the X-Y staging, it was realized that conventional mechanical staging could provided the necessary positioning accuracy and stability (see Section 3.5.1, detailed numerical calculations will be provided in the next chapter), thus this design concept was used. A customized AFM X-Y staging (the second concept) might of provided some advantage in terms of stability, but again the development effort required might very well exceed the time and resources available.

3.6.2 Experimental Verification

To verify that the kinematic coupling concept actually worked (i.e. is able to produce the required accuracy and precision), two experimental prototypes were tested. The first prototype consisted of a movable fixture piece with three ball locators, and a Kelvin clamp base (i.e. three ball X-Y locator, 'V' groove roll / yaw stop, and a pitch angle stop). The movable fixture is clamped against the X-Y locator and 'V' groove with O-rings to define an axis of rotation, and at the same time clamped against the pitch angle stop with a small magnet to establish the sample tilt angle. Note that the general dimensions of this prototype are approximately the same as those of the final device. The angular positioning repeatibility of the fixture was tested by clamping and unclamping the kinematic fixture 1000 times, and measuring the three-dimensional tilt angle of the fixture using a coordinate measuring machine (CMM)-- the Brown and Sharpe MicroVal PFx with a 1.2 *arc-sec.* angle measurement sensitivity for a 0.7" measurement length. By measuring the spatial locations of three distinct points on a reference surface (i.e. gage block attached to the movable fixture), it was possible to compute the plane representing the three dimensional tilt angle. The experimental data is shown in Figure 3.14; from the data it can be seen that the *kinematic coupling was able to*

tilt angle (theta_y) repeatibility

yaw angle (theta_x) repeatibility
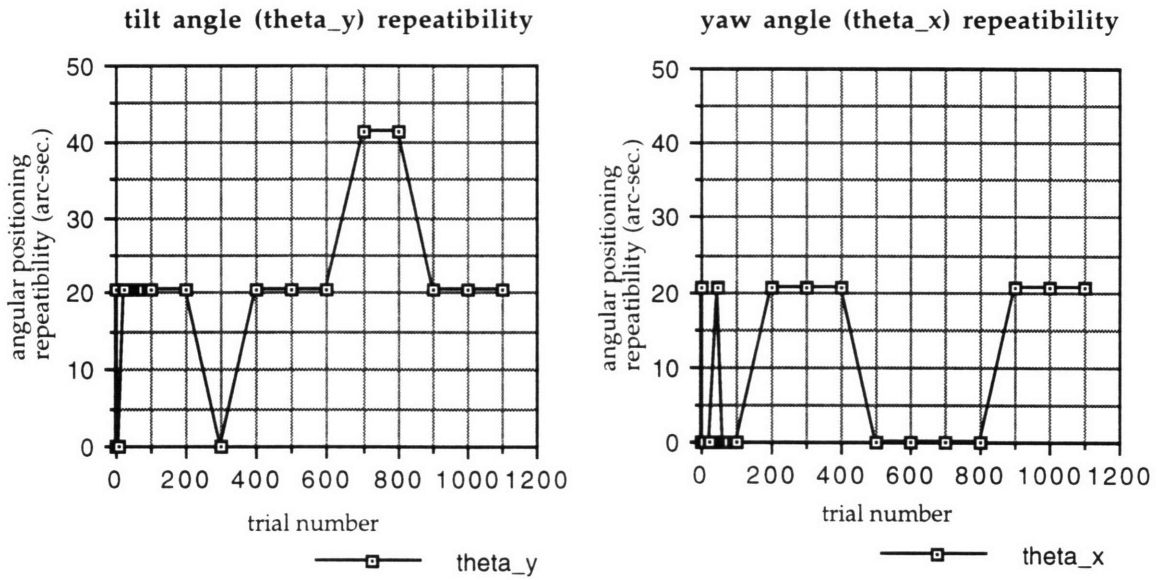
Figure 3.14: Angular positioning repeatibility of test prototype #1
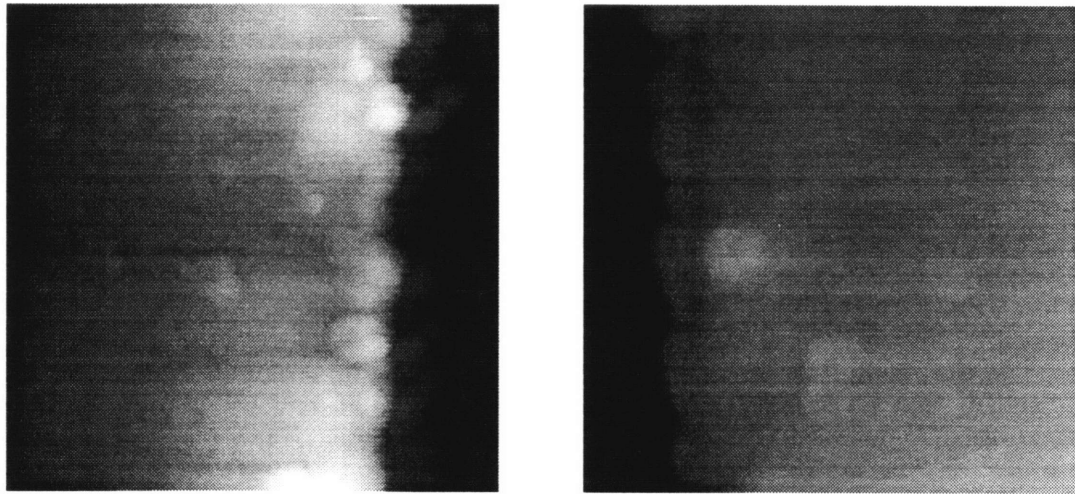
Figure 3.15: Typical sample edge shift error with test prototype #2; notice the matching features

achieve a sample tilt angle repeatibility of 20.63 arc-sec. (the target specification was ± 20 arc-sec.).

A second prototype (actually a temporary manual fixture) was built for the purpose of sample profiling on the AFM. The device has an inverted Kelvin clamp structure-- the three ball locators are attached to the base, while the X-Y, pitch/yaw/roll angle locators are on the sample holder. From the AFM measurements, it was possible to assess the magnitude of the axial shift upon flip sample error (δ_y). This was because for small scans of the sample tip region, clearly discernable edge features can be observed; by comparing the data from both of the sample, see Figure 3.15, the *axial shift error was found to be* $\approx \pm 1$ - *2 μm, (the target specification was* ± *1 μm).*

3.7 Summary

In this chapter, range-of-motion and error specifications for the sample positioning subsystem were first established. Based upon these specifications, design concepts were then generated for the sample 'flip' stage (precision servo gimbal stage, kinematic mechanical fixture, and coarse / fine positioner) and the X-Y stage (off-the-shelf stacked linear stages and customized AFM stage). The kinematic mechanical fixture concept for the sample 'flip' stage was chosen because it was the simplest solution which provided the necessary precision (verified experimentally) and functionality. Likewise, off-the-shelf linear stages were used because they met the required engineering specifications and allowed for rapid design implementation.

4 Sample Positioner Detailed Design

4.1 Introduction

The design of the sample positioner subsystem is described in depth in this chapter. First, the mechanical design is discussed-- topics include operation of the device, component and material selection, as well as positioning errors and mechanical vibration / thermal drift considerations. This is then followed by metrological considerations-- reference datums, measurement procedures, and calibration procedures.

4.2 Mechanical Design

4.2.1 Sample 'Flip' Stage

The 'flip' stage consist of three major subassemblies-- the sample holder, rotation drivetrain, and the tilt angle setting mechanism. To use the 'flip' stage, the sample is first loaded into the sample holder and aligned with the axis of rotation. The axis of rotation is defined by the X-Y-Z and roll / yaw stops on the base and the two locator balls on the sample holder. Since the stops and balls contact at five distinct points, kinematically this means that the sample holder is still free to rotate in the pitch direction.[1] To position at the tilt angle, the sample holder is rotated by a geared stepper motor to the near vicinity of the angle stop (position is sensed by a limit switch), once there, power to the motor is shut off and the holder is magnetically clamped against the angle stop; to unclamp, the motor is reenergized and made to turn in the opposite direction.

The sample holder, rotation drivetrain, and the angle setting stop subassemblies are described in greater detail below. In the sample holder, the sample body is clamped against a reference surface plane by a torsion spring clip-type clamp. The sample edge is aligned to the axis of rotation (the line connecting the centers of two locator balls) by two 0.090" length precision ground hardstops.

The rotation drivetrain consist of the X-Y-Z and roll / yaw stops, and a miniature 246:1 gear ratio stepper motor which is connected inline to the sample holder via a compliant coupling. The X-Y-Z stop (constructed out of three balls), the yaw / roll angle stops (consisting of two rods that form a 'V' two point constraint), and the axis locator balls on the sample holder are made of tungsten carbide (WC). Tungsten carbide was an ideal material for the following reasons:

> 1) *wear resistance*-- because of its extreme hardness[2], tungsten carbide is one of the most wear resistant materials known[C2]. Good wear resistance is required in order to maintain positioning accuracy and repeatibility;

---

[1] The sample holder is not truly kinematic(it is actually what I call 'quasi-kinematic') because it contacts the frame (i.e. the stationary part of the 'flip' stage at more than 6 points, (non-kinematic points of contact include the O-rings clamps and the motor coupling).

[2] On the Brinell hardness scale, diamond (the hardest material known) has a hardness of 10000, tungsten carbide a hardness of 1500, and for hardened stainless steel a hardness of 200 - 500 [C1].

2) *'fret' resistance* -- fretting is a corrosion process that occurs when two surfaces in intimate contact experience local welding of submicron surface features, upon seperation the welded material is torn from the surfaces; this process repeats with each contact cycle[B6]. Fretting is an especially acute problem problem for kinematic systems because of the high pressure point contact between mating surfaces; fret resistant materials include hardened '400' series stainless steel and ceramics such as tungsten carbide and silicon nitride [B6,C3].

The sample holder locator balls are preloaded against the X-Y-Z and roll / yaw stops with 70 durometer 'Buna-N' O-rings. Reasons for using O-rings include compliant clamping-- O-rings are highly elastic, so they have a minimal influence on the position set by the hard stops, in addition, they are very tough and durable (i.e. won't break). A disadvantage of using O-rings however is that there is rubbing contact between the rotating shaft and the O-ring which can generate microscopic contamination particles.

A critical portion of the 'flip' stage is the tilt angle setting subassembly, consisting of a locator ball (spaced 1.3125" away from the axis of rotation) which rests upon the reference flat of a custom gage block. For the present design, the allowable range of tilt angle is 8° to 15°, with two angles actually implemented-- 10° and 14°. The major design considerations for the tilt angle setting subassembly were the surface finish and wear performance of the contacting surfaces.

Because of the point contact nature of kinematic couplings, a good surface finish at the contacting surfaces is required to maintain positioning repeatability[3]. The most common quantitative measure of surface finish is the centerline average R_a, defined in Table 4.1 below; also listed are values for high quality surface finishes.
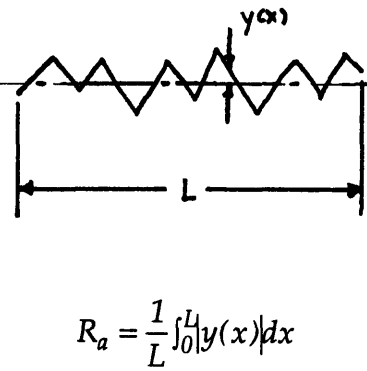
	Ra ($\mu in.$)	Methods of manufacture / typical surfaces
	32	Fine conventionally machined surfaces (i.e. fly-cutting).
	16	Typical surface grinder finish; used where smoothness / form is important.
	8	Fine surface produced by honing, lapping, or buffing, used in precision gages, instrument work, and bearing surfaces where lubrication is unreliable.
	4	Same manufacture processes as for 8 Ra but more refined; similar applications.
	1	Satin or highly polished, mirror like surface; used for fine /sensitive instrument parts and precision gage blocks.

$$R_a = \frac{1}{L}\int_0^L |y(x)|dx$$

Table 4.1 Definition for R_a and values for high quality surface finishes [C4], see [C5] for an in-depth assessment of the different production techniques.

---

[3] The most repeatable kinematic couplings use optical quality surface finish components [C3].

The tilt angle locator ball has a surface finish (R_a) of 0.7 $\mu in.$, while the tungsten carbide balls and rods have a R_a of 1-2.5 $\mu in.$ and 10 $\mu in.$, respectively, and the reference flat on the gage block has a 32 $\mu in.$ R_a. The somewhat high R_a value for the gage block is due to the fact that the flat is located in a depression, making it inaccessible to conventional surface grinding and other fine surface finish production techniques. It is still possible to get an approximate 50% reduction in R_a using electropolishing (i.e. go from 32 $\mu in.$ to 16 $\mu in.$), details of the process can be obtained from [C6]; this option however was not implemented in the prototype.

Another important consideration for the tilt angle setting subassembly was to minimize wear of the contact surfaces through proper material combination / properties selection. As mentioned earlier, kinematic couplings require the use of fret resistant materials, the most common being '400' series hardened stainless steel and tungsten carbide. Despite its superior wear resistance over hardened stainless steel, it was felt that tungsten carbide was *not* a good material to use for the following reasons:

1) *difficult to manufacture*-- tungsten carbide is a brittle and extremely hard material, hence WC parts tend to be simple in shape with no intricate features, parts are generally produced using powder metallurgy (P/M) or electrodischarge machining (EDM) methods[C2]; thus it was anticipated that to manufacture the (somewhat complicated shape) angle setting block out of tungsten carbide would be extremely difficult[4];

2) *impact resistance*-- the brittle nature of tungsten carbide also meant that chipping may arise from the impact that occurs when the locator ball is clamped against the reference flat; impact resistant grades of WC are available, although it should be noted that there is a tradeoff between wear and impact resistance.

Thus it was decided to use a material combination of hardened stainless steel on hardened stainless steel. The locator ball is made of through hardened (58 - 65 Rockwell 'C' scale (HRC) hardness) 440C stainless steel while the angle setting block is made of ion-nitride case-hardened [C7] 410 stainless steel (hardness 60 - 64 HRC). Compared to other case hardening methods, ion nitriding has a minimal effect on part dimensions (i.e. distortions) and surface finish[C8].

4.2.2 X-Y Stage

The 'X' stage is an off-the-shelf precision linear stage (Aerotech model ATS100-200-U-20P [B21] with 8" travel, ballscrew drivetrain and recirculating ball linear guides) driven by a low vibration 5 phase stepping motor (Oriental Motors 'Nanostep' RFK564BA [C9]). A unique feature of the linear stage is that it has been precalibrated for straightness, linear error, and flatness; error correction data has also been included for implementation in the user's own control program. For engineering specifications, see Appendix C.

Due to space limitations, the 'Y' stage had to be custom designed; it features all stainless steel (410) construction, a 0.75" height, and a 2" travel. The stage uses IKO CRW 2-150 cross roller way linear bearings [C10], the positioning actuator is a Newport

---

[4]Another possibility is to use a deposited (e.g. sputtered) film of tungsten carbide over a metal base.

860A-2 open-loop DC motor micrometer drive [B19]. For engineering specifications, see Appendix C.

4.2.3 HTM Based Profiling Errors Calculation Procedure

The profiling errors due to mechanical positioning errors in the AFM and sample positioning hardware was calculated using a procedure based on homogeneous transformation matrices (HTM). Basically the idea is to calculate and then compare the spatial orientation of the sample and AFM probe with respect to a single reference coordinate system in order to determine the positioning error. The transformation from the local (sample) coordinates to the reference coordinate is accomplished using a series of HTM's; each HTM incorporates the positioning error caused by a particular component. The calculation procedure is described below; actual numerical computations are shown in Appendix D.

The first step in the procedure is to establish a series of local coordinates; ideally they should be located where the positioning error can be measured. Using the notation X_i to represent the ith local coordinate system, from Figure 4.1 we have:

X_0 = reference coordinate system located on the granite;
X_1 = coordinate system of the 'X' stage, located on its top mounting surface;
X_2 = coordinate system of the 'Y' stage, located on the 'flip' stage centerline of rotation;
X_3 = coordinate system of the 'flip' stage, also located on the 'flip' stage centerline of rotation;
X_4 = coordinate system of the AFM 'Z' stage, located on its top mounting surface;
X_5 = coordinate system of the AFM probe.

The homogeneous transformation matrix (HTM) that takes one from the ith coordinate system to the jth coordinate system is denoted by ^jT_i ; in addition to a change of coordinates, each transformation matrix also incorporates the translational and rotational effects[5] due to the errors of the ith hardware component ($\delta_{x,i}$, $\delta_{y,i}$, $\delta_{z,i}$, $\varepsilon_{x,i}$, $\varepsilon_{y,i}$, $\varepsilon_{z,i}$). The HTM used were derived under the assumption of small angular errors (on the order of arc-seconds), for the hardware used this is definitely true. A translational (i.e. linear) stage has an HTM given by:

$$^jT_i = \begin{bmatrix} 1 & -\varepsilon z & \varepsilon y & a+\delta x \\ \varepsilon z & 1 & -\varepsilon x & b+\delta y \\ -\varepsilon y & \varepsilon x & 1 & c+\delta z \\ 0 & 0 & 0 & 1 \end{bmatrix} \qquad (4.1)$$

where the δ's and ε's are the positioning errors of the ith stage, and a, b, and c represent the origin offsets of the ith coordinate system with respect to the jth. For a rotational stage, the HTM is given by:

---

[5] All transformations are made with respect to the originally defined local coordinate system orientations; i.e. the 'pitch'-'row'-'yaw' system of transformations is used, this is different from the position transformations commonly used in the analysis of robotic systems.
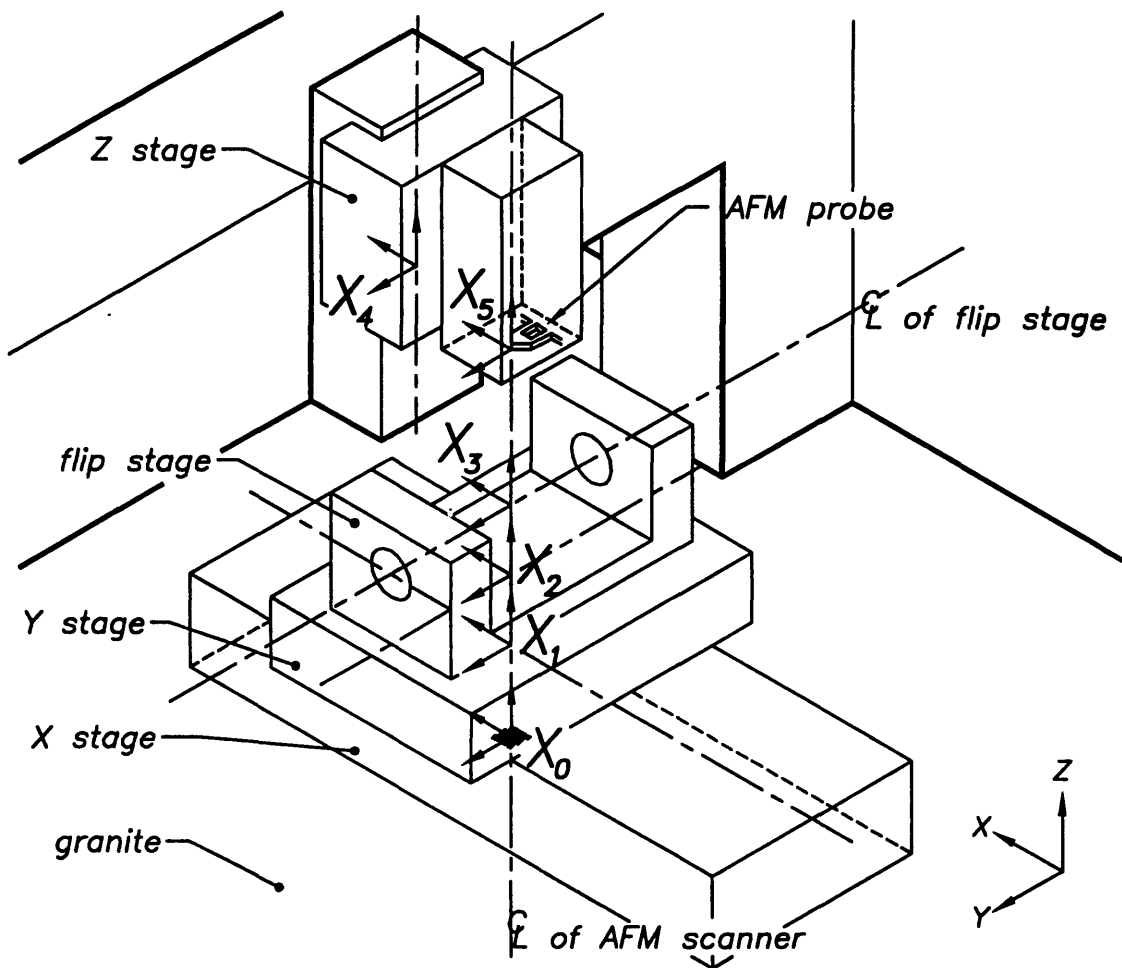
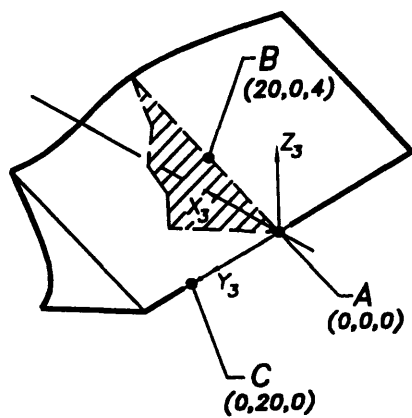Figure 4.1: HTM coordinate systems for sample positioning system

Figure 4.2: HTM based calculations: geometric model of sample
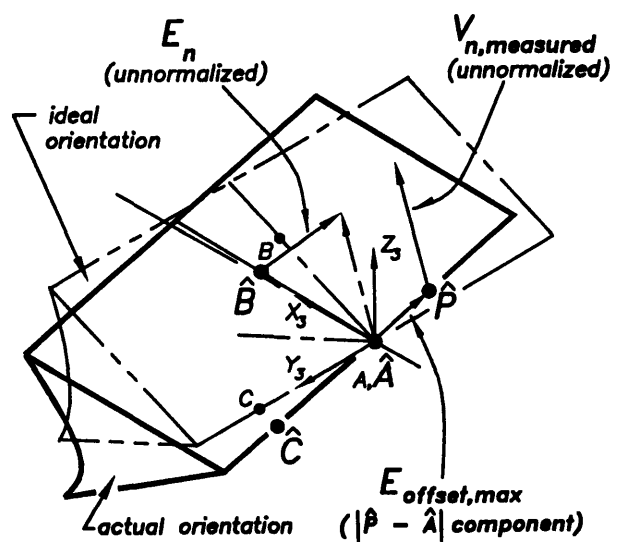
Figure 4.3: HTM based calculations: determination of error in measured profile

$$
{}^{j}\mathbf{T}_{i} = \begin{bmatrix} C\varepsilon zC\theta y - S\varepsilon zS\varepsilon xS\theta y & -S\varepsilon zC\varepsilon x & S\varepsilon zS\varepsilon xC\theta y + C\varepsilon zS\theta y & \delta x \\ S\varepsilon zC\theta y + C\varepsilon zS\varepsilon xS\theta y & C\varepsilon zC\varepsilon x & -C\varepsilon zS\varepsilon xC\theta y + S\varepsilon zS\theta y & \delta y \\ -C\varepsilon xS\theta y & S\varepsilon x & C\varepsilon xC\theta y & \delta z \\ 0 & 0 & 0 & 1 \end{bmatrix} \tag{4.2}
$$

where $'C'$ is the cosine of the angle, $'S'$ is the sine of the angle, and θ_y represents the ideal angular position (i.e. sample tilt angle). Using the notation ${}^{i}\mathbf{P}$ to represent a point in the ith coordinate system (note that $\mathbf{P}$ has the form $[x, y, z, 1]^{T}$), a point ${}^{3}\mathbf{P}$ in the sample coordinate system X_3 is transformed to the reference coordinate system X_0 by the formula:

$$
{}^{0}\mathbf{P} = {}^{0}\mathbf{T}_1 {}^{1}\mathbf{T}_2 {}^{2}\mathbf{T}_3 {}^{3}\mathbf{P} \tag{4.3}
$$

Note that if the $'X'$ and $'Y'$ stages are one unit (as in some stages), then ${}^{0}\mathbf{T}_1 {}^{1}\mathbf{T}_2$ would be a single matrix only. In a similar fashion, the location of the AFM probe tip in X_0 can be expressed by:

$$
{}^{0}\mathbf{P} = {}^{0}\mathbf{T}_4 {}^{4}\mathbf{T}_5 {}^{5}\mathbf{P} \tag{4.4}
$$

To determine the positioning error, the first step is to apply eq. (4.3) to three distinct points on the top face of the sample; the sample profile was modeled as a symmetric planar wedge with $T = 4$ μm at $D = 20$ μm (see Figure 4.2)[6], so the following points (in units of microns) were arbitrarily chosen:

$$
\{\mathbf{A}, \mathbf{B}, \mathbf{C}\} = \left\{ \begin{bmatrix} 0 \\ 0 \\ 0 \\ 1 \end{bmatrix} \begin{bmatrix} 20 \\ 0 \\ 4 \\ 1 \end{bmatrix} \begin{bmatrix} 0 \\ 20 \\ 0 \\ 1 \end{bmatrix} \right\} \tag{4.5}
$$

Numerical values for the offsets, δ's and ε's used in eq. (4.3) were based on the particular dimensions and error specifications (either from the manufacturers' data or estimated) of the positioning stages. Using the transformed values of $\{\mathbf{A}, \mathbf{B}, \mathbf{C}\}$, denoted as $\{\hat{\mathbf{A}}, \hat{\mathbf{B}}, \hat{\mathbf{C}}\}$ -- with each vector in the form $\begin{bmatrix} x & y & z \end{bmatrix}^{T}$ -- the angular orientation of the sample can then be computed using the vector cross product. From Figure 4.3, it can be seen that the vector normal to the plane containing the points $\{\hat{\mathbf{A}}, \hat{\mathbf{B}}, \hat{\mathbf{C}}\}$ is given by:

$$
\mathbf{N} = \begin{bmatrix} n_x \\ n_y \\ n_z \end{bmatrix} = (\hat{\mathbf{B}} - \hat{\mathbf{A}}) \times (\hat{\mathbf{C}} - \hat{\mathbf{A}}) \tag{4.6}
$$

Thus the equation for the top sample surface is simply:

---

[6]Form a non-wedge shape profile, the HTM must be applied to every point (i.e. an adequately spaced mesh) on the surface.

$$\mathbf{N} \bullet \begin{bmatrix} x & y & z \end{bmatrix}^{\mathrm{T}} = 0 \tag{4.7}$$

Note that the x, y, and z above refer to the local profiling coordinate system (i.e. $x = 0$ is the sample tip). A similar procedure can be applied to the other side of the sample by using the following points instead:

$$\{\mathbf{D}, \mathbf{E}, \mathbf{F}\} = \left\{ \begin{bmatrix} 0 \\ 0 \\ 0 \\ 1 \end{bmatrix} \begin{bmatrix} 20 \\ 0 \\ -4 \\ 1 \end{bmatrix} \begin{bmatrix} 0 \\ -20 \\ 0 \\ 1 \end{bmatrix} \right\} \tag{4.8}$$

The next step in the calculation procedure is to determine the positioning errors associated with the AFM probe tip; note that only mechanical positioning errors are considered, AFM particular errors (e.g. piezotube bending) are discussed in a seperate report. Because the AFM probe tip can be treated as a point, its positioning error is easier to determine. The probe position is given by eq. (4.4), so using $[0\ 0\ 0\ 1]^{\mathrm{T}}$ for $^5\mathbf{P}$ the following results:

$$^0\mathbf{P} = \begin{bmatrix} p_x \\ p_y \\ p_z \\ 1 \end{bmatrix} = {}^0\mathbf{T}_4\,{}^4\mathbf{T}_5\,{}^5\mathbf{P} \tag{4.9}$$

For subsequent error calculations, the vector $\hat{\mathbf{P}} = \begin{bmatrix} p_x & p_y & p_z \end{bmatrix}^{\mathrm{T}}$ will be used instead of $^0\mathbf{P}$. An additional source of mechanical positioning error comes from the angular misalignment of the AFM probe with respect to the X-Y plane every time a new probe cartridge is mounted or when the scanner unit is taken out and put back into place. Experimental investigations (from profiling an optical flat) showed that the maximum values for this tilt error ($\varepsilon_{x,\mathrm{mount}}$, $\varepsilon_{y,\mathrm{mount}}$) is approximately 0.13° and 0.07° in the 'X' and 'Y' direction respectively.

The final step in the calculation procedure is to determine the profile measurement error by comparing the position / orientation of the sample with respect to the AFM probe. Two types of positioning errors were examined-- first, the initial location offset error that occurs when the AFM probe is lifted from the sample and/or the sample is flipped, and secondly, the general profiling errors (i.e. E_{d2} and E_{t2}) due to angular orientation errors .

The maximum initial location offset error can be computed from the relative displacement of the 'zero' point on the sample with the AFM probe:

$$\mathbf{E}_{offset,max} = \begin{bmatrix} \delta_{x,offset} \\ \delta_{y,offset} \\ \delta_{z,offset} \end{bmatrix} = \left| \hat{\mathbf{P}} - \hat{\mathbf{A}} \right| + \left| \hat{\mathbf{D}} - \hat{\mathbf{A}} \right| \tag{4.10}$$

where $|\hat{\mathbf{P}} - \hat{\mathbf{A}}|$ is the offset positioning error due to the AFM 'Z' stage and $|\hat{\mathbf{D}} - \hat{\mathbf{A}}|$ is the offset positioning error due to the sample positioning stages. As mentioned in chapter 3, the sample tip is coarse aligned with the AFM probe in the 'X' direction before profiling, so $\delta_{x,offset}$ is always minimized[7]. Similarly, $\delta_{z,offset}$ has no effect on measurements because the AFM probe is brought down onto the sample surface before profiling; in addition, a relative 'Z' reference is used (i.e. the identified sample tip). Thus, the only significant error is $\delta_{y,offset}$.

To determine the general profiling errors (i.e. E_{d2} and E_{t2}) due to the angular orientation errors, the AFM profiling path is compared with the true profile, see Figure 4.3; this only needs to be done for one line trace because of the planar sample shape assumption (i.e. the measured profile is the same at all locations); in addition, the sample profile is generated one line at a time (i.e. the actual measurement data is rotated back about the located tip for that particular line, not the average edge)[8]. With this in mind, for the 'top' side of the sample, the spacial orientation of the true profile (i.e. directional vector) is given by the following:

$$V_{n,actual} = \frac{\mathbf{R}_y(-\alpha)(\hat{\mathbf{B}} - \hat{\mathbf{A}})}{\|\mathbf{R}_y(-\alpha)(\hat{\mathbf{B}} - \hat{\mathbf{A}})\|} \qquad (4.11)$$

where $(\hat{\mathbf{B}} - \hat{\mathbf{A}})$ are the vectors of equation 4.6, and $\mathbf{R}_y(-\alpha)$ is simply the 3 x 3 transformation matrix for a rotation about the 'Y' axis (with $\theta = -\alpha$, the tilt angle):

$$\mathbf{R}_y(\theta) = \begin{bmatrix} cos(\theta) & 0 & sin(\theta) \\ 0 & 1 & 0 \\ -sin(\theta) & 0 & cos(\theta) \end{bmatrix} \qquad (4.12)$$

For an AFM profiling path with an orthogonality error[9] of ε_{ortho}, the directional vector of the *measured* profile can be computed using equation 4.6 and 4.7, by first substituting $y = x\, tan(\varepsilon_{ortho})$ into equation 4.7 and solving for z as a function of x, then rotating the resultant vector (i.e. with the derived values of y and z) by $\mathbf{R}_y(\theta = -\alpha + \varepsilon_{y,mount})$ (note the inclusion of the error term $\varepsilon_{y,mount}$). The normalized directional vector (if $n_z \neq 0$) is therefore:

---

[7]Currently this alignment is done visually using the low magnification (180x) oblique camera view of the XL; the 'X' alignment error is estimated to be about ± 5-10 μm; better alignment can be expected on the M5 using the high magnification (up to 1350x)overview view camera. Note that the 'X' alignment error does have an effect on the measurement accuracy because the scanner position is typically offsetted for fine alignment with the sample tip-- this results in scanner positioning errors due to 'X'-'Z' cross-coupling effects (e.g. piezotube bending), this will be examined in a seperate thesis [A1].

[8]Part of the reason for this is computational simplicity.

[9]The orthogonality error has three components-- the angular error of the AFM 'Z' stage, the orthogonality travel error of the 'X'-'Y' stage, and the orthogonality mounting error of the 'flip' stage).

$$\mathbf{V}_{n,measured} = \cfrac{\mathbf{R}_y(-\alpha+\varepsilon_{y,mount})\begin{bmatrix} 1 \\ \cfrac{tan(\varepsilon_{ortho})}{n_x + n_y tan(\varepsilon_{ortho})} \\ -n_z \end{bmatrix}}{\left\| \mathbf{R}_y(-\alpha+\varepsilon_{y,mount})\begin{bmatrix} 1 \\ \cfrac{tan(\varepsilon_{ortho})}{n_x + n_y tan(\varepsilon_{ortho})} \\ -n_z \end{bmatrix} \right\|} \tag{4.13}$$

Note that the x term drops out of the equation (but keep in mind that all length measurements are in microns). Using equation 4.11 and 4.13, the error vector at $D = 1$ μm is given by:

$$\mathbf{E}_n = \mathbf{V}_{n,measured} - \mathbf{V}_{n,actual} \tag{4.14}$$

To compute the profile error (i.e. E_{d2} and E_{t2}), we can take advantage of the fact that the direction of the error vector $\mathbf{E}$ at a particular location (analogous formulation to equation 4.14) is the same as $\mathbf{E}_n$ because of the planar sample shape assumption and also that it scales linearly with the distance from the sample tip. The projection of $\mathbf{E}$ onto the 'X'-'Y' plane gives E_{d2} while its 'Z' component is E_{t2}.

To determine the profiling errors for the other side of the sample, a similar calculation procedure can be used.

4.2.4 Environmental Noise and Thermal Drift Considerations

In this section, design considerations for the minimization of environmental noise (including mechanical vibrations) and thermal drift are described. As can be expected of an instrument with sub-angstrom to nanometer resolution[10] (in both the lateral and vertical directions), great emphasis must be placed on minimizing the effects of external electrical and mechanical noise.[11] For this design, minimization of electrical noise basically meant shielding motor amplifers (PWM type for stepping motors)[12] and other electrical equipment . Note that one of the motivations for using a mechanically

---

[10]One must be careful in the interpretation of the manufacturer's specified vertical and laternal measurement noise, often referred to as the minimum measurement resolution, because such measurements are typically made under unusual scanning conditions; for example, a common claim is the ability to obtain 'atomic resolution'-- to achieve this, one must often scan an extremely small area (on the order of nanometers) continuously at the highest possible scan rate (to minimize the effects of mechanical vibrations). Another issue with the minimum measurement resolution, following PSI's procedure, is that it is ambiguously defined; the minimum vertical resolution determination procedure consist of scanning a small area on an atomically flat surface (e.g. graphite), then selecting a small flat region in the scanned image to compute the RMS roughness; depending on the scan area selected, the measured value can vary a lot, (for the experimental data, I use a selected area of 0.1 μm x 0.1 μm, this produces results which are comparable to PSI's specified values). Please see PSI software manual for instrumentation settings.

[11]For an examination of the intrinsic measurement noise (e.g. of the 'Piezolever'), see [A21] and the seperate thesis which focuses on the AFM aspects of the profilometer [A1].

[12]Linear amplifers could be used instead, although they are less efficient.

positioned design was to avoid / minimize the electrical noise from position sensors placed near the sensitive AFM probe sensor (the 'Piezolever'). .

The principal sources of external mechanical noise are acoustic and mechanical vibrations. The XL and M5 (in particular) have been carefully designed to minimize external mechanical noise (e.g. granite slab vibration isolation table and massive, total enclosure acoustic shielding). Even with this, effort was spent on reducing the effects of mechanical vibrations in the sample positioning system; this is highlighted below:

a) *rigid sample clamping* -- clamps with a large clamping surface area are used for the sample; in addition, the cantilevered distance from the sample tip to the sample body clamp is minimized; (as stated in chapter 2, one of the inherent disadvantages of the 'flip' stage concept is that the sample must be positioned with an overhang); in addition, all electrical control wires were carefully tied down to eliminate the transmittance of external disturbances to the sample[13].

b) *stable/stiff bearings* -- stable kinematic bearings are used in the 'flip' stage while high mechanical stiffness linear bearings (i.e. cross-roller ways and recirculating ball linear guides) are used in the 'X'-'Y' positioners.

c) *stable positioning actuators* -- positioning actuator jitter was avoided / minimized by using a mechanical locking mechanism for the 'flip' stage, stepping motors (with zero speed stability) and a stable open-loop DC micromotor pointscrew drive for the 'Y' stage (stability verifed experimentally[14]).

An important mechanical vibrations parameter is the minimum resonant frequency of the entire system. The bandwidth of the feedback loop that controls the position of the probe relative to the surface is limited by the minimum resonant frequency, the scanning speed, in turn, is limited by the feedback loop bandwidth[C11]. For large sample size system (i.e. sample size ≈ 75 - 200 *mm* in diameter), the minimum resonant frequencies arise from the bending modes of the microscopes' mechanical support structures; [C12] reports a horizontal bending mode frequency of 90 - 170 *Hz* (for two different instruments) and a vertical mode at 400 *Hz* (similar vertical performance in [B18]).[15] A rule-of-thumb is to limit the maximum scanning frequency to one tenth of the minimum resonant frequency in the system; (note that the XL has a maximum scanning frequency of 6 *Hz*). The minimum resonant frequency of the system will be investigated in the next chapter.

Finally, a different but equally important issue was the minimization of thermal drift. Preliminary investigations of the XL machine indicated a high drift rate in the range of 20 -60 *nm/min*. (the higher drift rates occur when the camera lights are left on[16]); by comparison, drift rates as low as 2 *nm/min*. have been reported for large sample systems [B18] (remember that positioning errors of a few nanometers are sought!) Well known strategies for minimizing thermal drift include:

---

[13]Simply touching the cable connected to one of the motors can cause a sudden jump (i.e. microslippage), typically 5-20 *nm* amptitude, but can be as high as 100 *nm*.

[14]This was done by observing the drift in the AFM scanned images of a 1 *μm* pitch grating; observed drift was negligible.

[15]Note that the tube type piezoelectric scanner commonly used in scanned probe microscopes typically have minimum resonant frequencies in the range of 1 - 20 *kHz* [C7, C8].

[16]In the new M5 machine, the overhead camera light is transmitted via optical fibers, so hopefully this will minimize the heat transmitted to the sample and / or scanner; as an added precaution, infared shields could be used.

a) *use of low thermal expansion materials and careful control of heat generation elements in the design* -- stainless steel (specifically 304 and 410, with a coefficient of thermal expansion of 9.6 and 5.5 x 10^{-6} in./in./F, respectively [C13], by comparison, 6061-T6 aluminum has a thermal coefficient of expansion of 13 x 10^{-6} in./in./F) was used extensively, in addition, heat-generating stepping motors are turned off or operated at reduced current while they are at a standstill;

b) *regulation of environmental conditions and shielding from external heat sources* -- place the instrument in a temperature-controlled environment; and from direct lighting and operator body heat (e.g. use a plastic cover);

c) *change scanning parameters* -- use a higher scanning rate, this however results in a lost of imaging detail (i.e. surface features are not resolved accurately).

Depending on the actual environment conditions, some of the items in b) and c) will be implemented.

4.3 Metrological Considerations

4.3.1 Reference Surfaces / Edges

In this section, the reference surfaces and edges used for measurements are described; (this should not be confused with reference calibration samples). First of all, the sample body is clamped against the sample holder mounting surface to establish a planar datum for the sample. In turn, the sample holder and the rest of the sample positioning subsystem, as well as the AFM assembly, are referenced back to a single master reference surface-- the granite surface on which all hardware components are mounted. Because measurements are made with respect to this *global* reference surface, it should be realized that in this application the AFM is used for *form* measurement [17] rather than the more common *surface texture* measurement application; for surface texture measurements, a first order plane is typically fitted to the data to remove the surface form component.

Instead of a single master reference surface, the possibility of using *two* local reference surfaces (mounted to the sample holder, one for each side of the sample) was also considered. The measurement process would then first involve measuring the local reference surface to determine the planar tilt orientation of the AFM probe to the sample holder mounting surface, and then using this information to correct the actual profile data. Possible reference surfaces include an optical flat (note that the highest quality flats are flat to within 20 *nm* over a 1″ area), and 'ultraflat' epiaxial silicon (used to fabricate certain semiconductor devices, this is flat to within 300 *nm* over a 8″ diameter area). The obvious advantage of this 'closed-loop' measurement procedure is that the sample needs not be positioned very repeatibility; disadvantages of the method include a longer measurement time because two additional surfaces need to be profiled, additional wear on the probe, and the need to establish an accurate planar reference over a very small distance (10 or 100 *μm*, depending the scanner used)-- a potentially major source of error being the 'X'-'Z' cross coupling of the piezotube scanner (due to the bending of the tube); for numerical estimates of this error, the reader is referred to the

---

[17] I like to think of the AFM profilometer as a sort of miniature coordinate measuring machine (CMM),in a 'macroscopic' CMM, the three dimensional form of the sample is also measured with respect to a global reference surface, usually a granite surface on which all hardware is mounted.

seperate report on AFM instrumentation [A1]. Because of these disadvantages, the local reference scheme was not implemented[18].

Aside from reference surfaces, another major consideration was how to align the sample edge with respect to the flip axis of rotation. Two possibilities were considered, one was to reference against the sample edge, as is currently done, another was to use the back edge (i.e. the unsharpened side) as the reference. Referencing to the back edge was not implemented because it is not very uniform in shape. With front edge referencing, care must be taken in aligning the sample against the hard stops; excessive (operator) force would result in large scale deflection of the fragile edge, resulting in edge misalignment[19]. This problem was minimized by using line contact hard stops (0.090" contact length each side) to reduce pressure on the edge.

4.3.2 Measurement Procedures

The profile measurement procedure consist of the following sequential operations:

1) load AFM probe and sample;
2) visually align the sample edge with the probe tip in the 'X' direction, and lower the AFM probe onto the sample surface, then use the AFM piezoscanner for fine lateral alignment with the sample tip;
3) scan the sample after setting the proper AFM measurement parameters;
4) flip the sample to the other side and repeat steps 2) to 3);
5) in the following sequence, filter, apply a 'deconvolution' algorithm, and locate the sample tip from the edge region (do for both sides of the sample);
6) rotate the data by $-\alpha$ (the tilt angle) to reconstruct the sample profile;
7) average the data if desired.

The measurement procedure is covered in depth in a seperate thesis [A1].

4.3.3 Calibration Procedures

The calibration procedures for the entire profilometer can be broken down into the followed catagories:

(1) *sample 'flip' stage performance*-- this mainly consist of measuring and checking the repeatability of the sample tilt angle α and the axial shift error δ_y(using a CMM and high power optical microscope / AFM, respectively), and minimizing the 'X' direction offset upon flipping the sample (to be done by precision grinding of the edge stops);

(2) 'flip'-X-Y stage-- calibration tasks here include aligning for straightness, orthogonality, and checking positioning accuracies / repeatability using dial and an avaiable high resolution capacitive sensor, note that some of the calibration data has already been provided by the linear stage manufacturer;

---

[18]The potential for higher measurement accuracy should not be dismissed however, given more time, the two reference surface scheme should be investigated further experimental to determine what is the maximum measurement accuracy that can be achieved.

[19]In the current flip stage used on another instrument, the problem is made worse by the fact that the hard stops have point contacts (i.e. dowel pins).

(3) *AFM calibration*-- this includes items such as check of the scanner measuring range and accuracy (linearity), and measurement resolution.

(4) *total system performance*-- this consists of an examination of the measurement accuracy /repeatibility of the combined AFM / sample positioning system; also examined will be the thermal drift and measurement resolution.

Due to time constraints, only preliminary results for (1) and (4) are presented in Chapter 5; (note that (3) and (4) are also be discussed in a seperate thesis [A1]).

4.4 Summary

In this chapter, the detailed design of the sample positioning system was described, with greater emphysis placed on the critical/unique features of the design. In additional, metrologically issues were also touched upon-- reference datums, measurement procedures, and calibration procedures.

5 Design Implementation

5.1 Introduction

In this chapter, the performance of the implemented design is assessed through a series of experiments. Due to time constraints, only preliminary experimental results are presented, although it should be noted that the system is still being worked on at this time to insure that all specifications are satisfactorily met.

5.2 Performance Evaluation

The performance of the actual profilometry system was assessed through a series of experiments. Before plunging into details, three items should be kept in mind; first, the primary focus of the experiments was to examine the performance of the *unique* aspects of the system-- the novel 'flip' stage, and the combined performance of the AFM and sample positioning stages. The performance of the AFM microscope and 'X'-'Y' stages are not examined here because detailed specifications / calibrations have been provided for by the respective manufacturer. A second thing to keep in mind is that due to time constraints, only preliminary experimental results will be discussed. Thirdly, actual sample measurement repeatibility and accuracy results are not presented here because they depend on the data processing algorithm(s) used as well as the hardware; the results for these are given in a seperate report.

5.2.1 'Flip' Stage

The performance of the 'flip' stage is examined in this section in terms of the positioning errors listed in Table 3.1-- the tilt and roll angle error (ε_y and ε_x), the sample edge shift error (δ_y), yaw angle error (δ_x), and planar AFM probe-to-sample tip alignment (ε_z).

5.2.1.1 Angular Positioning Repeatibility (Tilt Angle Error ε_y and Roll Angle Error ε_x)

The angular positioning repeatibility of the 'flip' stage was investigated in two experimental runs; each run consisted of automatically flipping the sample holder from one side to the other for 500 cycles and measuring the planar orientation of the sample holder (both sides) every tenth cycle using a coordinate measuring machine (CMM), the Brown and Sharpe PFx. The primary purpose of these experiments were to assess the effects of wear on positioning performance.

The 3-D plane procedure of the PFx was used for the measurements. In this procedure, the spacial location of three (or more) distinct points on the sample mounting surface[1] is measured and used to compute the unit normal vector of the best-fit plane[2]. The angular orientation about the 'X' and 'Y' axis is therefore given by $\theta_x = \tan^{-1}(n_x/n_z)$ and $\theta_y = \tan^{-1}(n_y/n_z)$. The PFx indicates position to 0.1 μm, so over a 15.2 mm distance (i.e. the maximum radial measuring distance on the holder) gives an angular

---

[1] When the sample holder is flipped over to the other side, the back surface of the holder is used for measurements.

[2] The same procedure was used for the concept verification experiments of section 3.6.2.

measurement sensitivity of $\approx \tan^{-1}(0.1 \ \mu m \ / \ 15.2 \ mm) = 1.4 \ arc\text{-}sec$. The CMM was calibrated by measuring 10°, 15°, and 30 ° angle gage blocks[3] with ± 10 *arc-sec.* accuracy; calibration results are given below:

Nominal angle	Accuracy	Repeatibility
10°	144 *arc-sec.*	$\approx \pm 10.8$ *arc-sec.*
15°	57.6 *arc-sec.*	$\approx \pm 14.4$ *arc-sec.*
30°	32 *arc-sec.*	$\approx \pm 14.4$ *arc-sec.*

Since the experiment was conducted over a period of hours, measurement drift was a major concern. However, a series of 30 calibration angle measurements made over 2 hours revealed negligible drift.

The actual measurement was conducted for the 14° angle setting on the 'flip' stage; results for the 10° angle are expected to be similar. The positioning repeatability of the tilt angle error (ε_y) and roll angle error (ε_x) for the right side position are shown in Figure 5.1 through Figure 5.4, and the results for the left side position are shown in Figure 5.5 through Figure 5.8. The measured average angle[4] (i.e. θ_y and θ_x) and corresponding standard deviations are listed below. The variation in the average could be attributed to the fact that the stage was taken apart and put back together between each run-- this can be eliminated thru the use of alignment pins and a final calibration (i.e. do not disassemble the stage) once all modifications have been made.

	Avg. Meas. Angle (θ_y)	Std. Dev. for θ_y	Avg. Meas. Angle (θ_x)	Std. Dev. for θ_x
1st Exp. Run (Right)	13.0498°	0.0094° (33.7″)	0.0459°	0.0077°(27.7″)
1st Exp. Run (Left)	13.1728°	0.0029° (10.4″)	0.0311°	0.0019° (6.8″)
2nd Exp. Run (Right)	13.0439°	0.0059°(21.1″)	0.0733°	0.0057°(20.7″)
2nd Exp. Run (Left)	13.1698°	0.0102° (36.9″)	0.0189°	0.0025° (9.0″)

Interesting results were obtained. In the first experimental run, for the right hand side, the angular positioning repeatability for both ε_y and ε_x was found to exhibit an ≈ 80 *arc-sec.* drift / wear over the first 500 cycles (see Figures 5.1 and 5.3); by comparison, the left hand side (see Figures 5.5 and 5.7) displayed a much smaller (almost negligible drift); this difference was attributed to two factors-- first, the holder sensing limit switch for the left side was set closer to the clamping magnet than the right side[5], hence the left side experienced much smaller/reduced impact wear. In addition, it was observed afterwards that that the angle setting assembly on the sample holder (i.e. the locator ball that is furthest out from the axis of rotation) shifted slightly in position (on the order of 0.001″ - 0.010″) due to mechanical vibrations from the impact loading; (note that from the geometry alone, a change in the radial length of 0.001″ can cause an angular change of 40 *arc-sec.*). This problem is currently being remedied through the use of alignment pins with the angle setting ball assembly; also, vibration resistant screws will be used.

---

[3] 8 and 12 degree angles were also measured as well, but this involved stacking two gage blocks one on top of the other, so measurement errors are likely to be larger.

[4] The average measured tilt angle is not equal to the nominal angle (14°) because final grinding adjustments have not been made.

[5] In the current design, it takes a lot of trial and error to set the limit switch at the position where the impact clamping force is minimized; so it should not be assumed that this condition will be always present.

Figure 5.1: Right side tilt angle error (ε_y) repeatibility (1st trial)

Figure 5.2: Right side tilt angle error (θ_y) repeatibility (2nd trial);
note the change in scale

Figure 5.3: Right side roll angle error (ε_x) repeatibility (1st trial)

Figure 5.4: Right side roll angle error (ε_x) repeatibility (2nd trial);
note the change in scale
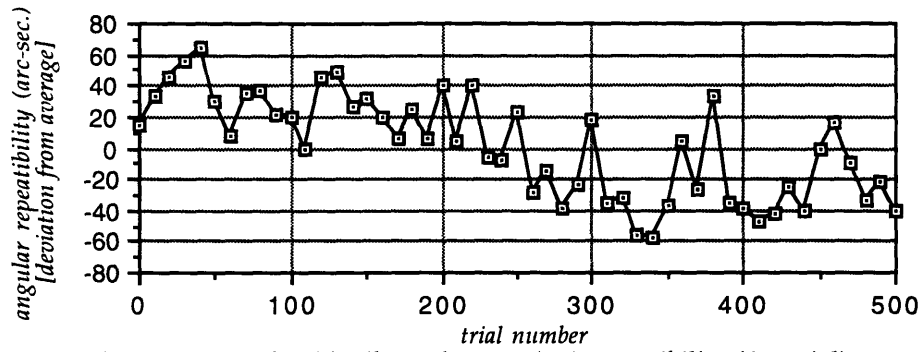
Figure 5.5: Left side tilt angle error (ε_y) repeatability (1st trial)
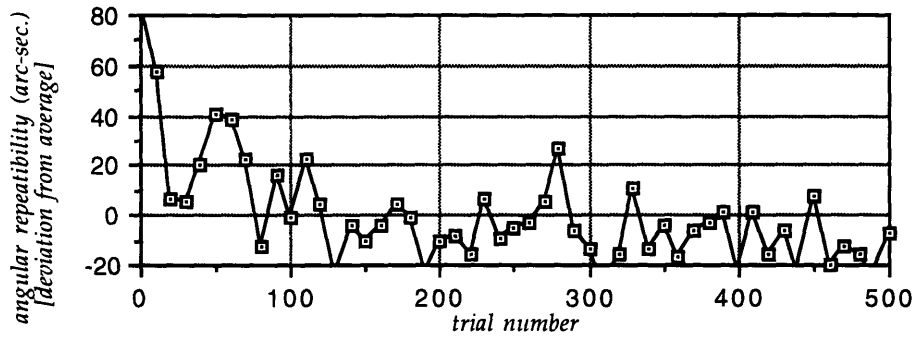

*Figure 5.6: Left side tilt angle error (ε_y) repeatability (2nd trial);
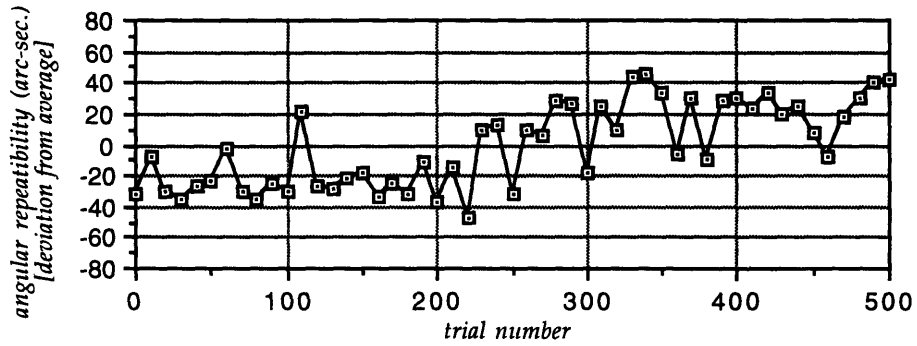note the change in scale*

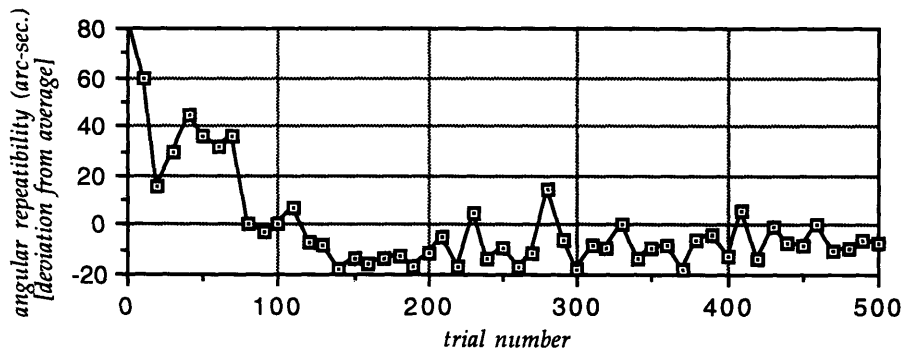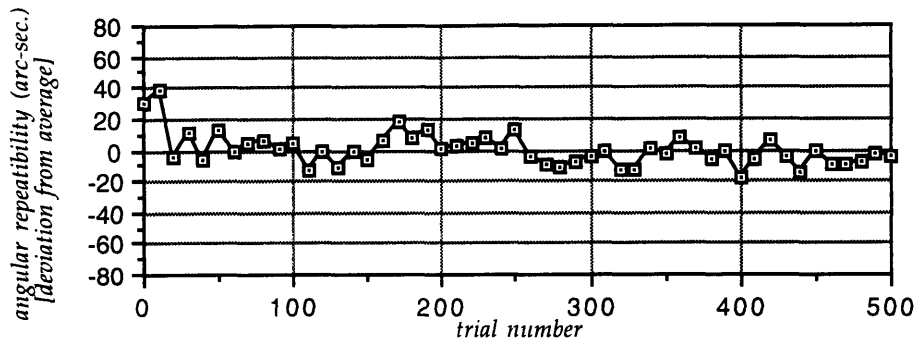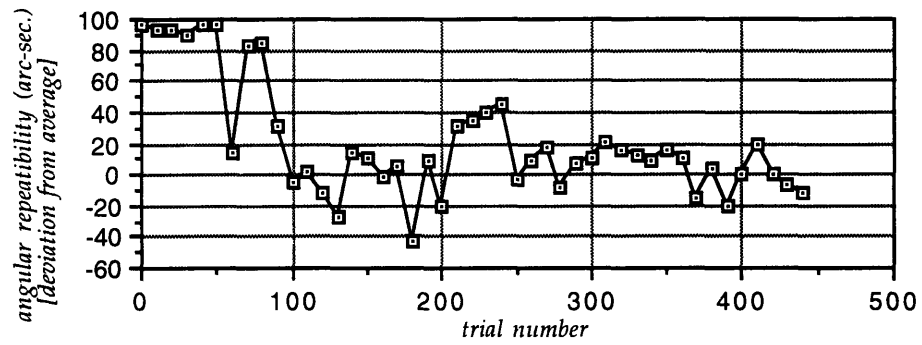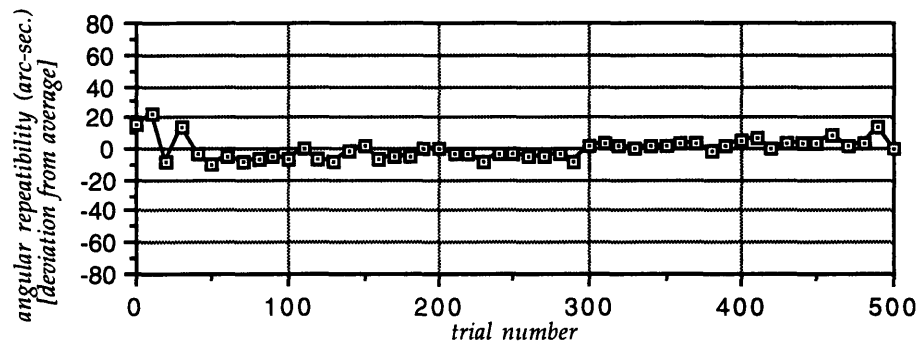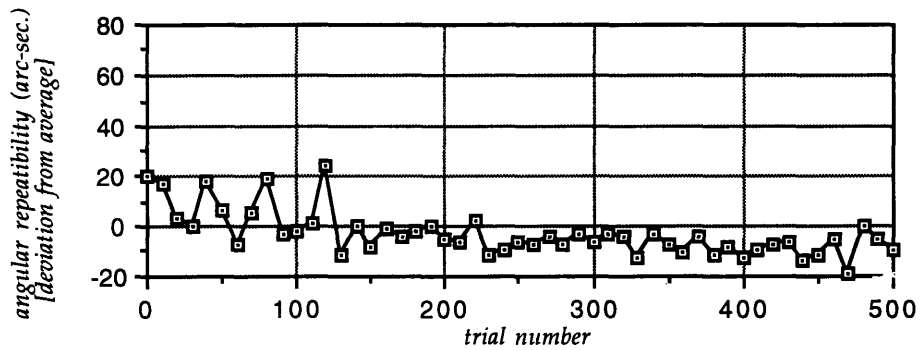*Figure 5.7: Left side roll angle error (ε_x) repeatability (1st trial)*

*Figure 5.8: Left side angle error (ε_x) repeatability (2nd trial);
note the change in scale*

In the second experimental run, an angular positioning error repeatibility of ± 20 *arc-sec.* was achieved (the target specification was ± 20 *arc-sec.* for ε_y and ± 40 *arc-sec.* for ε_x) after a wear-in period of about 100 cycles, (by comparison, [B12] reports a 50 cycle wear-in period). For this second run, it was suspected that the angle locator ball assembly on the sample holder had settled into a final position, so the large drifting problem observed in the first run was not present-- this hypothesis will be tested once the corrective changes to the design have been made.

5.2.1.2 Determination of Sample Edge Shift Error (δ_y)

When the sample is flipped from one side to another, the sample must remain aligned in the 'Y' direction to insure that the measured profile is representative of the true cross-section. From Table 3.1, the target value for this misalignment error ($\delta_{y,\text{flip offset}}$) was ≤ ± 1 *µm*. The magnitude and sources of this error were determined by first profiling a small region of the edge which has recognizable silhouette features, then measuring (with the built-in imaging processing software) the location shifts of those same features in subsequent scans after positioning moves (e.g. 'Z' stage retracted and then reengaged and / or 'flip' stage activated)[6].

In the first experiment, the sample was not moved, but the 'Z' stage was retracted about 800 *µm* above the sample and then reengaged again; this was repeated 10 times. From the data, it was found that the 'Z' stage had a positioning repeatibility of ≈ ± 0.13 *µm* in the 'Y' direction.

In the second experiment, the 'flip' stage was activated (with the 'Z' stage retracted and then reengaged, of course) 10 times. The positioning repeatibility in the 'Y' direction for one side (the right side) was found to be about ± 0.40 - 0.45 µ*m*. Assuming a worse case situation where the positioning errors are linearly additive, this means that the 'Y' positioning repeatibility of the 'flip' stage plus 'X'-'Y' stage can be on the order of ≈ ± 0.32 µ*m*.

In the third series of experiment, the total misalignment error was determined by flipping the sample from one side to another (12 times), and observing the shift in the 'Y' position of a prominent edge feature. Before the experiments were begun, it was noticed that flipping to the left side could result it the 'X' - 'Y' - 'Z' locator ball disengaging from one of the three reference balls (this problem was suspected to arise from the motor-to-sample holder coupling). Thus in the experiments, the locator ball was preloaded against the reference balls by hand before measurements were taken; in that case a $\delta_{y,\text{flip offset}}$ error of ≈ ± 0.75 *µm* was obtained. Specific 'fixes' include adjustment of the O-ring preload force, use a more axially/radially compliant motor coupling, or put in a seperate preload force for the sole purpose of aligning this locator ball.

5.2.1.3 Sample Edge to Axis of Rotation Alignment (Planar AFM Probe-to-Sample Tip Alignment Error δ_x and Yaw Angle Error ε_z)

---

[6]The high magnification overhead camera of the XL could be used along with a sizable two-sided edge feature of a known size, however, it was found that the camera's center of focus can shift considerably in 'X' and 'Y' when the depth of focus is changed (this is required because the stage has a z positioning error), so this method was not used for precise measurements. This method can be use for rough estimates however.

The sample edge is aligned to the 'flip' stage axis of rotation via. two flat stops; the target goal for the alignment was ± 10 μm.. This was to be achieved by first observing the offset error using a Nikon 30 x magnification industrial inspection microscope (equipped with 0.0001" (2.54 μm) positioning resolution sample stages[7]), then adjusting the stops using an Okamoto 8-20X precision surface grinder with position readout to 0.0001" (the stops were initially machined with a 0.010" grinding allowance). Unfortunately, the stops were grounded 0.002" over[8], thereby resulting in a 0.004" ($\approx$ 100 μm) δ_x flip offset. If the stops were precisely grounded, then edge realignment would be much more precise; (the 'flip' stage has high radial position repeatibility).

Better alignment will be attempted by applying the above procedure to another set of stops; this time, they will be grounded 0.002" to 0.003" undersized, with final adjustment to be done using shim stock (available in thicknesses of 0.0005", 0.001", and larger (in 0.001" increments)).

The yaw angle error was not investigated yet; it depends in part on the 'X'-'Y' stage alignment as well as 'flip' stage alignment; this will be characterized once the entire system is fully set up.

5.2.2 Total system performance

The 'Z' measurement sensitivity, thermal drift, and minimum natural frequency of the total system are discussed in this section. In order to get accurate performance assessments, actual scanning conditions / setups were used (i.e. profiling the sample as close to the tip as possible, without going over the edge).

5.2.2.1 'Z' Measurement Resolution

The 'Z' measurement sensitivity (actually noise) of the profilometer was found by computing the RMS roughness[9] of a 0.1 μm x 0.1 μm area near the edge of the sample. An implicit assumption is that the surface roughness of this region is sufficiently low so as not to significantly affect the measurements.[10] From an average of 15 measurements, the 'Z' measurement sensitivity was found to be 6.5 $\mathring{A}$; this is in the same order of magnitude as the AFM manufacturer's specified value of 2 to 3 $\mathring{A}$ (the 2 $\mathring{A}$ resolution is achieved under the most ideal environmental conditions with the stiffest sample mounts (e.g. sample is rigidly mounted to a heavy block of metal that is placed directly on the granite). Another point to remember is that a 6.5 $\mathring{A}$ (0.65 nm) 'Z' measurement noise comprises a small component of the allowable vertical measurement uncertainty (E_{T2}) of $\le \pm 5$ nm; from an error budgeting point of view this means that a greater error allowance can be allocated to other sources of error, such as thermal drift distortions and AFM particular errors (e.g. piezotube scanner bending).

---

[7] The much higher magnification overhead camera on the XL could also be used along with a two-sided edge feature of a known size as a length unit; however, the grinding adjustments was done at a different location, so this was not used.

[8] Note that for machined parts, dimensional tolerances of ± 0.001" is considered high precision; in addition, it was realized that even a misalignment of 0.001" is quite noticable when the sample is observed under the microscope.

[9] See the long footnote on the manufacturer's specified vertical and lateral measurement noise in chapter 4.

[10] Typically, the vertical sensitivity is measured using a sample with atomically flat surfaces (i.e. HOPG graphite), however, because of the small, thin nature of the sample, it was afraid that mounting a graphite sample (a large sample needs to be used because the graphite is fragile and flaky).

The 'X'-'Y' measurement resolution was not investigated due to a lack of a suitable nanometer scale 'X'-'Y' long range calibration sample[11]. This is currently one of the major issues in scanning probe microscopy; [C11] cites holographic gratings and C_{60} (with a 1.0 nm lattice constant) as possible distance / resolution calibration samples. However, it is known that that the 'Piezolever' probes have tip radii of ≤ 20 nm, thus a worse case lateral resolution of ≈ 40 nm (i.e. the maximum tip diameter) can be expected.

5.2.2.2 Thermal Drift

By observing and recording the vertical drift of a 0.9 μm length single line trace of a metal sample over a fixed period of time, it was possible to determine the 'Z' thermal drift rate; the drift rate was found to be $\approx 8 - 14$ nm/min.[12]; better results can be obtained by closely adhering to the guidelines listed in section 4.2.4.

The 'X'-'Y' thermal drift was investigated thru observations of the lateral drift in the position of the sample edge over several continuous scans; the observed drift was found to be negligible.

5.2.2.3 Minimum System Natural Frequency

The minimum natural frequency of the profilometer was found by exciting the system with an impulse load (e.g. a sharp blow on the granite table with a metal tool) while the instrument was profiling a smooth[13], flat area (e.g. the edge region of the sample was used). By observing the largest non-zero harmonic peak in the FFT of the scan trace, the minimum system natural frequency was found to be ≈ 180 Hz; this is comparable to the performance of other large sample size systems [C12].

5.3 Summary

In this chapter, the implemented profilometer system is presented along with an initial assessment of its performance. Test results are encouraging because they indicate that the implemented design is capable of meeting the original system specifications, although much work remains to be done to insure that the system operates robustly.

---

[11]The relatively low rigidity of large sample systems makes it difficult if not impossible to obtain atomic resolution images; in addition, atomic resolution images are typically taken over a few nanometers only (because atomically flat planes occur only over such scale), making them unsuitable for long range · calibrations.

[12]The exact state of the profilometer system during the drift experiments was: 1) AFM electrical cover not in place, 2) AFM optical camera lights left on, and 3) 'X' stage motor turned off.

[13]This is to minimize the magnitude of the non-zero frequency harmonics in the FFT scan trace due to sample roughness.

6 Conclusions and Recommendations

6.1 Discussion

In this chapter, the actual performance of the profilometer is briefly summarized, followed by recommendations for future work.

The AFM profilometer was successfully used to measure the profile of two-sided samples. Preliminary performance testing of the sample positioning system shows that it is capable of meeting the original positioning specifications-- in particular, the tilt angle positioning repeatibility and the maximum allowable flip offset error ($\delta_{y, flip\ offset}$). In addition, the sample positioning system was shown to provide the necessary mechanical and drift stability for demanding nanometer scale measurements. At the same time, specific problems (i.e. 'bugs') were found in the 'flip' stage (e.g. disengagement of the 'X'-'Y'-'Z' locator ball from one of the reference balls).

6.2 Suggestions for Further Work

Much work remains to be done before the machine can be considered fully operational. These include the following specific actions:

1) *corrective design*: fix the bugs (particularly the ball disengagement problem) in the 'flip' stage and perform tests to insure the necessary accuracy, reliability and robustness of the device;
2) *assess measurement accuracy and repeatibility* through sample measurements.

Lastly, based upon the experience gained with the 'flip' stage prototype, the following design changes (to the 'flip' stage) should be investigated:

1) *addition of damper(s) to the sample holder*: this will lessen the impact wear on the angle setting block / sample holder;
2) *placement of the angle block sensing limit switches on the sample holder itself*, this will eliminate the need to adjust limit switch positions every time a different tilt angle is used;
3) *optimal clamping force / release mechanism*: determine the optimal angle clamping force (I suspect the current clamping force is larger than necessary), alternately implement some sort of clamp release mechanism; these steps will prolong the life of the rotation axis bearings and motor;
4) *better / incorporate (other than tilt) angle adjustments*: currently this is done thru careful adjustments of the clamping screws, better alignment can be achieved thru wedge adjustment cams.

Appendix A: Probe Alignment in a Two Probe AFM Configuration (written 6 / 16 / 94)

At the first engineering review meeting, the possibility of a "two probe-on-one scanner" configuration was discussed. This was investigated, with the findings presented below.

Experimental Work

The alignment of the probe tips was investigated using the fixture jig shown below, a Nikon 30x magnification industrial inspection microscope, and 4 mounted Piezolevers (which were factory rejects-- probably, the ends of the probe tip had broken off). To determine alignment, each probe cartridge was placed on the 3 ball kinematic mount, and the X and Y position shift of the probe tip was measured with respect to the position of one of the probes. Results are as follows:
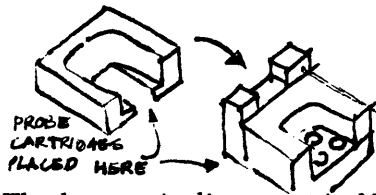
Probe #	deltaX	deltaY
2	180 μm	135 μm
3	135 μm	135 μm
4	157 μm	135 μm

The large misalignment in X and Y probe tip positions can be attributed to the fact that: 1) the Piezolevers are connected to large silicon blocks (from the micromachining process) which have no reference edges, hence it is difficult to align the probe (and maintain alignment) during assembly, and 2) the probes are affixed to the ceramic substrate with cynoacrillate ("Crazy Glue"), so some shifting in probe position is likely due to glue shrinkage. Looking at the data, it can be seen that there is good alignment in Y; the large difference between the first probe and the others may be because the first probe came from a seperate production batch. More probes have to be examined before a definitive conclusion can be reached.

Using the alignment jig, two probes were aligned under the optical microscope to about 33 and 15 μm in X and Y, respectively. The poor alignment achieved was due to the particular mechanical design used; better alignment can be expected with a flexure type stage (to be described later). Note that when viewed under the optical microscope with backlighting, a Piezolever is semitransparent (because it is made of a very thin layer of crystalline silicon), with the location of the probe tip clearly marked by a small black dot. Thus with a better alignment jig and higher optical magnification (with sufficient depth of field, perhaps a few thousandths of an inch), the probes can be expected to be aligned to a few microns.

Design considerations

Based on the experience above, possible mechanical configuration for the "two probe-on-one scanner" design are described below:

59

Confiugration	Advantage(s)	Disadvantage(s)
Two probes glued onto a single ceramic substrate	+ compact design	- custom probe configuration could be costly to manufacture; - if one probe is broken, entire cartridge (both probes) must be discarded;
Each probe mounted on its own ceramic substrate; with the two probes aligned via. a flexure jig (which is also mounted to the scanner)	+ probes are aligned (probably to a few microns); + if one probe breaks, the other can still be used (because it is mounted on a seperate cartridge)	- alignment jig (which will also be mounted to the scanner) is likely to be large in size; significant design and experimentation work required to insure that basic AFM performance, i.e. maximum scan speeds, resonant frequencies, rigidity is not compromised.
Each probe mounted on its own ceramic substrate; but probes are not aligned; some method of determining the relative positions of the probes required. (Note that this idea was suggested by one of the company engineers)	+ relatively compact design (basic AFM performance probably not an issue) + if one probe breaks, the other can still be used (because it is mounted on a seperate cartridge)	- blade has to be moved in X and Y by a few hundred microns (corresponding to the offsets)

Aside from the mechanical alignment problem, there is also the very important question of probe calibration-- i.e. tolerance in probe performance). This needs to be investigated in greater detail.
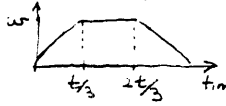
Appendix B: Motor Torque / Speed Requirements for a Gimbal Mount 'Flip' Stage

NOTE: CALCULATIONS DIFFER FROM STATED TEXT VALUES, BUT DO ILLUSTRATE PROCEDURE (CALCULATION IN TEXT UPDATED FROM CALC'S PRESENTED HERE)

Angle to move ~130°
Time to move ~5 sec. } $RPM_{avg} = \frac{1 \, rev}{10 \, sec.} = 0.1 \, rpm$

Trapezoid profile $\alpha_{max} = \frac{9\Omega}{2t^2} = \frac{9}{2} \cdot \frac{\pi \, rads}{(5 \, sec.)^2} = 0.56549 \, rad/sec.^2$

$\omega_{max} = \frac{3}{2} \cdot \frac{(\pi \, rads)}{(5 \, sec.)} = 0.94248 \, rad/sec.$

$\Sigma T = I\alpha$

$T_m - T_s - T_g - T_{sr} = I\alpha \Rightarrow T_m = I\alpha + T_g$

ASSUME ZERO

$I = \left(J_{motor} + J_{reducer} + \frac{J_{load}}{N^2} \right) N\alpha$

SAMPLE HOLDER

where $J_{reducer}$ and N are the gear/transmission ratios

Calculate inertia

STEEL

1" LONG
0.5"
1.75"
₵ OF ROTATION
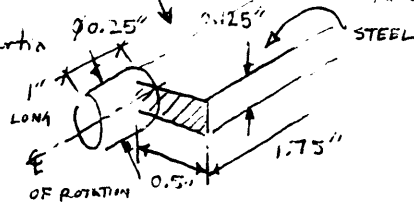
$\rho_{STEEL} = 7.9 \times 10^{-6} \, kg/mm^3$
$= 7900 \, kg/m^3$

for shaft $I = \frac{1}{2}mr^2$, $m = (\frac{\pi}{4} d^2 \ell)\rho$

$= \frac{1}{2}(0.003547 \, kg)(0.125 \, in.)^2 [2.54 \times 10^{-2} \, m/in.]^2 = 3.2030 \times 10^{-8} \, kg-m^2$

for 'plate' $I_c = \frac{mw^2}{12} = \frac{(0.5 \, in.)(1.75 \, in.)(0.125 \, in.)(7900 \, kg/m^3)[2.54 \times 10^{-2} \, m/in.]^3 (0.5 \, in.)^2}{12}$

$= 1.9031 \times 10^{-7} \, kg-m^2$, by the parallel axis theorem,

$I = I_c + md^2$

$T_g = dmg = (0.25 \, in.)(0.04159 \, kg)(9.81 \, m/s^2)[2.54 \times 10^{-2} \, m/in.]$

$= 0.00088201 \, N \cdot m$

$= 1.9031 \times 10^{-7} \, kg-m^2$
$+ (0.04159 \, kg)(0.25 \, in.)^2$
$= 7.6124 \times 10^{-7} \, kg-m^2$

Iteratively select a motor that (in the ideal case matches load inertia) and produces an approximate 2-3 times torque margin at the maximum speed (see manufacturer's motor catalogues).

63

POSITIONING STAGES

Linear, Low Profile, High Accuracy
ATS100 Series

- Travel range of 50 to 200 mm (2 to 8 in)
- Designed for high stiffness and stability
- Long life linear motion guide bearing system
- Ultra fine resolution to 0.1 micron
- Average accuracy better than
  ± 1 micron/25 mm (± 0.00004 in/in)
- Integral bellows waycovers
- Low profile, compact design

Shown with 50SMB2 Motor

The ATS100 series motor driven linear stages provide the high resolution and repeatability required for semiconductor wafer testing and fabrication, automated microscope inspection systems, and precision micro-machining applications.

Outstanding Construction Features

ATS100 series stages are machined from a special cast aluminum alloy to provide a high strength to weight ratio, and long term stability. The base is a box design that provides exceptional stiffness and stability. Optional models with all-steel construction are also available for severe temperature environments.
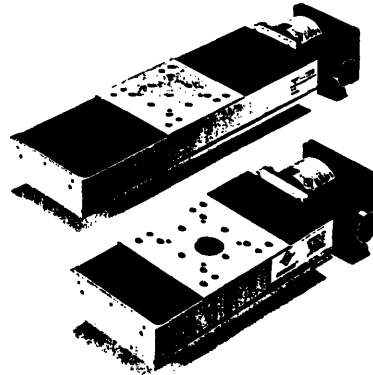
ATS100 series stages employ a precision ground ballscrew. The ballscrew is pre-loaded to eliminate backlash and the nut has wipers to prevent contamination and maintain high accuracy throughout the life of the stage. High quality, pre-loaded duplex bearings are used to eliminate axial play.

All ATS100 series stages incorporate linear motion guide bearing systems to provide high load capability and high stiffness. The LMG design provides a compact stage with continuous carriage support over the entire travel and good cantilevered load capability. Integral wipers on the bearing trucks help insure stage travel life in excess of 100 million inches. Highly accurate optical limit switches and cushioned end stops are also standard.

Integral bellows type waycovers protect the drive and bearing system from contamination. Metal surfaces are protected with an attractive clear anodized finish. Mounting holes on the stage table are ¼-20 on a one inch square grid pattern or M6 on a 25 mm grid pattern.

HAL Option for Improved Accuracy

The HAL option applies Aerotech's advanced motion control electronics to the ATS100 stages to provide submicron accuracy positioning systems. Each HAL stage is manufactured to exacting tolerances for superior straightness and flatness, then matched with a HAL-capable Aerotech UNIDEX motion controller for electronic compensation of leadscrew error. Every HAL stage is certified for better than ± 1 micron/200mm positioning accuracy and 0.3 micron bi-directional repeatability.

Precision XY and XYZ Configurations

Multi-axis ATS100 series configurations with optional precision alignment to provide orthogonality within 5 arc seconds are available. For Z-axis applications, Aerotech provides a choice of L-brackets. The HDZ1 accommodates stages up to the ATS100-125. The HDZ1L accommodates all stages in the series. See the Application of Aerotech Positioning Stages section for more information.

High Performance Drive Systems

ATS100 series stages are available with microstepping or DC servo motors. Speeds to 100 mm/sec are available, depending upon the drive system. ATS100 series stages can achieve resolutions as fine as 0.1 micron with microstepping drives. Servo motor equipped stages include a rotary encoder for closed loop position feedback.

Encoder position verification can be added to stepping motor driven stages to insure that the stage attains commanded position. Encoder verification is available with several UNIDEX motion controllers.

Vacuum Preparation

ATS100 series stage systems can be prepared for vacuum operation to 10^{-6} torr. Drive components are lubricated with vacuum compatible greases or solid lubricant. Polymeric materials are replaced or removed and teflon-coated wiring is used.

ATS100 Series Positioning Stage Specifications

Basic Model			ATS100-50	ATS100-100	ATS100-150	ATS100-200
Total Travel			50 mm (2 in)	100 mm (4 in)	150 mm (6 in)	200 mm (8 in)
Mechanical Drive System			Precision ground ballscrew			
Linear Resolution (2mm lead)			1,0 μm (40 μin) @2000 steps/rev motor resolution (0,1 μm to 10 μm available)			
Max. Travel Speed[1]	Stepping Motor		50 mm/sec (2 in/sec); 100 mm/sec (4 in/sec) with motor option 6 or 7			
	DC Servo Motor		100 mm/sec (4 in/sec)			
	HAL Option		25 mm/sec (1 in/sec)			
Max. Load Carrying Capability[2]	Horizontal		22,7 kg (50 lb)			
	Vertical		10.0 kg (22 lb)			
	Side		11,4 kg (25 lb)			
Accuracy[3]	Standard		± 2 μm (± 80 μin)	± 3 μm (± 120 μin)	± 5 μm (± 200 μin)	± 6 μm (± 240 μin)
	HAL Option		± 0,5 μm (± 20 μin)	± 0,5 μm (± 20 μin)	± 0,75 μm (± 30 μin)	± 1 μm (± 40 μin)
Repeatability	Standard		± 0.7 μm (30 μin) bi-directional			
	HAL Option		± 0.3 μm (12 μin) bi-directional			
Straightness and Flatness of Travel	Differential	Std.	2 μm/25 mm (80 μin/in)			
		HAL	1 μm/25 mm (40 μin/ in)			
	Maximum Deviation	Std.	± 1 μm (± 40 μin)	± 2 μm (± 80 μin)	± 2 μm (± 80 μin)	± 3 μm (±120 μin)
		HAL	0,5 μm (30 μin)	1,0 μm (40 μin)	1,5 μm (60 μin)	1,75 μm (70 μin)
Nom. Stage Weight	Less Motor		0.9 kg (2 lb)	1 kg (2.3 lb)	1.1 kg (2.5 lb)	1.2 kg (2.6 lb)
	With Motor[4]		2.4 kg (5.3 lb)	2,6 kg (5.6 lb)	2.7 kg (5.8 lb)	2.8 kg (6.1 lb)
Material			Aluminum			
Finish			Stage and Table: Clear Anodize			

Notes: 1. Non standard encoder resolution and/or screw pitch may limit speed to lower values.
Maximum speed with HAL option should be observed to minimize inaccuracies due to thermal expansion of the ballscrew.
2. Payload specifications are for single axis system and based on ballscrew and bearing life of 2500 km (100 million inches) of travel.
3. Values are maximum plus/minus deviation over full travel of stage
4. Add 0.7 kg (1.5 lb) for motor with tachometer.

Resolution Information

Resolution		Encoder	
Code	Travel/Step	Steps/Rev[2]	Model
20; 21[1]	1.0 μm (for 2 mm ballscrew)	2000	E500AS; E500LD
99	N/A	N/A	Home Marker (stepping models only)

Notes: 1. Code 21 and 41 specify line driver-type (LD) encoders.
2. Assumes times-4 interpolation by controller for encoder models.

Drive Information

Motor				Driver
Code	Type	Model	Cable	
1	Stepping	50SMC2N	Integral	DM4001
2	DC Servo	1035LT-DC2	Integral	DSL4020 or DS16020
3	DC servo + Tach	1035DC-MSOF	DC-MSO	(40 V bus; 4A)
4	Stepping	50SMB2	SMS-O	DM4001
			SMC	U100M
5	DC Servo	1035LT-MSOF	DC-MSO	DSL4020 or DS16020 (40 V bus; 4A)
			DCC	U100S
6	Stepping	101SMC2N	Integral	DM4005
7	Stepping	101SMB2	SMS-0 SMC	DM4005
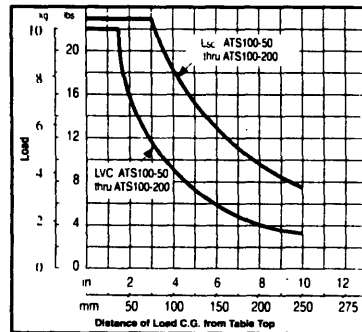
Lvc and Lsc Cantilevered Load Capability (ATS 100 Series)

Loading vs. Travel Life (ATS100 Series)

7

ATS100 Series Positioning Stage Dimensions
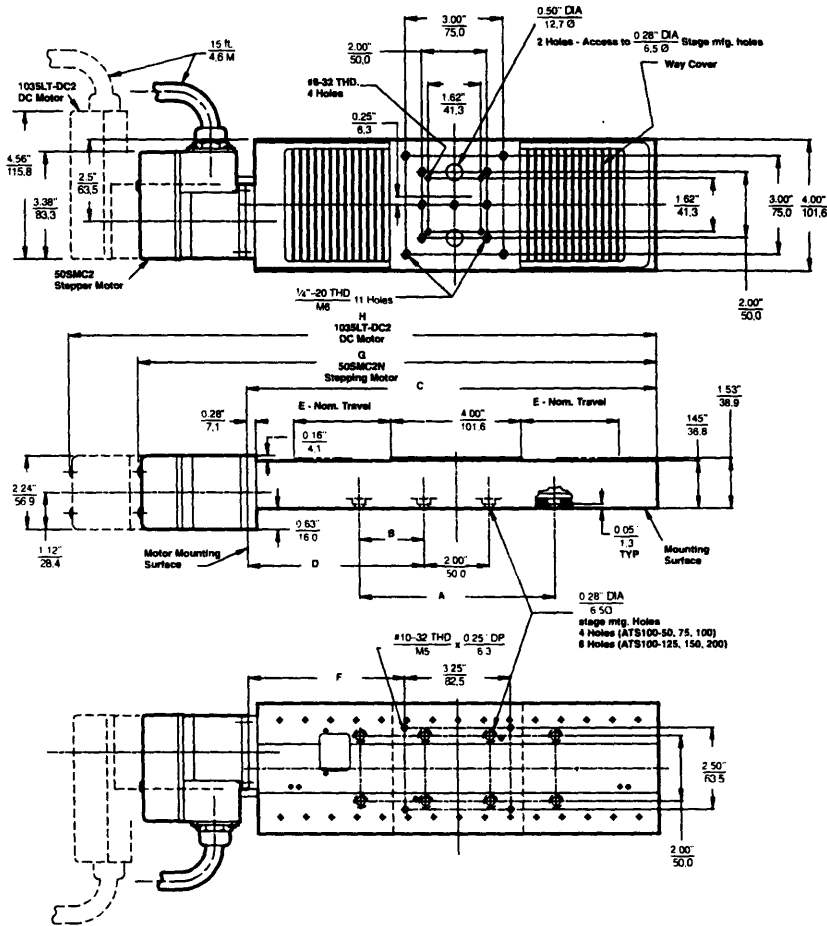
Basic Model	A	B	C	D	E	F	G	H
ATS100-50	—	—	8.60"/218,4	3.47"/88,5	1.00"/25,4	2.84"/72,3	11.92"/302,8	14.02"/356,1
ATS100-100	—	—	10.60"/269,2	4.47"/113,9	2.00"/50,8	3.84"/97,7	13.92"/353,6	16.02"/406,9
ATS100-150	6.00"/150,0	2.00"/50,0	12.60"/320,0	5.47"/139,3	3.00"/76,2	4.84"/123,1	15.92"/404,4	18.02"/457,7
ATS100-200	6.00"/150,0	2.00"/50,0	14.60"/370,8	6.47"/164,7	4.00"/101,6	5.84"/148,5	17.92"/455,2	20.02"/508,5

ATS100 Series Positioning Stage Ordering Information

Example: ATS100 - 50 - M - 20P - 1 - 99/ NPA/

ATS100	-50	-U	-20P	-1	-99	-(Opt.)/
Series	Travel	Mounting and Grid Pattern	Drive Screw	Motor Option	Encoder Resolution[1] (steps/rev)	Stage and Assembly Options
	50 = 50 mm 100 = 100 mm 150 = 150 mm 200 = 200 mm	M = Metric U = English	20P = 2 mm/rev precision ground ballscrew	1 = Stepping motor with integral cable 2 = DC servo motor with integral cable[1] 3 = DC servo motor and tachometer with connector[1] 4 = Stepping motor with connector 5 = DC servo motor with connector[1] 6 = High torque stepping motor with integral cable 7 = High torque stepping motor with connector	00 = No encoder or marker 20 = 2000 21 = 2000[2] 99 = Stepping motor home marker	- A - K - HAL - STEEL - VAC MP100/ NPA/ PAxxx/

Notes: 1. Servo motors require encoder (resolution) option.
2. Resolution option 21 specify line driver-type encoders.

Basic Model	Description	Price
ATS100-50	50 mm (2 in) travel stage with limits	$ 2,375
ATS100-100	100 mm (4 in) travel stage with limits	$ 2,655
ATS100-150	150 mm (6 in) travel stage with limits	$ 2,835
ATS100-200	200 mm (8 in) travel stage with limits	$ 3,140

Options

-M	Metric dimension mounting pattern and holes	N/C
-U	English dimension mounting pattern and holes	N/C
-20P[1]	2 mm/rev precision ground ballscrew	N/C
-1	Stepping motor 50SMC2N with 4.6 m (15 ft) integral cable	$ 350
-2	DC servo motor 1035LT-DC2 with 4.6 m (15 ft) integral cable	$ 470
-3[1]	DC servo motor/tach 1035DC-MSOF with connector	$ 580
-4[1]	Stepping motor 50SMB2 with connector	$ 295
-5[1]	DC servo motor 1035LT-MSOF with connector	$ 460
-6	Stepping motor 101SMC2N with 4.6 m (15 ft) integral cable	$ 415
-7[1]	Stepping motor 101SMB2 with connector	$ 360
-20,-21	Encoder and resolution	$ 295
-99	Home marker (one count per rev) for stepping motors only	$ 175
-A	Aperture table and base	$ 255
-K	Manual positioning knob (stepping motor only)	$ 40

-HAL	High accuracy system	$ 560
-STEEL	All-steel construction	Add 15% to base price
-VAC	Vacuum preparation to 10⁻⁶ torr	$ 1,275

Notes: 1. Requires motor-to-controller cable. Refer to specification section for proper cable selection.

Stage Assembly Options

NPA/[1]	Non precision XY, XZ or XYZ assembly	$ 120
PA10/[1]	XY assembly; 10 arc sec orthogonal	$ 360
PA10B/[1]	XZ or YZ assembly with L-bracket; 10 arc sec orthogonal	$ 560
PA5/[1]	XY assembly; 5 arc sec orthogonal	$ 560
PA5B/[1]	XZ or YZ assembly with L-bracket; 5 arc sec orthogonal	$ 765

Notes 1. See "Standard Assembly Configurations" in the stage application section for multi-axis assembly information

Accessories

HDZ1/	Right angle L-bracket	$ 305
HDZ1L/	Right angle L-bracket	$ 385
MP100/	Base mounting plate	$ 70

Axis Calibration - HAL2000

LABEL ON EEPROM / FILE : _____ (TABLE ON PAGE 2)
CUSTOMER ORDER # _____ *51916 B* _____
AXIS: _____
STAGE MODEL & SERIAL # *ATS100-200 (MFC108-47/13)*
MOTOR MODEL & SERIAL # _____
DRIVE MODEL & SERIAL # _____
RESOLUTION: _____ *,0005 MM* _____
Laser Interferometer Model # *HP 5505A* _____

OTHER PARAMETERS:

1. Torque on bolts _____ *30 IN-LBS* _____
2. Air Temperature _____ *21.1 °C* _____
3. Stage Temperature _____ *21.9 °C* _____
4. Motor Flange Temperature _____ *24.1 °C* _____
5. Stage Base Temperature _____ *23.9 C* _____
6. Stage Far End Temperature _____ *21.5 °C* _____
7. Flatness Specification of Supporting Table *5 u. inch/inch*
8. Calibration Distance _____ *200 MM* _____
9. Number of Calibration Points _____ *400* _____
10. Distance from Ball Screw to measurement axis (Vertical) *60 MM*
11. Distance from Ball Screw to measurement axis (Horizontal) *0 MM*
12. Maximum Operating Speed _____
13. Maximum Duty Cycle _____
14. Backlash _____ *0* _____
15. Home Offset (Linear Encoders) _____

NOTES:

1. Any frictional heating of the ball screw is to be avoided to maintain specified accuracies.
2. Thermal expansion characteristics of the ball screw are as specified in the data sheet on page 3.
3. For linear encoder applications; accuracies can only be achieved from the home offset position.

Calibration performed by: *J Gorala* _____ Date: *10/31/*

Linear Error Plot - X-Axis (4/18/94 9:00:06 AM)

Error in um

Machine Name:	ATS100-200-U-20P	Environment Data: Metric
File Name:	mit.lin	
Operator:	R.C	
Location:	1.75"/35,0mm ABOVE	
Serial No:	MFC108-47/13	
Comments:		

Numerical Analysis:

Machine Position in mm

75

FLATNESS   Error Plot - X-Axis (10/29/94 7:36:50 AM)

Error in um

Machine Position in mm
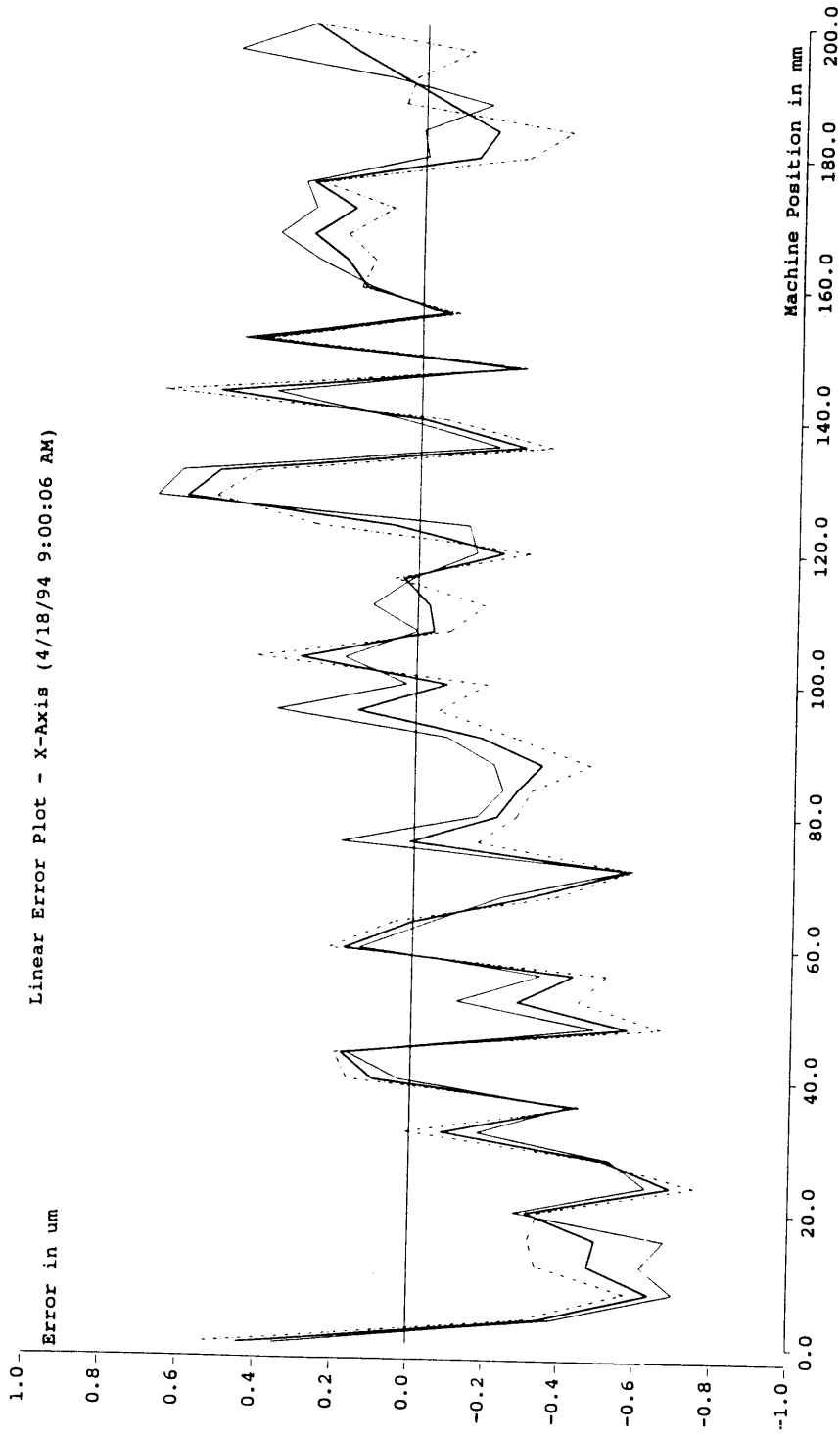
Numerical Analysis:

Machine Name:	ATS100-200-U-20P
File Name:	200.str(Mod)
Operator:	R.C
Location:	1.75" ABOVE TABLE
Serial No:	MFC108-47/13
Comments:	
MAX ERROR +3 MICRONS	
MIN ERROR -3 MICRONS	

Environment Data: Metric

STRAIGHTNESS   Error Plot - X-Axis (10/24/94 4:48:56 PM)

Error in um

Machine Position in mm

Numerical Analysis:	Machine Name:	ATS100-200-U-20P	Environment Data: Metric

File Name: 200.str
Operator: R.C
Location: 1.75" ABOVE TABLE
Serial No: MFC108-47/13
Comments:
MAX ERROR +3 MICRONS
MIN ERROR -3 MICRONS

SPECIFICATIONS

<table>
<tr><th rowspan="2" colspan="2">Unit Model</th><th>Single Shaft</th><th>RFK543AA</th><th>RFK544AA</th><th>RFK545AA</th><th>RFK564AA</th><th>RFK566AA</th><th>RFK569AA</th></tr>
<tr><th>Double Shaft</th><th>RFK543BA</th><th>RFK544BA</th><th>RFK545BA</th><th>RFK564BA</th><th>RFK566BA</th><th>RFK569BA</th></tr>
<tr><td rowspan="8">M O T O R</td><td>Holding Torque [1]   oz-in (kgcm)</td><td></td><td>18.1 (1 3)</td><td>25.0 (1.8)</td><td>33.3 (2.4)</td><td>58.3 (4.2)</td><td>115 (8.3)</td><td>231 (16.6)</td></tr>
<tr><td>Rotor Inertia   oz-in² (gcm²)</td><td></td><td>0 19 (35)</td><td>0.30 (54)</td><td>0.37 (68)</td><td>0.96 (175)</td><td>1.53 (280)</td><td>3.06 (560)</td></tr>
<tr><td>Rated Current</td><td></td><td colspan="3">0.75 A / phase</td><td colspan="3">1.4 A / phase</td></tr>
<tr><td>Step Angle (Full)</td><td></td><td colspan="6">0.72"</td></tr>
<tr><td>Insulation Class</td><td></td><td colspan="6">Class B [266°F (130°C)]</td></tr>
<tr><td>Insulation Resistance</td><td></td><td colspan="6">100MΩ or more under normal ambient temperature and humidity when the megger reading between the windings and the frame is 500V DC.</td></tr>
<tr><td>Dielectric Strength [2]</td><td></td><td colspan="6">Under normal ambient temperature and humidity, sufficient to withstand 1.0kV at 60Hz applied between the windings and the frame for one minute following a period of continuous operation.</td></tr>
<tr><td colspan="8"></td></tr>
<tr><td rowspan="17">D R I V E R</td><td colspan="2">Power Consumption</td><td colspan="3">24V DC ± 10% 1.1A Max.</td><td colspan="3">24V DC ± 10% 1.7A Max.</td></tr>
<tr><td colspan="2">Output Current</td><td colspan="3">0.15 ~ 0 75 A / phase</td><td colspan="3">0.17 ~ 1.4 A / phase</td></tr>
<tr><td colspan="2">Excitation mode:</td><td colspan="6">Microstep</td></tr>
<tr><td rowspan="6">I n p u t   S i g n a l s</td><td>• Input Signal Circuit</td><td colspan="6">Photocoupler Input (optically isolated). Input Impedance: 220Ω. Input Current 20mA max.
H : 4 ~ 5V   L : 0 ~ 0 5V</td></tr>
<tr><td>• Pulse Input</td><td colspan="6">Step Command Input
Pulse width: 1 μ sec. minimum. Pulse rise/pulse fall time 2 μ sec. maximum. Motor moves at pulse rising edge (Negative logic pulse input)</td></tr>
<tr><td>• Direction-of-Rotation Input</td><td colspan="6">Directional Input
Pulse width: 1 μ sec minimum. Pulse rise/pulse fall time 2 μ sec maximum. Motor moves at pulse rising edge. (Negative logic pulse input)</td></tr>
<tr><td>• Resolution select input (RS1/2)</td><td colspan="6">At Level "H", a step angle will be selected between 0.72° and 0.00288° as preset by Step Angle Setting Switch RS1.
At Level "L", the step angle will be selected between 0.72 and 0.00288° as preset by Step Angle Setting Switch RS2.</td></tr>
<tr><td>• All Windings OFF Input</td><td colspan="6">At H level, the current set by RUN potentiometer is supplied to the motor.
At L level, the current to the motor is cut off and the shaft can be rotated by hand.</td></tr>
<tr><td></td><td colspan="6"></td></tr>
<tr><td rowspan="2">O u t p u t   S i g n a l s</td><td>• Output Signal Circuit</td><td colspan="6">Photocoupler, Open-Collector Output
External use condition: 24V DC maximum, 10mA Max.</td></tr>
<tr><td>• Excitation-Timing Output</td><td colspan="6">Signal is output every time the excitation sequence returns to step 0. (Photocoupler is ON)
0.72°/Step (Resolution 1): Signal is output every 10 pulses
0.072°/Step (Resolution 10): Signal is output every 100 pulses</td></tr>
<tr><td colspan="2">Functions</td><td colspan="6">Automatic-Current-Cutback at Motor Standstill, Pulse input mode change</td></tr>
<tr><td colspan="2">Driver Cooling Method</td><td colspan="6">Convection Cooling</td></tr>
<tr><td rowspan="2">Weight</td><td>Motor lbs (kg)</td><td></td><td>0.55 (0.25)</td><td>0.66 (0.3)</td><td>0.88 (0.4)</td><td>1.33 (0.6)</td><td>1.76 (0.8)</td><td>2.87 (1.3)</td></tr>
<tr><td>Driver lbs (kg)</td><td colspan="6">0.79 (0.36)</td></tr>
<tr><td rowspan="2">Ambient Temperature</td><td>Motor</td><td colspan="6">+14°F ~ +122°F (–10°C ~ +50°C)</td></tr>
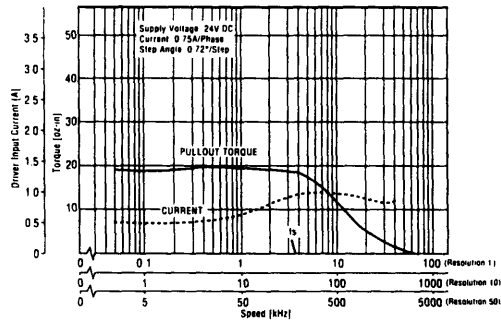<tr><td>Driver</td><td colspan="6">+32°F ~ +104°F (0°C ~ +40°C)</td></tr>
</table>

① The value given for holding torque is the value operated by dedicated driver with rated current and 4-phase excitation.
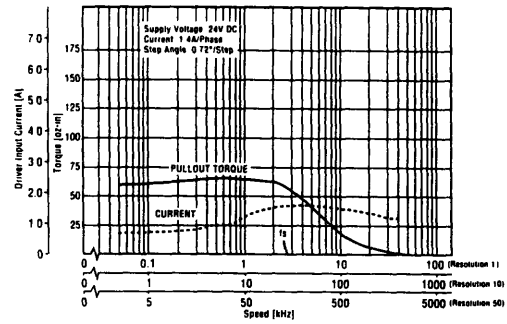② Dielectric strength for RFK54 □A type is 0.5kV at 60Hz.

2

SPEED vs. TORQUE CHARACTERISTICS

RFK543AA
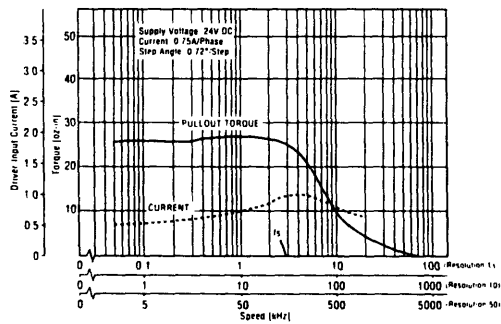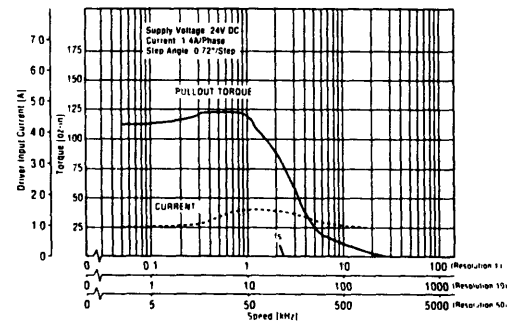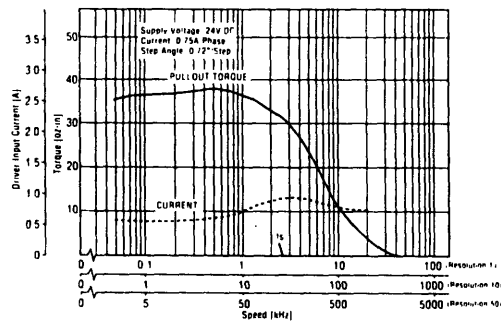**RFK543BA**

RFK564AA
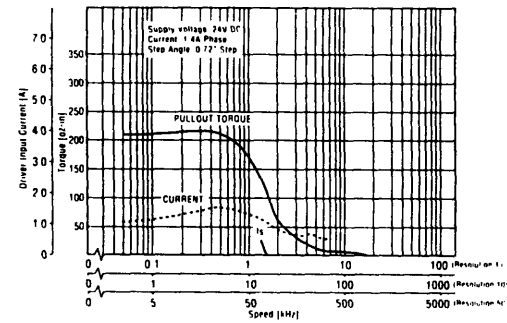**RFK564BA**

RFK544AA
RFK544BA

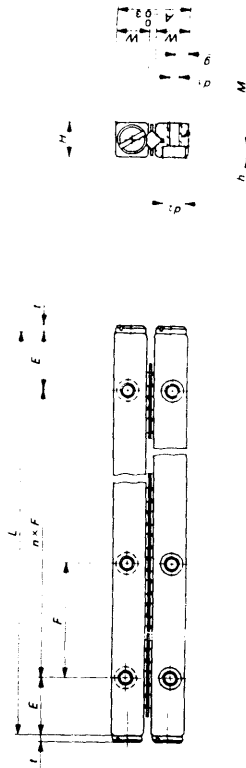**RFK566AA**
RFK566BA
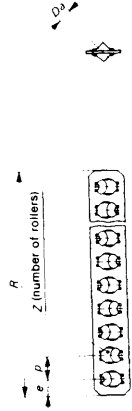

RFK545AA
RFK545BA

RFK569AA
RFK569BA

● **Step resolution does not affect torque based on the speed (rpm) of the motor.**

3

Crossed Roller Way CRW

Main dimensions / Nominal dimensions

Model number	Weight Way (kg/m)	Weight Roller cage (g)	A	H	L (n×F)	E	De	R	Z	p
CRW 1- 20	0.12	0.38	8.5	4	20 (1×10)	5	1.5	16.5	5	3
CRW 1- 30					30 (2×10)			25.5	8	
CRW 1- 40					40 (3×10)			31.5	10	
CRW 1- 50					50 (4×10)			37.5	12	
CRW 1- 60					60 (5×10)			43.5	14	
CRW 1- 70					70 (6×10)			52.5	17	
CRW 1- 80					80 (7×10)			61.5	20	
CRW 2- 30	0.24	0.98	12	6	30 (1×15)	7.5	2	29.6	7	4
CRW 2- 45					45 (2×15)			41.6	10	
CRW 2- 60					60 (3×15)			53.6	13	
CRW 2- 75					75 (4×15)			65.6	16	
CRW 2- 90					90 (5×15)			77.6	19	
CRW 2-105					105 (6×15)			89.6	22	
CRW 2-120					120 (7×15)			101.6	25	
CRW 2-135					135 (8×15)			113.6	28	
CRW 2-150					150 (9×15)			125.6	31	
CRW 2-165					165 (10×15)			137.6	34	
CRW 2-180					180 (11×15)			149.6	37	
CRW 3- 50	0.50	2.96	18	8	50 (1×25)	12.5	3	42	8	5
CRW 3- 75					75 (2×25)			62	12	
CRW 3-100					100 (3×25)			82	16	
CRW 3-125					125 (4×25)			102	20	
CRW 3-150					150 (5×25)			122	24	
CRW 3-175					175 (6×25)			142	28	
CRW 3-200					200 (7×25)			162	32	
CRW 3-225					225 (8×25)			182	36	
CRW 3-250					250 (9×25)			202	40	
CRW 3-275					275 (10×25)			222	44	
CRW 3-300					300 (11×25)			242	48	

Mounting dimensions / Load ratings

e	W	g	M	d_1	d_2	h	t	Basic dynamic load rating C_u (kgf)	Basic static load rating C_{ou} (kgf)	Allowable load F_u (kgf)	Model number
2.5	3.9	1.8	M2	1.65	3	1.4	1.7	13	12	4	CRW 1- 20
											CRW 1- 30
											CRW 1- 40
											CRW 1- 50
											CRW 1- 60
											CRW 1- 70
											CRW 1- 80
3.8	5.5	2.5	M3	2.55	4.4	2	1.5	31	30	10	CRW 2- 30
											CRW 2- 45
											CRW 2- 60
											CRW 2- 75
											CRW 2- 90
											CRW 2-105
											CRW 2-120
											CRW 2-135
											CRW 2-150
											CRW 2-165
											CRW 2-180
3.5	8.3	3.5	M4	3.3	6	3.1	2	68	62	21	CRW 3- 50
											CRW 3- 75
											CRW 3-100
											CRW 3-125
											CRW 3-150
											CRW 3-175
											CRW 3-200
											CRW 3-225
											CRW 3-250
											CRW 3-275
											CRW 3-300

Z (number of rollers)

Advanced 2/4-Axis Open Loop Motorizer Controller
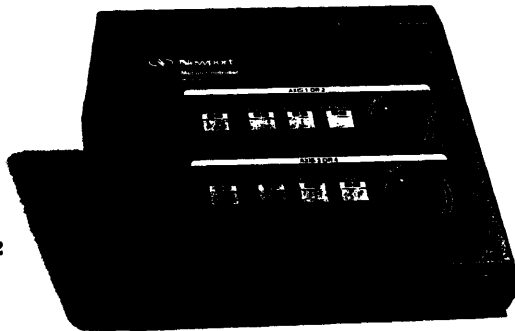
860-C2

- **Simultaneous control of two or four motorized devices**

- **Advanced velocity servo provides continuously-variable speed control**
  A high degree of load-independence provides excellent bi-directional motion reproducibility

- **Dynamic braking for precision start/stop**

- **Built-in joystick port**

- **TTL/analog ports for automated control**

The advanced **Model 860-C2 Motorized Drive Controller** provides continuously-variable, virtually load-independent free-running (RUN) and increment (JOG) motions of two out of four axes at a time under manual or automated control.

Motion parameters are easily selected and commanded by front-panel buttons and knobs or TTL and analog control lines. Front-panel indicator lights operate under manual or automated actuation to show direction of travel, limit/stall conditions, power-on, and RUN or JOG mode for each axis. 860-C2 features a novel limit/stall protection strategy with automatic back-off to protect motors and gearboxes and prevent jamming. Its built-in universal power supply provides world-wide compatibility.

Intuitive, responsive manual control

From the front panel, select RUN or JOG mode, dial-in the desired velocity, and press and FORWARD or REVERSE buttons to commence motion. JOG mode allows very short bursts or motion which have been interferometrically demonstrated down to 0.1 µm using standard 860A drives.

860-C2 features a connector for any PC-compatible game joystick such as our Model PMC200-J. This provides especially intuitive manual control for one- or two-axis positioning applications such as microscopy and probing.

Versatile automation features

860-C2 features TTL control, axis-select and status lines plus analog velocity-command lines for setting speed. Very fine incremental motions can be commanded by pulsing the TTL lines.

Provided with each 860-C2 is a sample program — documented in the manual — which allows motion execution directly from the keyboard of any PC-compatible via the

parallel printer ports standard in any PC. By sending standard ASCII characters out the parallel port, you can set the port's TTL lines as desired to control the 860-C2. For Macintosh users, free for the asking is a sophisticated LabVIEW™ driver which provides jog, run and velocity control and facilitates easy integration of the 860-C2 into complex setups via National Instruments' popular MIO-Series analog/digital I/O boards.

Specifications

|	
Device compatibility	860 860A
Number of axes	Simultaneous 2-axis control. 2 out of 4 total axes may be selected
Minimum 860A increment	0.2–0.5 µm typical, 0.1 µm demonstrated
860A speed range	50–100 µm, sec ±10% typical. 0–12 lb. axial load
Weight	5 lb. (2.3 kg)
Size	10 · 8 · 4 inches (254 · 203 · 102 mm)
Power	90–132 180–250 VAC, 47–63 Hz; meets FCC 20870 and VDE 0871 requirements; includes AC line filter
Control ports	PC-compatible joystick; DB-25 TTL, parallel I-O control port; DB-9 analog velocity control port
Utility software	PC keyboard control (requires cable, DOS 2.0 or later); LabVIEW 2.x driver (free on request; requires Newport LA-NB-MIO Series or equivalent A D I O board)

Ordering Information

	Model	Price
Dual-axis controller	860-C2	$1,418
Joystick (860-C2 only)	PMC200-J	$ 168
10 ft. interconnecting cable	860I-10	$ 15

9.24   *U. S. Domestic Prices Shown*   Newport

Open-Loop Motorized Drives
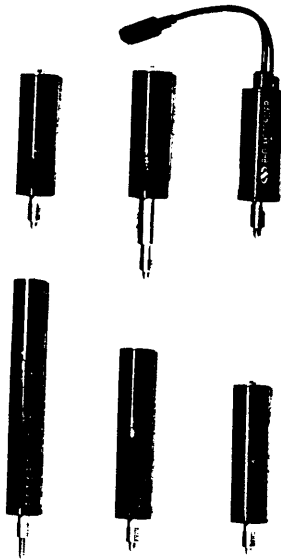
860A Series

- **Sub-μm minimum incremental motion**
  Interferometrically verified remote positioning capability to 0.1 to 0.5 μm

- **Long-travel drives are easily interchangeable with micrometers in Newport mounts and stages**

- **Smooth, cool-running DC servo motors**
  Continuously variable speed; high thrust; stable with power on or off

- **Choice of controllers**
  Choose from an inexpensive hand-held controller (861) or sophisticated manual computer-controllable multi-axis controllers.

Newport's 860A Motorized Drives incorporate many of the same robust construction features and precision assembly of the new 850B Closed-Loop Actuators. They are ideal for applications where position feedback or display are unnecessary, or when an external encoder or feedback device is used. 860A drives are useful in a broad range of applications:

— They provide sub-μm remote actuation when limited-access or hazardous conditions inhibit manual adjustment of micrometers.

— They eliminate the inevitable disturbances that occur when a sensitive component's micrometers are touched. Controlled by our advanced **860-C² Motorized Drive Controller**, they can be integrated into automated closed-loop applications incorporating external interferometry or other advanced direct-motion metrology techniques.

— The 860-C² controller also provides a joystick port to provide especially intuitive simultaneous control of two motorized drives — ideal for probing and microscopy applications.

Very often, a component's micrometers may be quickly replaced by 860A series actuators without disturbing experiment setups.

Precision construction for sub-μm motion

Like the 850B closed-loop actuators, these inexpensive motorizers incorporate precision-ground and electropolished stainless-steel leadscrews and low-backlash reduction gears. Smooth, cool-running DC motors are integrated into the assembly via a patented technique that allows the motor-gearbox assembly to float, decoupling slight drivetrain eccentricities from the rotating spindle without introducing friction (U.S. Patent 4,496,865). Spindle position indicators are visible through hard windows and are referenced against permanently-engraved English and metric-unit scales.
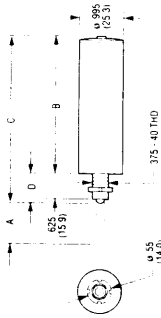
Ordering Information

m. (mm)	Model	Price
Actuator travel		
0.25 (6)	860A-025	$425
0.5 (13)	860A-05	$410
0.5 (13)	860A-05MM*	$447
1.0 (25)	860A-1	$431
2.0 (51)	860A-2	$483
1.0 (102)	860A-4	$541
High-speed versions		
0.5 (13)	860A-0.5-HS	$593
1.0 (25)	860A-1-HS	$688
2.0 (51)	860A-2-HS	$746

*Versions, Models 861 and 862 stages, and 860-C² and 865 series motor mounts

860A SERIES

MODEL 860A-05MM

| MODEL	A	B	C	D
860A-025	.250 (6.4)	2.59 (65.8)	1.27 (83.1)	6.8 (17.3)
860A-05-HS	.500 (12.7)	3.09 (78.5)	3.77 (95.8)	6.8 (17.3)
860A-05MM	.500 (12.7)	3.09 (78.5)	4.96 (124.5)	6.8 (17.3)
860A-1-HS	1.000 (25.4)	3.66 (93.0)	4.58 (116.3)	8.8 (22.4)
860A-2-HS	2.000 (50.8)	4.72 (119.9)	5.64 (143.3)	8.8 (22.4)
860A-4	4.000 (101.6)	6.91 (175.5)	7.83 (198.9)	8.8 (22.4)

PM500 Ultra-Resolution Motion Systems

- **Sub-micron incremental motion**
- **Glass scale encoder on the output shaft**
- **Non-rotating tip design**

The **PM500** family offers the broadest line of ultra-resolution motion devices in the industry: our micrometer-replacement actuators incorporate an integral glass-scale encoder on the output shaft, virtually eliminating all sources of error due to mechanical buildup in the drive-train. Coupled with a non-rotating tip design, this actuator provides performance unmatched in the industry. For complete information, see page **5.4**.

PM500-A1 Micrometer-Replacement Actuator
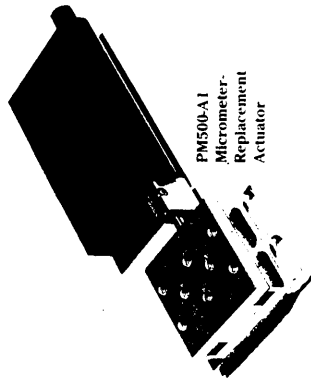
MicroMo® MOTORS

Stepping Gearmotor Series AM1524

- 24 Steps Per Revolution (step angle: 15°).
- High Holding Torque.
- High Speed Operation.
- Available With a Variety of Gearheads Including Our 15/2, 15/3, 15/5, 15/6, 15/8, 16A, and 16/7 (Ratios 3.45 to 235,067:1).
- Double Shaft Standard, Single Shaft Available.

Actual Size
with Gearhead

Electrical Specifications:

	Voltage Mode			Current Mode
For Type	V-6-35	V-12-150	V-24-590	A-0.25-12.5
Phase Resistance (Ohms):	35	150	590	12.5
Phase Inductance (1kHz) mH:	15	65	239	5.5
Nominal Current/Ph (2 ph on) A:	0.15/6V	0.075/12V	0.037/24V	0.25
Nominal Current/Ph (1 ph on) A:	0.20/8V	0.100/15V	0.052/34V	0.35
Back EMF Amplitude V/K steps/second:	6	12	24	3.5
Dielectric Test (1 min):	500 Vrms All Types			
Electrical Time Constant:	0.4 msec All Types			

Mechanical Specifications:

Nominal Holding Torque (2 phase on)[1]:	6mNm (0.84 oz-in) All Types
Holding Torque (2x nominal current)[1]:	10mNm (1.4 oz-in) All Types
Detent Plus Friction Torque[1]:	0.9mNm (0.12 oz-in) All Types
Absolute Angular Accuracy[2] (2ph on, full step):	± 3% of Full Step All Types
Rotor Inertia:	6.4×10^{-6} oz-in-sec^2 All Types
Nominal Acceleration:	130,000 rad/sec^2 All Types
Resonant Frequency:	120 Hz All Types
Thermal Resistance Coil-Air:	55°C/W All Types
Maximum Coil Temperature:	130°C (266°F) All Types
Operating Temperature[3]:	-20°C to +45°C (-4 F to +113°F) All Types
Thermal Time Constant:	220 sec All Types
Maximum Shaft Loading:	
Radial:	0.5N (1.8 oz) All Types
Axial:	0.5N (1.8 oz) All Types
Bearings:	Sleeve (Ball Bearing Optional) All Types
Maximum Bearing Play:	
Radial; with 0.72 oz Load:	0.59×10^{-6} in All Types
Axial; with 0.72 oz Load:	5.9×10^{-6} in All Types
Weight:	12g (0.42 oz) All Types

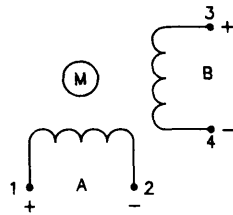(1) With bipolar driver.
(2) Requires balanced phase currents.
(3) For higher temperatures, derate phase current.

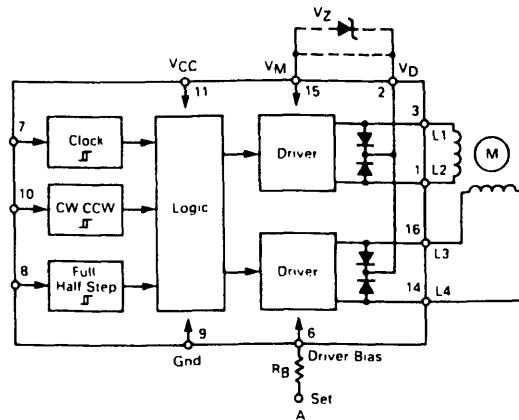—Specifications Subject to Change—

STEPPING GEARMOTORS

| Phase A	B	Direction of rotation
+	+	
−	+	
−	−	CW ⬇ CCW
+	−	
Driving sequence Full step 2 phases ON		

Recommended Voltage Mode Driver (Motorola SAA 1042)

The SAA1042 drives a two phase stepper motor in the bipolar mode. The device contains three input stages, alogic section and two output stages.
- Drive stages designed for motors from 6 to 12V.*
- 500m/A coil drive capability.
- Built in clamp diodes for over voltage protection.
- Wide logic supply voltage range; (V_CC=5V to 18V)*.
- Accepts commands for CW/CCW and Half/Full Step operation
- Inputs compatible with popular logic families; MOS, TTL, DTL.

*Use the SAA1042A for 24V motors

Recommended Current Mode Driver (Ericsson PBL3770A)
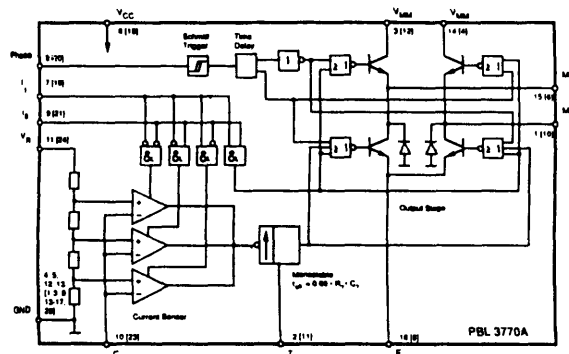
This PBL3770A is a bipolar monolithic circuit intended to control and drive the current in one winding of a stepper motor. The circuit consists of a LS-TTL compatible logic input stage, a current sensor, a monostable multivibrator, and a high power H-bridge output stage. The circuit is pin-compatible with the PBL3717 industry standard driver.
- Half-step and full-step operation
- Switched mode bipolar constant current drive.
- Wide rnage of current control 5 - 1800mA.
- Wide voltage rnage 10 - 45V.
- Designed for unstabilized motor supply voltage.
- Current levels can be selected in steps or varied continuously.
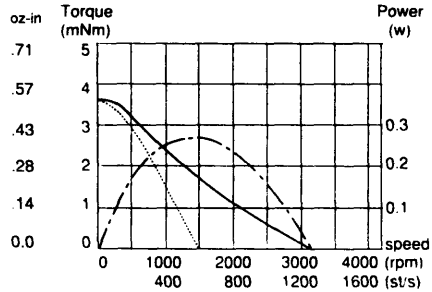- Thermal overload protection.

Stepping Gearmotor Series AM1524
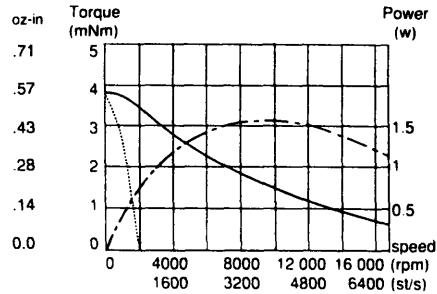
Dimensional Outlines: DYNAMIC CHARACTERISTICS

AM1524–V–...
Voltage Mode Characteristics Shown Using The
Motorola SAA 1042(A) Driver (24 volt version)

AM1524–A–...
Current Mode Characteristics Shown Using The
Ericsson PBL3770A Driver 18V


```
........  Start-stop mode
          Load inertia: 10⁻⁸kg·m·  (1.41 x 10⁻⁶ oz-in·s²)

          Slew mode operation
          Load inertia: 8 x 10⁻⁸kg·m·  (1.13 x 10⁻⁵ oz-in·s²)

          Mechanical power
```

Ordering Information:

Example: To order a 6 volt AM1524 Motor with rear shaft intended to fit our 15/5 Gearhead, specify:

Motor   AM1524 V 06 35 06 ... + 15/5 , 141:1

- Series
- Mode
  - V = Voltage
  - A = Current
- Voltage/Current Options
  - 06 = 6 volt
  - 12 = 12 volt
  - 24 = 24 volt
  - 25 = 25 Amp
- Desired Gear Ratio
- Desired Gearhead Series
- Special Order Numbers (where applicable)
- Shaft Type
  - With rear shaft 04* = 1.5mm dia. x 6.3mm shaft end
  - Without rear shaft 05* = 1.5mm dia. x 6.3mm shaft end
  - With rear shaft 06 = E pinion for Gearheads 16A, 15/2, 15/3, 15/5, 15/6, 15/8
  - Without rear shaft 07 = E pinion for Gearheads 16A, 15/2, 15/3, 15/5, 15/6, 15/8
  - *04 or 05 version required for 16/7
- Phase Resistance
  - 35 = 35 Ohms (6v version)
  - 150 = 150 Ohms (12v version)
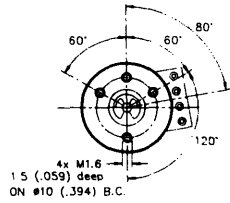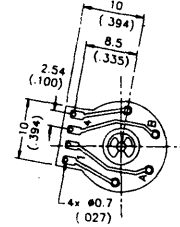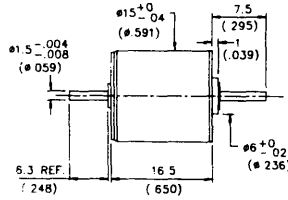 - 590 = 590 Ohms (24v version)
  - 12.5 = 12.5 Ohms (Current version)

Stepping Gearmotor Series AM1524

Dimensional Outlines:

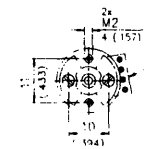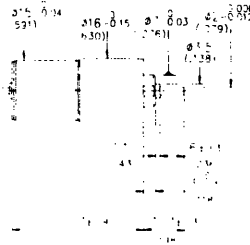**Front View**
Motor AM1524 ...

Rear View

Front View
With Gearhead 16A

Gear Ratio	L1 mm	in
11.8:1	26.0	1.02
22:1	27.8	1.10
41:1	27.8	1.10
76:1	29.6	1.17
141:1	29.6	1.17
262:1	31.3	1.23
485:1	31.3	1.23
900:1	33.1	1.30
1670:1	33.1	1.30
3101:1	34.8	1.37
5752:1	34.8	1.37
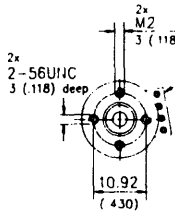
Front View
With Gearhead 15/5, 15/6, 15/8*
*15/8 Available with ratios 76:1 through 900:1 only.
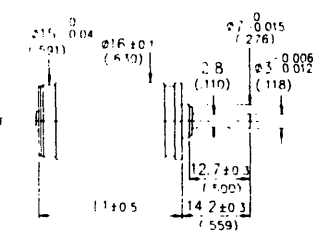
Gear Ratio	L1 mm	in
6.3:1	30.1	1.19
11.8:1	30.1	1.19
22:1	33.8	1.33
41:	33.8	1.33
76:1	35.9	1.41
141:1	35.9	1.41
262:1	38.0	1.50
485:1	38.0	1.50
900:1	40.1	1.58
1670:1	40.1	1.58
3101:1	42.2	1.66
5752:1	42.2	1.66
10683:1	44.3	1.74
19813:1	44.3	1.74
36796:1	46.4	1.83
68245:1	46.4	1.83
126741:1	48.5	1.91
235067:1	48.5	1.91
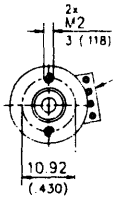
Front View
With Gearhead 16/7
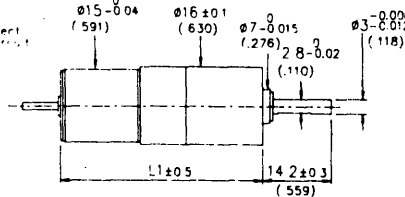
Gear Ratio	L1 mm	in
3.71:1	33.3	1.31
14:1	38.0	1.50
43:1	42.1	1.66
66:1	42.1	1.66
134:1	46.2	1.82
159:1	46.2	1.82
246:1	46.2	1.82
415:1	50.3	1.98
592:1	50.3	1.98
989:1	50.3	1.98
1526:1	50.3	1.98
2608:1	54.4	2.14
4365:1	54.4	2.14
5647:1	54.4	2.14

97

I B 4 6 2 • I B 4 6 3

MINIATURE HIGH PERFORMANCE BIPOLAR STEPPING MOTOR DRIVES

FEATURES

- LOW COST
- SINGLE SUPPLY
- HIGH INPUT VOLTAGE (+40 V)
- HIGH OUTPUT CURRENT (2 / 3.5 AMPS)
- ISOLATED INPUTS
- 20 KHz CHOPPING RATE
- ON BOARD PHASE LOGIC
- PC OR CHASSIS MOUNTABLE
- EXTREMELY SMALL SIZE
- FULL OR HALF STEP

DESCRIPTION

Intelligent Motion Systems has succeeded in developing a line of miniature high performance stepper motor drivers for todays quality minded — price sensitive market. Recognizing the wide variety of needs in a rapidly growing motion market, IMS has responded with some of the smallest, low cost stepper drives available today.

IMS has included features usually found only in the larger expensive drives — single supply, optically isolated inputs, half and full step, and a chopping rate of over 20KHz that eliminates audible noise.

Their small size make the IB462 and IB463 ideal for PC board mounting but they can also be frame or chassis mounted and will accept .200/.196 center connec-tors or plug type terminal strips.

The IB462 and IB463 are just two in our growing line of high performance, cost effective drives.

IB462

A MINIATURE PACKAGE...
The IB462, our smallest and lowest priced drive, packs a powerful 160W in less than 3 cu.in.

...HIGH OUTPUT CURRENT...
IB462 will effortlessly output up to 2 Amps per phase.

...HIGH INPUT VOLTAGE
The IB462 operates from 12 to 40 Volts. This high voltage allows for greater speeds at higher torque without resorting to expensive drives or larger motors.

The high efficiency of the IB462 chopper drives, along with its miniature size, makes it ideally suited to replace the less efficient L/R drives. In addition, the low cost and off-the-shelf availability of the IB462 permits an immediate cost effective solution to an in house design.

IB463

HIGHER OUTPUT CURRENT...
With an output capability of up to 3.5 Amps / phase. The IB463, which is only slighter larger than the IB462, can deliver 1.4 times more power.

...IN A MINIATURE PACKAGE
Although the IB463 circuit fits into an area of less than 3.6 cu.in., it is capable of delivering a powerful 230 Watts!

The IB463 is ideal for those applications requiring more power, but where size and cost are still important factors.

S P E C I F I C A T I O N S

ELECTRICAL

	IB462		IB463
INPUT VOLTAGE		+12 TO +40 VDC	
DRIVE CURRENT (PER PHASE)	0 TO 2 AMPS		0 TO 3.5 AMPS
LOGIC INPUT CURRENT (TO OPTO)		7.0 mA (TYP)	
STEP FREQUENCY (MAX)		40 KHz	

MECHANICAL
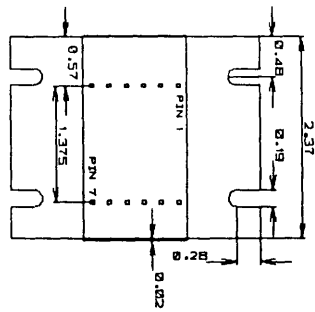
DIMENSIONS IN INCHES
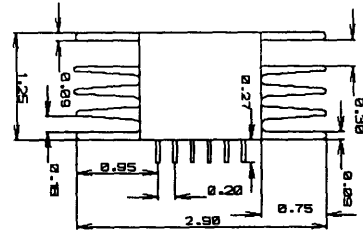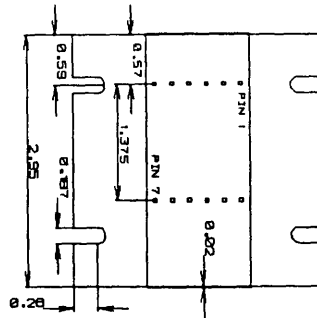
TEMPERATURE

STORAGE	−40 TO +125 °C
OPERATING	0 TO +50 °C
* CASE (MAX)	+80 °C

* EXTERNAL HEATSINK MAY BE REQUIRED TO MAINTAIN CASE TEMPERATURE

PIN FUNCTIONS

1. ENABLE	12. PHASE A
2. LOGIC GND	11. PHASE $\overline{A}$
3. HALF/FULL STEP	10. PHASE $\overline{B}$
4. STEP CLOCK	9. PHASE B
5. DIRECTION	8. V +
6. CURRENT ADJUST	7. GND

Ball with Concentric Blind Hole
Hardened Stainless Steel
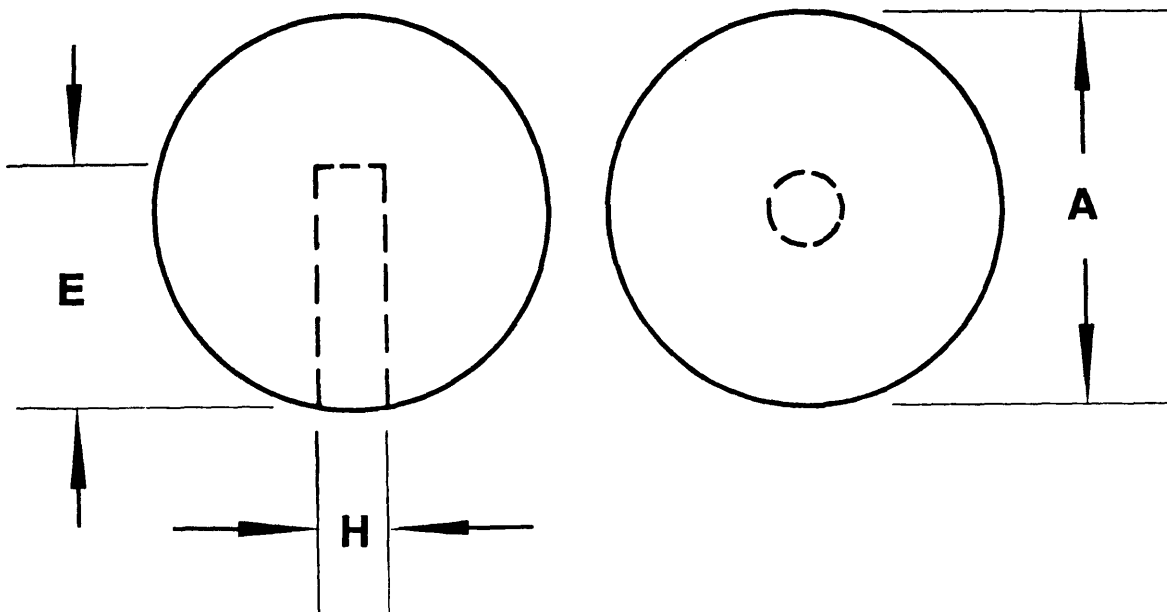
This general purpose component is most widely used by the gage industry.

They are used to construct ball bars, ball trees, reference spheres, etc.

They make good elements for kinematic systems, where this simple design can be applied.

Bal-tec ™

1550 E. Slauson Ave.
Los Angeles CA 90011 USA
Phone 213-582-7348
FAX 213-582-0934

Part No.	A-Diameter ±.0001"	H-Diameter ±.002"	E-Depth Reference
25-BBH	.250" 6.35 mm	.0625" 1.587mm	.125" 3.175mm
312-BBH	.3125" 7.9375mm	.09375" 2.381mm	.125" 3.175mm
375-BBH	.3750" 9.525mm	.09375" 2.831mm	.125" 3.175mm
50-BBH	.500" 12.700mm	.125" 3.175mm	.250" 6.35 mm
75-BBH	.750" 19.05mm	.125" 3.175mm	.300" 7.620mm
100-BBH	1.00" 25.4mm	.125" 3.175mm	.300" 7.620mm

9.

Truncated and Threaded Cylinder

Hardened Stainless Steel
with extended glue line and tapped holes
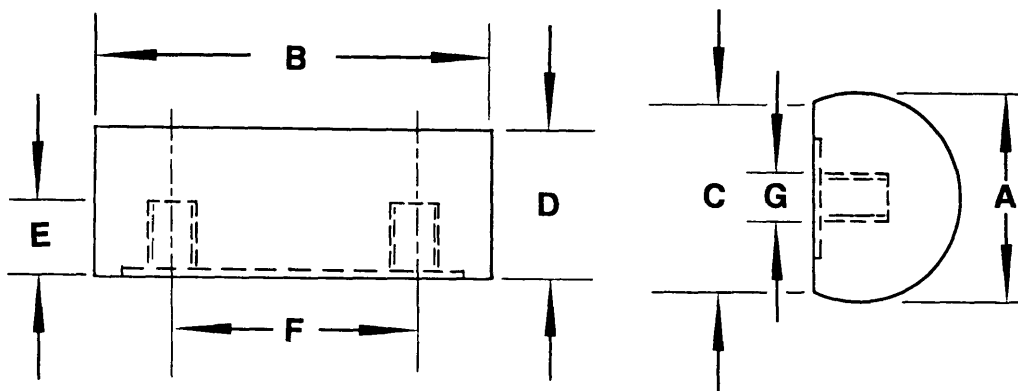
This design has a .005" deep recess on its flat surface that is made very rough by Electrical Discharge Machining. When maximum reliability is required, glue may be applied to this rough surface to form a permanent bond between this component, the machine screw, and the mounting surface.

Part No.	A-Diameter ±.0001"	B-Length Reference	C-Width Ref.	D-Heighth ±.002	Screw Size	E-Depth Ref.	F-Center Line
25-TCR-T	.250" 6.35 mm	1.5" 38.100mm	.235" 5.97mm	.167" 4.242mm	6-32	.125" 3.175mm	1.00" 25.4mm
312-TCR-T	.3125" 7.9375mm	1.5" 38.100mm	.294" 7.468mm	.208" 5.283mm	6-32	.154" 3.91mm	1.00" 25.4mm
375-TCR-T	.3750" 9.525mm	1.5" 38.100mm	.353" 8.966mm	.250" 6.35mm	10-32	.200" 5.08mm	1.00" 25.4mm
50-TCR-T	.500" 12.700mm	1.5" 38.100mm	.471" 11.963mm	.334" 8.484mm	1/4-20	.250" 6.35mm	1.00" 25.4mm

Because this cylinder is held from behind with machine screws, there is no interruption of the cylindrical surface. This provides a smooth, clean working surface.

The truncated and threaded cylinder is our most widely used cylindrical component.

The land left around the edge of the flat due to the recess forms an extremely stable mounting surface.

These hardened and dimensionally stabilized stainless steel cylinders are precision ground and machine lapped to provide excellent cylindricity with close dimensional tolerance.

The highly-regular low micro inch surface texture generated by the machine lapping leads to low hysterisis and excellent repeatability

Two parallel mounted cylinders, held in place by machine screws, form a very high quality substitute for the hard-to-manufacture vee groove.

13.

Appendix D: HTM Based Profiling Errors Calculation

The HTM based profiling errors calculation has two components; the first is the error that results when the sample is flipped from one side to the other side, the second component is the error that arises when the sample is moved to different locations along the edge (i.e. move along the 'Y' axis). The example calculation below is for the top side of the sample at one 'Y' location ('Y' = 0); it can be easily extended to the other side of the sample and also to different 'Y' locations.

Numerical values for the error terms / constants of chapter 4's homogeneous transformation matrices are given, followed by the explanations / assumption(s) made.

		1	2	3	4	5	6	7	8	9
	HTM matrix*	ε_x	ε_y	ε_z	a	b	c	δ_x	δ_y	δ_z
A	$^0T_1$ (X stage)	1.004 arcsec	0.288 arcsec	0	x = 0	0	1.53″	±.1142 µm	± .0105 µm	± 0.0026 µm
B	$^1T_2$ (Y stage)	0	0	20 arcsec	0	y=0	0.74″	0	0	0
C	$^2T_3$ (flip stage)	±20 arcsec	±20 arcsec	20 arcsec	0	0	0.73″	0, (± 10 flip offset)	0	0
D	$^4T_5$ (AFM tip)	0	0	20 arcsec	-2.75″	0	0	0 (init. align. <5 µm)	0	0
E	$^0T_4$ (AFM Z stage	0	16.5 arcsec	16.5 arcsec	2.75	0	z = 3″	0.012 µm	0.012 µm	0

* See figure 4.2 for location of HTM's.

Explanation / Assumptions
A1: change due to straightness error, data computed from X stage straightness calibration data (see Appendix C); (i.e. compute the angle from the inverse tan of change in straightness error divided by measuring height above table (1.75 in.);
A2: similar to A1, except done for flatness error;
A3: reference axis, therefore set to zero;
A4: position during profiling, same at all 'Y' points (i.e. along edge);
A7: actual incremental change in positioning error (i.e. leadscrew periodic error) from calibration data (see Appendix C);
A8: actual incremental change in straightness error (see Appendix C);
A9: actual incremental change in flatness error (see Appendix C);
Note for A7-A9:

	position error δ_x	straightness error δ_y	flatness error δ_z
Maximum (from spec)	± 1 µm	± 1.75 µm differential: 1µm/25mm	± 1.75 differential: 1µm/25mm
Maximum (from calibration curves)	≈ ± 0.7 µm	± 0.6 µm	+ 0.9 µm - 1.5 µm

Actual incremental over 280 µm travel at 141.22 mm position (actual profile location) (total change / 2)	± 0.1142 µm	± 0.01045 µm	± 0.00255 µm

B1: 'Y' stage does not move when one point is profiled;

B2: same as B1;

B3: estimated alignment possible;

B5: mid point of Y stage taken as zero reference;

B7: 'Y' stage does not move when one point is profiled; at different locations, est. for error is 0.001"/6.25" (specifed straightness and flatness);

B8: same as B7, but (positioning error) includes 2.5 µm (backlash) and leadscrew periodic error (not determined yet);

B9: same as B7;

C1: estimated angular positioning repeatibility of 'flip' stage;

C2: same as C1;

C3: estimated alignment possible (to 'Y' stage);

C7: assume when AFM tip engaged, alignment error is negligible; for worse case, use ± 10 µm (target alignment);

C8: if calculate error for top side only, use zero, else

C9: no 'Z' reference, measured from located tip;

D1: no error for a point; angular error would come from AFM;

D2: same as D1;

D3: estimated alignment possible (to 'Z' stage);

D7: assume when AFM tip engaged, alignment error is negligible;

D8: zero because no 'Y' reference point;

D9: no 'Z' reference, measured from located tip;

E1: assume negligible;

E2: angular error computed from specifed (Daedeal cross-roller stage) straightness (0.00008 in. / in.); note that Daedeal engineer states that error can be larger (up to 45 arc-sec.);

E3: same as E2;

E7: positioning error from straightness, assume only need to travel short distance (max. 150 µm) during initial alignment, i.e. 150 µm, so error is 0.00008 in./in. x 150 µm = 0.012 µm;

E8: same as E7;

E9: no 'Z' reference, measured from located tip;

Appendix D: HTM Based Profiling Errors Calculation

Sample error calculation for top side of the blade (actually the 'left' side) at Y=0; to calculate error for different 'y''s, need to change 'y' stage errors

Calculations done using DERIVE & MAPLE (math packages) using 32 digit precision.

For the AFM probe tip:

$$\hat{P} = {}^{0}T_{4} \, {}^{0}T_{5} \begin{bmatrix} 0 \\ 0 \\ 0 \\ 1 \end{bmatrix} = \begin{bmatrix} 0.012 \\ -5.5755309 \\ 76205.5875851 \\ 1 \end{bmatrix} \quad \text{(UNITS OF MICRONS)}$$

For the sample:

$$\hat{A} = {}^{0}T_{1} \, {}^{1}T_{2} \, {}^{2}T_{3} \begin{bmatrix} 0 \\ 0 \\ 0 \\ 1 \end{bmatrix} = \begin{bmatrix} 0.1665335554 \\ -0.1712938351 \\ 76200.00255 \\ 1 \end{bmatrix} \quad \text{(UNITS OF MICRONS)}$$

$$\hat{B} = {}^{0}T_{1} \, {}^{1}T_{2} \, {}^{2}T_{3} \begin{bmatrix} 20 \\ 0 \\ 4 \\ 1 \end{bmatrix} = \begin{bmatrix} 20.5570816989 \\ -0.1673370193 \\ 76200.468789008 \\ 1 \end{bmatrix} \quad \text{(UNITS OF MICRONS)}$$

$$\hat{C} = {}^{0}T_{1} \, {}^{1}T_{2} \, {}^{2}T_{3} \begin{bmatrix} 0 \\ 20 \\ 0 \\ 1 \end{bmatrix} = \begin{bmatrix} 0.1624550336 \\ 19.8287057793 \\ 76200.004586616 \\ 1 \end{bmatrix} \quad \text{(UNITS OF MICRONS)}$$

$$\underbrace{(\hat{B} - \hat{A}) \times (\hat{C} - \hat{A})}_{\substack{\text{use } 3\times1 \text{ column vectors} \\ \text{(take last row element out)}}} = \begin{bmatrix} -9.3247720037 \\ -0.0433364 3997 \\ 407.8149700 \end{bmatrix}$$

$$\underset{\text{(unnormalized)}}{V_{n,\,actual}} = Ry(\theta = -10^{\circ})(\hat{B} - \hat{A}) = \begin{bmatrix} 20.0000053076 \\ 0.0037068159 \\ 3.9999 72043 \end{bmatrix}$$

$$\underset{\text{use } 3\times1 \text{ vector}}{}$$

$$\underset{\text{(unnormalized)}}{V_{n,\,measured}} = Ry(-10^{\circ} - 0.07^{\circ}) \begin{bmatrix} 1 \\ 9.6963 \times 10^{-5} \quad \longleftarrow \varepsilon_{y,\,mmt} \\ \dfrac{-9.3247720037 + (-0.0433643997) \cdot (9.6963 \times 10^{-5})}{-407.8149700} \end{bmatrix}$$

ε_{x} of AFM tip

$$= \begin{bmatrix} 0.9305968564 \\ 9.6963 \times 10^{-5} \\ 0.1973641890 \end{bmatrix}$$

References

[A1] Cheng-Jung Chiu, *Data Processing in Nanoscale Profilometry*. Mechanical Engineering M.S. Thesis, (M.I.T., 1995).

[A2] e. g. resolution of the "S-4500 Ultrahigh-Resolution Scanning Electron Microscope", *Hitachi Technology '94* (Hitachi Review Special Issue).

[A3] S. T. Smith and L. P. Howard, "A precision, low-force balance and its application to atomic force microscope calibration," *Review of Scientific Instruments*, Vol 65, April 1994, p. 903.

[A4] D. G. Chetwynd and S. T. Smith, "High Precision Surface Profilometry: From Stylus to STM" in *From Instrumentation to Nanotechnology*.

[A5] J. Jahanmir, B.G. Haggar, and J. B. Hayes. "The Scanning Probe Microscope." *Scanning Microscopy*. Vol. 6, No. 3, 1992, pg. 625-660.

[A6] Eric Betzig \& Jay K. Trautman. "Near-Field Optics: Microscopy Spectroscopy, and Surface Modification Beyond the Diffraction Limit." in *Science*. Vo. 257. July 10, 1992.

[A7] e. g. the "Aurora" NSOM from Topometrix, 5403 Betsy Ross Drive, Santa Clara, CA 95054, Tel. (408) 982-9700, Fax. (408) 982-9751.

[A8] Y. Martin, C. C. Williams, and H.K. Wickramsasinghe. "Atomic force microscope-force mapping and profiling on a sub 100 angstrom scale." *Journal of Applied Physics*. Vol. 61. pg. 4723-4729.

[A9] H. Heinzelmann, E. Meyer, H. Rudin and H.J. Guntherodt. "Force Microscopy." in *Scanning Tunneling Microscopy and Related Methods*.

[A10] C.C. Williams and H.K. Wickramasinghe. "Scanning thermal profiler." *Applied Physics Letters*. Vol. 49. pg. 1587-1589.

[A11] D. Rugar, H.J. Mamin, P. Guethner, S.E. Lambert, J.E. Stern, I. McFadyen and T. Yogi. "Magnetic force microscopy: "General principles and application to longitudinal recording media." *Journal of Applied Physics*. Vol. 68. pg. 1169.

[A12] Y. Martin, D. W. Abraham and H. K. Wickramasinghe. *Applied Physics Letters*. Vol. 52. pg. 1103.

[A13] C. C. Williams, W. P. Hough, and S. A. Rishton. "Scanning capacitance microscopy on a 25 nm scale." *Applied Physics Letters*. Vol. 55. pg. 203-205.

[A14] V. K. Adamchuk, A. V. Ermakov and S. I. Fedoseenko. "Scanning tunneling microscope with large scan range." in Proceedings of STM'91 (published in *Ultramicroscopy*, Vol. 42-44. pg. 1602).

[A15] O. Wolter, Th. Bayer, and J. Greschner. "Micromachined silicon sensors for scanning force microscopy." *Journal of Vacuum Science and Technology*. Vol. B9 pg. 1353.

[A16] O. Marti, H.O. Ribi, B. Drake, T. R. Albrecht, C. F. Quate, and P. K. Hansma. "Atomic force microscopy of an organic monolayer." *Science*. Vol. 239. pg. 50.

[A17] H. Tsai and D. B. Bogy. "Critical Review: Characterization of diamond-like carbon films and their application as overcoats on thin film media for magnetic recording." *Journal of Vacuum Science and Technology*. Vol. A5 pg. 3287.

[A18] D. Keller, D. Deputy, A. Alduino, and K. Luo. "Sharp, vertical-walled tips for SFM imaging of steep or soft samples." in Proceedings of STM'91 (published in *Ultramicroscopy*, Vol. 42-44. pg. 1481-1489).

[A19] G. Binnig. "Force microscopy." in Proceedings of STM'91 (published in *Ultramicroscopy*, Vol. 42-44. pg. 7-15).

[A20] H. Kawakatsu, Y. Hoshi, T. Higuchi and H. Kitano, *J. Vaccum Science and Technology*. B 9, 651 (1991).

[A21] D. Nyyssonen, L. Landstein, and E. Coombs, *J. Vaccum Science and Technology*. B 9, 3612 (1991).

[A22] M. Tortonese, R. C. Barrett, and C. F. Quate, "Atomic resolution with an atomic force microscope using piezoresistive detection." *Applied Physics Letter*, Vol. 62 (8), February 22, 1993, p. 834-836.

[A23] Park Scientific Instruments, 1171 Borregas Ave., Sunnyvale, CA 94089, Tel. (800)-SPM-1602, Fax. (408) 747-1601.

[A24] Digital Instruments, Inc., 520 E. Montecito St., Santa Barbara, CA 93103.

[B1] J. F. Song and T. V. Vorburger, "Stylus profiling at high resolution and low force," *Applied Optics*, Vol. 30, No. 1, Jan. 1, 1991.

[B2] Model MM-3M-R Rotary Stage from National Aperture, Inc.. 27A Roulston Rd, Windham, N.H. 03087, Tel. (603) 893-7393, Fax. (603) 893-7857.

[B3] e.g. see stepper motor specifications in Compumotor catalog, Compumotor, 5500 Business Park Drive, Rohnert Park, CA 94928. Tel. (800) 358-9070.

[B4] S. Ueha and Y. Tomikawa, *Ultrasonic Motors: Theory and Applications*, Oxford University Press, New York, 1993.

[B5] Keyence general catalog (sensors), 17-17 Route 208 North, Fair Lawn, NJ 07410, Tel. (201) 791-8811, Fax. (201) 791-5791

[B6] Slocum, Alexander H., *Precision Machine Design*. Prentice Hall, New Jersey, 1992..

[B7] Lucas Aerospace "Free-frex pivot", 211 Seward Ave, PO Box 457, Utica NY 13503, Tel. (315) 793-1200, Fax. (315) 793-1415.

[B8] NMB Corporation 1992 Bearing Catalog, 9730 Indepence Ave., Chatsworth CA 91311, Tel. (818) 341-0820, Fax. (818) 709-0387.

[B9] Barden Precision Ball Bearings Catalog C-8C, 200 Park Avenue, Danbury, Connecticut 06810, Tel. (203) 744-2211.

[B10] J. Clerk Maxwell, "General considerations concerning scientific apparatus," *The Kensington Museum Handbook*. pp 1-21 (Chapman and Hall, London, 1876).

[B11] I. Sherrington and E. H. Smith, "Design and performance assessment of a Kelvin clamp for use in relocation analysis of surface topography." *Precision Engineering*, April 1993 Vol. 15 No. 2, pp 77-85.

[B12] A. Slocum and A. Donmez, "Kinematic couplings for precision fixturing-part 2: experimental determination of repeatibility and stiffness," *Precision Engineering*, Vol. 10, No. 3, July 1988, pp. 115-121.

[B13] Francis T. Farago, *Handbook of Dimensional Measurement*, Industrial Press, New York, 1968.

[B14] e.g. < 0.1 μm resolution motorized screw actuator ('Picomotor') is available from New Focus, Inc. 1275 Reamwood Avenue, Sunnyvale, CA 94089, Tel. (408) 734-8988, Fax. (408) 734-8882, fine manual screws with ≈ 0.1 - 0.5 μm minimum incremental motion are commonly available, see [B19].

[B15] piezostacks of various positioning range and sizes can be obtained from Physik Instrumente, 23 Midstate Drive, Suite 104, Auburn MA 01501, Tel. (508) 832-3456.

[B16] K. Nakamura, M. Kurosawa, S. Ueha, M. Umeda, and K. Ohnishi, *Transactions of the Institute of Electrical Engineers of Japan*, 111-C, p. 462-9.

[B17] M. Suzuki, T. Fujii, T. Onuki, M. Miyashita and M. Matsushiro, "Scanning tunneling microscope coaxially arranged with an optical microscope," *Ultramicroscopy*, 42-44 (1992), p. 1553-1557.

[B18] M. Yasutake and C. Miyata, "Scanning tunneling microscope combined with optical microscope for large sample measurement", *J. Vac. Sci. Technology* A 8 (1), Jan./Feb. 1990.

[B19] Newport catalog (1994), Newport Corporation, 1791 Deere Ave., Irvine, CA 92714, Tel. (800) 222-6440, Fax. (714) 253-1680.

[B20] Daedal Manual & Motorized Positioning Systems (1993-4), Daedal, Box 500, Harrison City, PA 15636, Tel. (800) 245-6903, Fax. (412) 744-7626.

[B21] flatness calibration curve for Aerotech HAL option (high precision) ATS-100-200mm travel linear stage, data obtained by measuring with an interferometer the linear displacement of a reference mirror located 1.75" above the tabletop mounting surface; Aerotech, Inc., 101 Zeta Drive, Pittsburgh PA 15238, Tel. (412) 963-7470, Fax. (412) 963-7459.

[B22] Normag, 25026 Anza Drive, Santa Clarita, CA 91355, Tel. (805) 257-0216, Fax. (805) 257-2037.

[B23] e.g. the 'ServoGlide' X-Y planar stage uses dual interferometer beam angle sensing and proprietary software; Anorad Corporation, 110 Oser Avenue, Hauppauge, N.Y. 11788, Tel. (516) 231-1995, Fax. (516) 435-1612.

[B24] Dektak SXM Atomic Force Microscope from Veeco Sloan Technology, Tel. (805) 963-4431 or (516) 349-8300.

[B25] Gurley Precision Instruments, 514 Fulton Street, P.O. Box 88, Troy, N.Y. 12181, Tel. (518) 272-6300, Fax. (518) 274-0336.

[B26] Canon, One Canon Plaza, Lake Success, N.Y. 11042, Tel. (516) 488-6700, Fax. (516) 354-1114.

[B27] Kaman Instrumentation Corporation, P.O. Box 7463, 1500 Garden of the Gods Road, Colorado Springs, CO 80933, Tel. (719) 599-1132.

[B28] Mechanical Technology Inc., 968 Albany-Shaker Road, Latham, N.Y. 12110, Tel. (800) 342--2203, Fax. (518) 785-2806.

[B29] Kaman Instrumentation Corporation, P.O. Box 7463, 1500 Garden of the Gods Road, Colorado Springs, CO 80933, Tel. (719) 599-1132.

[B30] Lucas Schaevitz, 7905 N. Route 130, Pennsauken, N.J. 08110, Tel. (609) 662-8000, Fax. (609) 662-6281.

[C1] S. Kalpakjian, *Manufacturing Engineering and Technology*, Addison-Wesley Publishing Company, Reading, Massachusetts, 1992.

[C2] K. Brookes. *Cemented Carbides For Engineers and Tool Users*, International Carbide Data, 1993.

[C3] Kinematic coupling components (as well as information on them) can be obtained from BAL-TEC, 1550 E. Slauson Avenue, Los Angeles, CA 90011, Tel. (213) 582-7348, Fax. (213) 582-0934.

[C4] C. Jensen and J.D. Helsel, *Engineering Drawing and Design*, McGraw-Hill, New York, 1990.

[C5] E. Oberg, F. D. Jones, H. L. Horton, and H.H. Ryffel, *Machinery's handbook* (24th Edition), Industrial Press, Inc., New York.

[C6] see literature from Able Electro-Polishing, 2904 West 26th Street, Chicago, IL, 60623, Tel. (312) 847-1631, Fax. (312) 847-1985.

[C7] Sun Steel Treating Inc, 550 Mill Street, Box U, South Lyon, Michigan 48178, Tel. (313) 471-0840, Fax. (313) 437-3140.

[C8] in ion nitriding, the part to be hardened is placed in a vaccum where a high voltage electrical energy is used to form a plasma of nitrogen ions; the ions are accelerated towards the workpiece, heating it, cleaning the surface, and provide active nitrogen for the hardening process; a detailed description of the process is given in the *Metals Handbook, 9th Edition, Vol. 4: Heat Treating*, American Society for Metals, Metal Park, OH.

[C9] Oriental Motor U.S.A. Corp., New York office: 369 Passaic Ave., Fairfield N.J. 07004, Tel. (201) 882-0480, Fax. (201) 740-0693.

[C10] IKO International, Inc., Fox Hill Ind. Park, 91 Walsh Drive, Parsippany, N.J. 07054, Tel. (800) 922-0337, Fax. (201) 402-0441.

[C11] J. E. Griffith and D. A. Grigg, "Dimensional metrology with scanning probe microscopes," *J. Applied Physics*, Vol. 74 (9) November 1, 1993. p. R83 - R109.

[C12] G. B. Picotto, S. Desogus, and G. Barbato, "Two scanning tunneling microscope devices for large samples," *Review of Scientific Instruments*, Vol. 64 (9) September 1993. p. 2699 - 2701.

[C13] 1994 Materials Selector Issue, *Machine Design*, Cleveland, OH 1993.